The impact of senescence on bioartificial organ design and performance

**A thesis submitted in fulfilment of the requirements of
the University of Brighton for the degree of
Doctor of Philosophy**

Neda Heidari

August 2022

1

Declaration

I declare that the research contained in this thesis, unless otherwise formally indicated within the text, is the original work of the author. The thesis has not been previously submitted to this or any other university for a degree and does not incorporate any material already submitted for a degree.

Neda Heidari

August 2022

Abstract

Acute liver failure (ALF) and acute chronic liver failure (ACLF) are life-threatening conditions with mortality rates of up to 85%. The only reliable treatment is orthotopic liver transplantation but there is a shortage of organ donors. Bioartificial livers (BALS) have been developed to overcome the limitations associated with non-biological devices and to replace the metabolic activities of the liver as a bridge to transplant or organ recovery after liver decompensation. These comprise hepatocytes within a biocompatible matrix. However, there is no evidence for enhanced patient survival, for unknown reasons, contact with the plasma of individuals with liver failure severely reduced hepatocytes key metabolic functions. Although overall cell viability was unaffected this loss of function completely compromised device function and represents an important barrier to the development of working BAL systems. Since senescence contributes to altered hepatocyte function in cirrhosis and the combination of an altered phenotype and unaffected viability in response to physiological stressors seen in BAL hepatocyte populations is highly reminiscent of cellular senescence. The aim of this study was therefore to investigate the role and significance of senescence on bio-artificial liver performance using an alginate modified p (HEMA)-MBA cryogel prototype seeded with hepatocytes and consider mechanisms by which to mitigate any effects on bio-artificial liver function using protective resveralogues. In this study, HEMA-MBA cryogels modified with alginate were used as a hepatocyte extracellular matrix to provide a 3-D environment for human hepatocyte studies. A model of hepatocyte senescence induction was developed using etoposide-treated HepG2 cells. To understand the role of senescence on bioartificial liver function, HepG2 cells were exposed to a non-cytotoxic concentration of senescence-inducing drug such as etoposide and analysed for potential markers of cellular senescence. The impact of hepatocyte senescence on key metabolic functions was analysed by measuring albumin and urea production. The data showed that etoposide treatment induced a senescent phenotype in HepG2 cells that combines growth arrest and loss of key functional phenotypes. The percentage of cell proliferation markers including 5-ethynyl-2'-deoxyuridine (EdU) ($p < 0.001$) and Ki67 ($p < 0.0001$) labelling decreased significantly after 48h treatment with 10µM etoposide. In addition, HepG2 senescence caused a significant reduction in albumin ($p<0.05$) and urea production ($p<0.001$) at the 3-D surface. HepG2 cells were treated with a liver toxins

3

cocktail at physiological doses and over clinically relevant periods (6h) and the effect of liver toxins on HepG2 cells proliferstion was measured. Also, the effect of senescence inhibitor compounds (resveratrol and resveralogues) on rescuing HepG2 cells from liver toxins effects and reversion of senescence effects were studied. The results of this study showed that HepG2 cells enter a senescent state in response to the liver toxin and inflammatory cytokine exposure which was confirmed by a significant reduction in the percentage of EdU and Ki67 positive cells ($p<0.0001$). However, senescence induction was inhibited by pre-treatment with 5µM resveratrol and resveralogues including V31, V34 and V29, and resulted in a significant increase in the percentage of EdU positive cells compared to liver toxins-treated cells ($p<0.001$). A multi-layered HEMA-MBA-alginate cryogel bioreactor was used as a *vitro* model of liver failure to assess induction of senescence and its role in declining device function and also evaluate the effect of resveratrol may reverse bio-artificial liver prototype failure. In line with the earlier results of this study, liver toxins induced senescence in HepG2 cells after 6h exposure and resulted in a significant reduction in albumin and urea synthesis ($p < 0.001$), and a considerable increase in cytokines production including IL-6 ($p< 0.01$) and IL-8($p < 0.001$). However, resveratrol at 5 µM concentration either before or during exposure to liver toxins cocktail preserves their capacity to produce both urea and albumin and suppresses cytokine production. In conclusion, this study showed that senescence plays a significant role in lost metabolising hepatocyte cell fraction over time and in the reduction of BAL synthetic and detoxification functions. However, this can be prevented by the use of polyphenolic compounds to protect the cells in the device from senescence-associated phenotypic changes, via both SIRT1-dependent and independent pathways.

Dedication

This thesis is dedicated to my lovely parents Mr Mansour Heidari, Mrs Zari Riahi and my kind brother Nima Heidari for their unconditional love, blessing and support throughout my life.

Acknowledgements

I would like to take this opportunity to express my unreserved gratitude to Dr Susan Sandeman for considering my application for research leading to the degree of Doctor of Philosophy and for selecting me for a project under her supervision. Her support and guidance throughout the project are highly appreciated.

I have been fortunate to have the pleasure of a prominent and one of the leading professors whose research in the field of ageing is known worldwide on the supervisory team. I express my heartfelt gratitude to Professor Richard Faragher for his support in conducting this research where his in-depth knowledge had the ultimate impact on the completion of this research work which would have been impossible otherwise. Professor Richard Faragher's constant encouragement throughout the project not only motivated me to engage in this research area but to learn how to conduct scientific research which I take as an asset in my career as a researcher. My thanks would be incomplete not to mention his role in securing a postdoctoral research post at the Royal Veterinary College. I am truly grateful to you.

I extend my thank you to Dr Marcus Dymond for the preparation and provision of 3D printing of connectors and spacers for the bioreactor experimental setup.

It would be hard not to mention the help and support of my fellow PhD friends, in particular, Flavia, Media, Gheed, Elahe, Emma, Grace, Sulef and Meriem. I do not think I would have made it without you.

Table of Contents

10

Table of Figures

14

15

ABBREVIATIONS

ACLF   Acute on chronic liver failure

ALD   Alcohol-related liver disease

ALF   Acute liver failure

ATM   Ataxia telangiectasia mutated

ATR   Ataxia telangiectasia and the RAD3-related

BrdU   Bromodeoxyuridine

BALs   Bioartificial livers

BSA   Bovine serum albumin

CDKi   Cyclin-dependent kinase inhibitor

DDR   DNA damage response

DMEM   Dulbecco's Modified Eagle Media

DMSO   Dimethyl sulfoxide

DPP4   Dipeptidyl peptidase 4

ECM   Extracellualr matrix

EdU   5-ethynyl-2'-deoxyuridine

ELAD   Extracorporeal liver assist device

ELISA   Enzyme-linked immunosorbent assay

EMT   Epithelial–mesenchymal transition

FBS   Fetal bovine serum

H_2O_2 Hydrogen peroxide

HCV   Hepatitis C virus

HCCs   Hepatocellular carcinomas

HSC   Hepatic stellate cells

ICC   Immunocytochemistry assay

IF   Immunofluorescence

IL-6   Interleukin-6

IL-8   Interleukin-8

IHC   Immunohistochemistry

LB1   Nuclear lamin B1

MARS   Molecular Adsorbent Recirculating System

MELS   Modular extracorporeal liver support

MMPs   Matrix metalloproteinases

mtDNA Mitochondrial DNA

MTT   3-(4,5-Dimethylthiazol-2-yl)-2,5-diphenyl tetrazolium bromide

NAFLD Non-alcoholic fatty liver disease

NASH   Non-alcoholic steatohepatitis

NK   Natural killer cells

OIS   Oncogene-induced senescence

PD   Population doubling

PDGF-AA Platelet-derived growth factor AA

RPA   Replication protein A

Rb   Retinoblastoma

ROS   Reactive oxygen species

SDF   Senescence-associated DNA-damage foci

SASP   Senescence-associated secretory phenotype

SPAD   Single pass albumin dialysis

SA-β-Gal Senescence-associated β-galactosidase

SAHF   Senescence-associated heterochromatin foci

TGF-β Transforming growth factor-beta

TRFs   Telomere restriction fragments

TNF-α   Tumor necrosis factor – α

UV   Ultraviolet

VEGF   Vascular endothelial growth factor

WB   Western-blot

Chapter 1. Introduction

1.1. Overview

The liver performs hundreds of functions including bile production, plasma protein synthesis, detoxification of drugs, metabolic waste processing, storage of dietary nutrients, and immunoregulation. In the course of liver failure, metabolites normally processed by the liver accumulate and promote hepatotoxicity through disruption of hepatocyte activity. The accumulation of liver toxins may promote cell death due to activation of apoptotic pathways or inflammation, mitochondrial damage, and oxidative stress which disrupt hepatocyte function and contribute to the progression of liver failure. Acute liver failure (ALF) and acute chronic liver failure (ACLF) are life-threatening conditions with mortality rates of up to 85% [1]. The only reliable treatment is liver transplantation but there is a shortage of organ donors. In the UK ~29% of patients wait for more than 6 months on the transplant list, and 8% die before receiving a transplant[2]. The shortage of organ donors and high mortality rates has created an urgent need for alternative functional liver replacement strategies that either bridge patients to transplantation or temporarily support liver function allowing it to recover. Approaches include non-cell-based liver dialysis devices and cell-based therapies including extracorporeal bioartificial liver, hepatocyte transplant, whole organ xenotransplantation and liver tissue engineering transplants.

Although non-cell-based artificial liver support devices have been developed, these systems are not able to replicate liver function effectively and have shown no clinical efficacy in terms of long-term survival benefits. The detoxification functions can be partially addressed by artificial and albumin dialysis devices but the synthetic functions of the liver can only be performed by living cells. Thus, biological liver replacement devices incorporating a hepatoma cell line or primary hepatocytes into a bioreactor to process blood or plasma have been developed to partially replace the synthetic and regulatory function of the liver in addition to patient plasma detoxification. However, no devices to date have shown significant survival benefits in patients with acute liver failure [3, 4]. A potential explanation for limitations to current biological device efficacy could be the impact of biological toxins, inflammatory and immunogenic stimulus on hepatocyte viability, and metabolic functional characteristics after exposure to patient plasma. One factor linked to altered liver function which may be promoted by exposure to high toxin levels is the induction of senescence in which cell death does not occur, but cells permanently exit the cell cycle and exhibit

radically altered phenotypic characteristics. It is known that cellular senescence plays a key role in the human response to injury and disease and is potentially associated with organ transplant failure [5, 6]. In the context of liver disease, it is known that hepatocyte senescence plays a role in the progression of fibrosis, but nothing is known about the impact of senescence on hepatocyte function within biological liver replacement devices. This chapter summarises our current understanding of senescence, its role in the development of liver failure, its potential role as a causative factor in the failure of current biological liver replacement devices and potential mechanisms by which the impact of senescence may be reduced for improved device longevity.

1.2. What is senescence and why does it exist? A broad range of stressors exists in all living cells. Cells can be damaged when they are exposed to different stress factors such as environmental stress or DNA damaging agents. They can respond to damage in different ways, ranging from the activation of pathways that develop survival or promote cell death to removing damaged cells. So, the damage can initiate a reversible (repair) or irreversible (senescence or apoptosis) response in cultured cells which ultimately determines the fate of the damaged cells. Also, the initial cell's response to stress is dependent on the level and duration of the insult as well as cell type. Cells undergoing apoptosis (programmed cell death) die and disintegrate rapidly in response to persistent stimuli or damage [7]. In recent years, apoptosis has been considered the main response to cellular stress. However, in some circumstances, cells undergo senescence as a consequence of less severe damage. In contrast to apoptosis, senescent cells lose their proliferative capacity but remain viable and metabolically active and they can also secrete a great number of inflammatory substances in their surrounding environment [8].

Cellular senescence is the state of permanent and irreversible cell cycle arrest of previously growing cells which is distinct from other forms of cell cycle arrest including quiescence (transient growth arrest), necrosis, and apoptosis. Quiescent cells are non-proliferating cells, and they can enter growth arrest due to a lack of nutrition and growth factors. However, they can re-enter the cell cycle when the growth condition is restored. In opposite to quiescence, senescence, an irreversible and stable cell cycle arrest, happens as a result of

20

ageing, DNA damage and other mutagens which can prevent or limit the transmission of damage to the next cell generation. No normal physiological stimuli are known that can stimulate senescent cells to re-enter the cell cycle [9]. Recent studies show that the proliferative potential of damaged or cloned cells during senescence is limited by the induction of stable cell cycle arrest. This mechanism can prevent damage from being transmitted to the next cell generation. It can also act as a barrier to carcinogenesis and cancer formation by preventing the clone of cells from accumulating and developing procarcinogenic mutations. Therefore, the transient presence of senescent cells can be beneficial in modulating tissue homeostasis by limiting the proliferation of damaged cells in tissue and acts as a tumour suppressor mechanism [10, 11].

Cellular senescence was first discovered by Leonard Hayflick and Moorhead in 1961 [12] when they observed that cultured normal human fibroblasts in *vitro* ceased to proliferate after 40 to 60 sub-cultivations. These cells were grown in a suitable condition, but they stopped proliferation after about 50 population doublings. They showed that the death of cultured normal cells was independent of growth medium contamination, medium components, and culture conditions[12]. A flattened and enlarged morphology was observed in human primary fibroblasts when they lost their proliferative capacity after a finite number of replications or when they reached their maximum capacity for replication. This maximum potential for replication was reduced in cultured cells derived from older donors compared to human embryos which shows an inverse relationship between the age of a human donor and the replicative capacity in *vitro.* Therefore, Hayflick introduced the theory of ageing at the cellular level based on this result. He proposed a three-phase model in normal cultured fibroblast cells. Phase I was the primary culture and normal cells were usually growing rapidly at this phase and it was followed by phase II when the cells were proliferating and multiplied. Phase II represents sub-cultivated cells during the period of exponential replication which the number of cells increases and the level of cell proliferation is more than cell death. Then, cells replicated slowly at phase III and stopped dividing after a limited number of divisions (Hayflick limit). He named this phase "senescence" when cultured cells stopped proliferation permanently (figure 1.1) [12]. Along this line, in the early 1970s, it was realised that the ends of linear DNA molecules cannot be completely copied because the end of the linear chromosome is capped with nucleoprotein complexes called

telomeres. Telomeres are placed at the end of chromosomes to protect the end of the DNA from degradation and a chromosomal end-to-end fusion. It was observed that telomeres gradually became shorter in diploid cells with every cell division, and ultimately become critically short, inducing replicative senescence. The telomere or telomerase system has been identified as a mediator of replicative capacity[13].
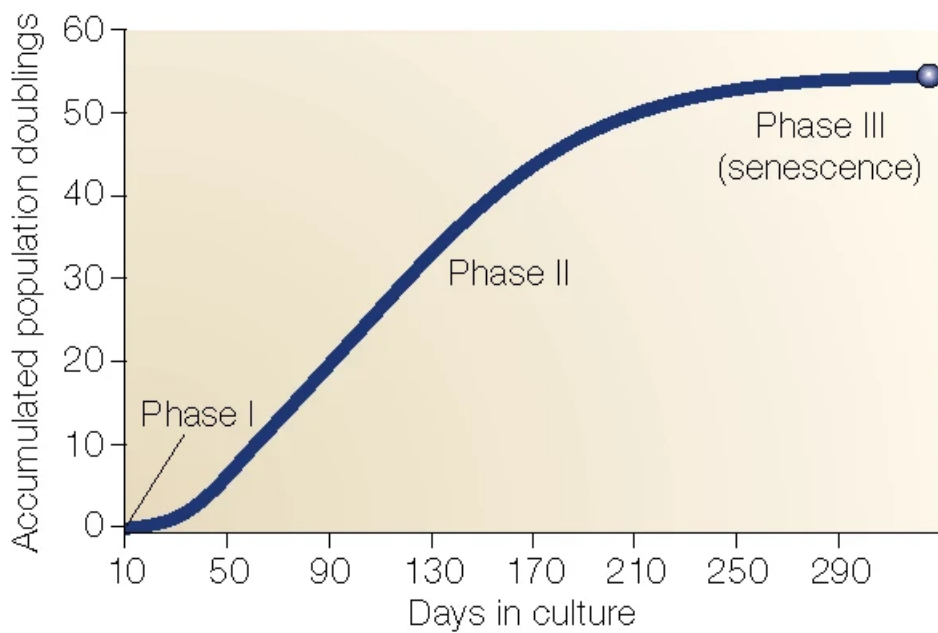
Figure 1.1.Three phases of cultured normal human fibroblasts [12]. Phase 1 indicates the primary culture. Phase II indicates the proliferation of the cultured cells. Phase III shows that cultured cells stopped dividing after a limited number of replications.

Telomere-dependent replicative senescence is the primary mode of entry into senescence-like growth arrest in *vitro* for human fibroblasts. Another type of cell has also behaved analogously to human fibroblasts in *vitro*. Cell types known to undergo replicative senescence include endothelial cells, epidermal keratinocytes, vascular smooth muscle cells, adrenocortical cells, lymphocytes, keratinocytes, and chondrocytes [14-16]. So, replicative senescence is not just limited to fibroblasts, and it can happen in different cell types. However, the process of cellular senescence is likely to be cell-type specific. In a study by Bodnar *et al. in* 1998 [17], two telomerase-negative normal human cell types including retinal pigment epithelial cells (RPE) and foreskin fibroblasts (BJ) were transfected with the reverse transcriptase subunit of human telomerase MPSV-hTRT vectors which encode the

22

human telomerase. This study showed that telomerase-expressing cells had reduced senescence biomarkers including reduced staining for β-galactosidase in both cells and increased their normal lifespan from 60 population doubling (PD) in telomerase-negative BJ fibroblast to 85-90 PD in telomerase positive fibroblasts and 20 PD in telomerase-negative RPE to 55-57 in telomerase-positive cells suggesting a relationship between telomere erosion and cellular senescence in *vitro*. Therefore, the reintroduction of telomerase into human cells resulted in a life-span extension and prevented replicative senescence [17].

In general, normal cells in *vitro* can undergo senescence after a finite number of divisions but, cultured cells may bypass the senescence process and show an unlimited life span in *vitro* and then become immortalised. Cells with an unlimited growth proliferation in *vitro* which display the characteristic of cells derived from malignant tissue, are abnormal and result in the development of a malignant phenotype [18]. This form of spontaneous immortalisation is a rare event that can be dependent on primarily species type. The spontaneous immortalisation has already been reported in different cell lines such as mouse embryonic fibroblasts (MEFs), liver sinusoidal endothelial cell line (LSEC) generated from mouse liver, and mouse and rat epithelial cells [19, 20]. Genetic instability including mutation in the p53 gene and changes in chromosomes are considered the main facilitators of spontaneous immortalisation in the mentioned cell lines. Inactivation of apoptotic pathways with loss of the p53 and pRb pathways is another possible route for immortalisation [20].

In summary, normal somatic cells grown in culture are unable to proliferate indefinitely and they usually cease to proliferate after a limited number of divisions despite having access to sufficient growth factors, nutrients, and space. This phenomenon of permanent growth arrest is known as replicative senescence because it happens by replication. Senescent cells cannot replicate anymore because they have reached the end of their replicative life span which is termed the Hayflick limit [12]. Cells with unlimited growth potential in *vitro* are referred to as immortal or continuous cell lines which can escape from senescence and acquire an infinite lifespan. Immortalised cell lines can be categorised into two different groups. Spontaneously immortalised cells or tumorous cells can undergo some genetic changes and become resistant to senescence. These cells acquire an infinite life span which can be produced from human cells such as HepG2 or HeLa cells. By contrast, non-

tumorigenic cells are artificially manipulated cells that have the unlimited proliferative capacity and can be cultured for a long time [21]. These cells are usually immortalised by using viral genes such as the simian virus 40 (SV40) T antigen or through the expression of Telomerase Reverse Transcriptase protein (TERT), especially for cells that are affected by telomere length including human cells.

1.2.1 Mechanisms of entry into senescence

Permanent and irreversible cell cycle arrest is one of the most important features of senescent cells which is controlled by activation of the p53/p21^{CIP1} and the p16^{INK4a}/Rb tumour suppressor pathways (figure 2). This growth arrest is usually induced by a continuous DNA damage response (DDR) in response to either intrinsic stimuli such as progressive telomere shortening, changes in telomere structure, oxidative damage or external insults including radiation, oxidative and genotoxic stress and chemotherapeutic agents[22]. Progressive telomere shortening which happens as a result of replicative senescence is the most known reason for induction of senescence, and DDR in this type of senescence depends on telomere length. During replicative senescence of human fibroblasts, telomeres become critically short leading to an uncapped and double-stranded chromosome-free end and subsequently initiating a DDR [22]. However, it is important to note that senescence in some cells happens irrespectively of telomere length and it can be mediated by the activation of tumour suppressor pathways (p53/p21 or p16/Rb) [23]. For example, replicative senescence occurs in primary human astrocytes (NHAs) after 20 PD in a p53-dependent but telomere-independent manner. The majority of cells (~80%) were immunopositive for p21 and showed a low level of Bromodeoxyuridine (BrdU) labelling (1%) and high SA β-gal index (90 %) after approximately 20 PD. Furthermore, telomere length didn't change significantly during the replicative life span in the culture and the final arrest or M1 in astrocytes was associated with significant changes in cyclin-dependent kinase inhibitor expression. A significant increase in p16INK4A expression (30-fold) was observed at M1 in comparison to presenescent-proliferating cells suggesting that final arrest in NHAs occurred independent of telomere length but resulted from the p53 activation [24]. Regardless of which stressors cause DNA damage, the DDR is characterized by activation of protein kinases ataxia telangiectasia mutated (ATM) and ataxia telangiectasia and the RAD3-related (ATR) kinases cascade. Different DNA damage sensors such as replication protein A

24

(RPA), the RAD9-RAD1-HUS1 (9-1-1) and MRE11-RAD50-NBS1 (MRN) complexes detect single and double-stranded breaks respectively and recruit ATM and ATR to the site of damage[25]. Both ATM and ATR strengthen the DDR signal by increased deposition of γ-H2AX (DNA damage protein) at the site of injury which helps in the gathering of other DNA repair complexes to form nuclear foci and activation of a kinase cascade. Once ATM and ATR are phosphorylated, they block cell cycle progression by activation of downstream cell cycle regulators CHK1 and CHK2 leading to the P53 stabilisation. Subsequently, P53 activates the transcription of the cyclin-dependent kinase inhibitor (P21) which binds to a cyclin-dependent kinase (CDK) 2 complex resulting in hypo phosphorylated retinoblastoma (Rb) and consequently prevents E2F-mediated transcription of proliferation-promoting genes causing G1 cell cycle arrest [10] ([figure 1.2](#)).

The response of the p53–p21 and p16Ink4a–RB effector pathways to the primary growth arrest signal is dependent on the type and duration of stress. Either p53 or p16 pathways become activated and both may eventually be involved to sustain senescence. When proliferating cells are subjected to transient stress, p53 induction can activate a quiescence state and DNA repair processes. Induction of p53 pauses the cell cycle at the G1, S, or G2 phases of the cell cycle to prevent DNA synthesis and mitosis in the presence of unrepaired DNA damage. Once the DNA damage is resolved, then the cell can resume cell cycling. However, p16INK4a, an inhibitor of CDK4 and CDK6, is activated in the presence of persistent stress and unrepaired DNA damage resulting in permanent cell cycle arrest or senescence[22]. Senescence can be mediated through p16 activation which binds specifically to the CDK4 and CDK6 and displaces cyclin D thereby inhibiting the Rb phosphorylation. Retinoblastoma protein (pRb) is a tumour suppressor protein that is considered the master brake of the cell cycle. When RB is in a hypo-phosphorylated state it binds specifically to transcription factor E2F1 and inhibits transcription of E2F1 target genes which are necessary for DNA replication and cell proliferation. Therefore, P16 activates the G1-S checkpoint and inhibits the kinass activities of CDK4 and CDK6 via the prevention of pRB phosphorylation's response which is essential to establish permanent growth arrest or long-term maintenance of senescence phenotype[22, 26] ([figure 1.2](#)).
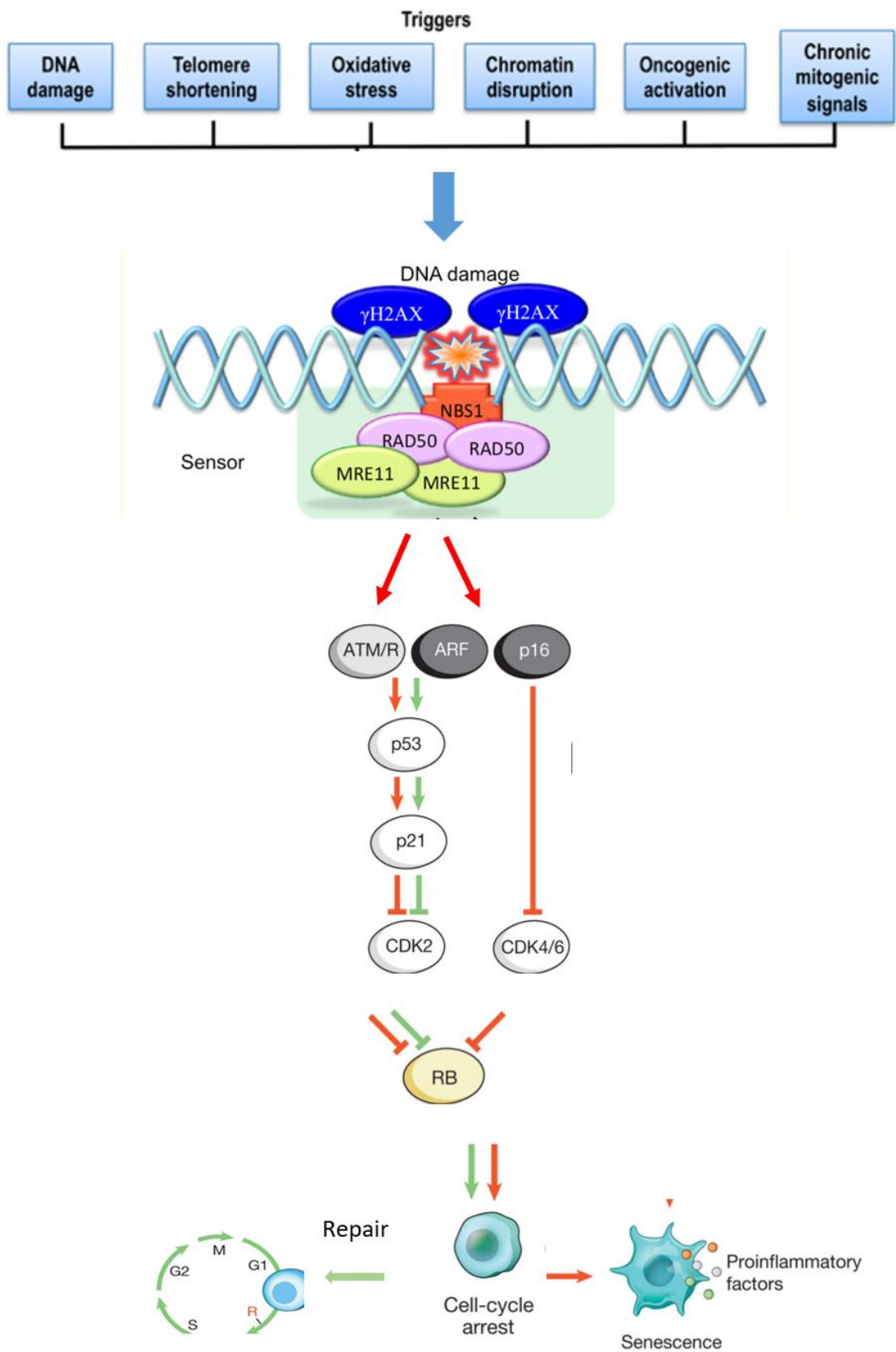
Figure 1.2. Mechanism of cellular senescence. Different cell-intrinsic and extrinsic stresses can trigger cellular senescence by initiating DNA damage response which resulted in p53, p16Ink4a, or both activations. Both p21 and p16 inhibit CDKs and prevent the inactivation of Rb protein leading to inhibition of transcription of E2F1 target genes and G1 cell cycle arrest. Upon moderate and transient stress (green arrows), the cell can re-enter the cell cycle and resume proliferation. In contrast, cells exposed to severe stress (red arrows) which causes permanent damage age to enter the permanent cell cycle arrest and transit into a senescence state[10].

1.2.2 Stress-induced premature cellular senescence

In human and mouse cells premature senescence can be induced by oxidative stress through increased intracellular levels of reactive oxygen species (ROS) that cause damage to lipids, proteins and DNA. ROS are oxygen-containing radicals comprising the superoxide anion (O_2-), hydrogen peroxide (H_2O_2), and hydroxyl radicals ($OH\cdot$). The ROS produced from either endogenous sources such as mitochondria or exogenous sources including ultraviolet/ionising radiation, smoke exposure, and chemotherapeutic drugs induce cellular senescence via a DNA damage response pathway[11]. Stress-induced premature senescence occurs in many types of cells including normal and tumour cells when they were exposed to ionising radiation or oxidative stress[27]. The oxidative stress responses of human endometrium-derived mesenchymal stem cells (hMESCs) were studied after exposure to the sublethal H_2O_2 doses. 200 µM H_2O_2 induced premature senescence in hMESCs after 1 h treatment. Senescent-like morphology was observed after 24 h treatment and cells become enlarged and flattened. An increase of senescence-associated beta-galactosidase (SA-β-Gal) staining (95% H_2O_2- treated cells), lack of Ki67 staining and increased levels of p21 confirmed the permanent growth arrest and irreversible loss of proliferative potential in treated cells. So, hMESCs lost their proliferative potential and entered the state of premature senescence in response to oxidative stress [28].

Oxidative stress and DNA damage similar to telomere damage initiate the DNA damage response (DDR), a signalling pathway in which ATM or ATR kinases block cell-cycle progression through stabilisation of p53 and transcriptional activation of the cyclin-dependent kinase (Cdk) inhibitor p21. Then the growth arrest phenotype is established by

27

P53/P21 pathway[23]. Zhan et al (2010)[29] investigated the role of ATM in mediating the action of oxidative stress to induce premature senescence in endothelial cells. The ATM-dependent Akt/p53/p21 signalling pathway was activated in human umbilical vein endothelial cells (HUVECs) through induction of unrepairable DNA damage and persistent oxidative stress. An increase in ATM phosphorylation, p53, and p21 expressions was confirmed after exposure to 100 μM H_2O_2 for 1 h as an inducing agent of oxidative stress. This data suggests that oxidative stress-activated ATM and p53 phosphorylation which was followed by the up-regulation of p21 expression. ATM likely activated p53 phosphorylation which is the downstream signalling molecule of ATM/Akt. Then, p21 expression, a downstream target of p53, was upregulated after activation/phosphorylation of ATM and p53. These actions were abolished in H_2O_2 -treated cells in which ATM was knocked down using RNA interference(siRNA) and resulted in reduced ATM mRNA and protein levels expression with inhibition of Akt and p53 phosphorylation and decreased p21 gene expression ($p < 0.05$). In addition, the level of SA-β-gal-positive cells in H_2O_2 -treated cells decreased significantly ($p < 0.05$) after ATM knockdown by siRNA. Thus, the phosphorylation of ATM, Akt, and p53 and up-regulation of p21 expression regulated the cellular response to oxidative stress in endothelial cells. In addition to ATM phosphorylation, the number of SA-β-gal positive cells were significantly increased in H_2O_2- treated cell, compared with cells incubated without H_2O_2 treatment. In conclusion, oxidative stress induced DNA damage and premature senescence in endothelial cells as confirmed by SA-β-gal staining and was associated with the ATM-dependent Akt/p53/p21 signalling pathway. This signalling pathway have a key role in mediating the action of oxidative stress and induction of premature senescence in HUVECs and can be considered as new therapeutic target for cardiovascular diseases [29].

1.2.3 Oncogene-induced senescence

Oncogene-induced senescence (OIS) is a potent defensive mechanism against tumour progression and cancer which arrest cell cycle progression upon oncogenic signalling. DNA damage induced by oncogenic stimuli happens independently of telomere length. Oncogene activation during early tumorigenesis initially triggers a high degree of DNA replication (hyperproliferative phase) which induces cellular senescence. The mitotic signals increase the usage of DNA replication origins which leads to stalled replication forks and produces

numerous double-stranded DNA breaks and eventually activates DDR. DDR activates several tumour suppressors' networks, including the p16^{INK4A}/RB and p19ARF/p53/p21 pathways which cause OIS, leading to cell cycle arrest after a few cell cycle divisions [30]. For example, Di Micco et al (2006) [31] showed that oncogene-induced senescence following an activated oncogene (H-RasV12) in normal human cells, happened because of DDR activation. A hyper-replicative phase occurred immediately after the expression of oncogenic Ras resulting in DDR and OIS and most of the cells that underwent OIS have detected positively senescence-associated DNA-damage foci (SDF), containing the activated ATM (84%), NBS1(73%), and the complex containing ATR (85%), ATRIP (ATR-interacting protein, 89%) and RPA (replication protein A,87%). Activation events related to DNA damage include an increase in the p21 and p16 cyclin-dependent kinase inhibitors together with p53 and hypo-phosphorylated Rb gene product accumulated in senescent cells. It was also shown that the inactivation of the DDR pathway increased the fraction of growing cells which restarted DNA synthesis, confirmed by a significant increase in the incorporation of BrdU and inactivation of p16 (p<0.05) and increased cell numbers (P < 0.04). In summary, these data show that OIS is linked with the presence of DNA damage. Complete activation of the DDR mechanism is necessary for the establishment and maintenance of OIS. Also, the knockdown of the main DDR kinases abolished OIS and develop cell transformation.

1.2.4   The altered phenotypes of senescent cells

Permanent exit from the cell cycle is considered the main characteristic associated with senescent cells. However, many studies showed that irreversible cell cycle arrest was not the only feature of senescent cells which distinguishes them from normal growing cells. For example, Shelton et al in 1999 [32] showed that senescent cells have altered patterns of gene and protein expressions and secrete matrix remodelling enzymes plus, inflammatory chemokines and cytokines. In this study, the level of soluble factors secreted by five human fibroblast strains, derived from embryonic lung (WI-38, IMR-90), neonatal foreskin (BJ, HCA2), or adult breast (hBF184) was measured by antibody arrays and senescence was induced in these cells by either replicative exhaustion or by treating them with 10 Gy of ionising radiation. Senescent cells expressed higher levels of inflammation-associated genes including chemokines (MCP-1 and Gro-α), cytokines (IL-15 and IL-1β, TNF-α, IL-6, IL-8) compared to the normal fibroblasts. Also, these secretory phenotypes of senescent cells

29

were not dependent on whether senescence was induced by replicative exhaustion, telomere erosion or genotoxic stress. Once the cell's proliferation is permanently arrested, they start to express different secreted molecules which are known as senescence-associated secretory phenotype (SASP) factors. SASP was developed by senescent cells 4 to 7 days after DNA damage and it reached the maximum level on day 10. Consequently, senescent cells started to be considered metabolically active viable cells with permanent growth arrest which is unique to the senescent phenotype[32].

SASP is responsible for many positive and negative impacts attributed to senescent cells. One of the major functions of SASP is to act in an autocrine fashion to reinforce the cell cycle arrest and facilitate the immune clearance of senescent cells. The secretion of SASP factors including proinflammatory cytokines and chemokines mediate the activation and recruitment of the immune system to eliminate senescent cells. The SASP components recruit adaptive and innate immune cells including macrophages, natural killer cells (NK), neutrophils, and T lymphocytes to eliminate senescent cells. Also, the proteins responsible to remodel the extracellular matrix facilitate the entry of immune cells to the areas of senescent cell localisation for their removal and secrete growth factors to stimulate the proliferation of surrounding cells for subsequent replacement of eliminated cells and maintain the tissue homeostasis[33]. For example, In study by Kang and co-workers (2011) showed that senescent hepatocytes communicated with their environment by producing different cytokines and growth factors and these secretory phenotype can have anti-tumorigenic effects . Firstly, oncogene-induced senescence occurred in the mouse liver by delivering transposable elements 7 expressing oncogenic Nras (NrasG12V) into hepatocytes and sescence was confirmed by positive stainings of p21, p16 and SA-β-gal in NrasG12V -expressing hepatocyte. Then, neutrophils, lymphocytes, and monocytes/macrophages were found in immune cell clusters around senescent hepatocytes (hepatocytes expressing NrasG12V) and accompanied by the increased number of NK cells, macrophages, dendritic cells, and CD4+ and CD8+ lymphocytes quantified by flow cytometry. These liver-infiltrating immune cells mediated the clearance of senescent hepatocytes (known as 'senescence surveillance') which depends on an intact CD4+ T-cell-mediated adaptive immune response. 6 days after delivery of oncogenic NrasG12V or NrasG12V/D38A in *vivo,* similar numbers of Nras-positive and p21- and p16-positive senescent cells were found in mouse liver.

However, time-course analysis confirmed a rapid loss of Nras-positive and senescent cells over time with only 6 ± 1.4% of Nras-positive cells remaining at day 12 and complete loss of Nras-positive cells after 60 days. It was also reported that immune surveillance of pre-malignant senescent hepatocytes was abrogated by an impaired adaptive immunity in mouse model with impaired adaptive immune response and resulted in the development of murine hepatocellular carcinomas (HCCs). In summary, the results of this study showed that the autocrine activity of senescent cells has a positive effect because of the activation of the immune system which leads to removing damaged cells and preventing the accumulation of senescent cells within a tissue (anti-tumour barrier). In addition, senescence surveillance plays a key role to inhibit tumour progression and liver cancer development in *vivo* [34].

Specific components of SASP such as proteases and other factors secreted by SASP including growth factors may play a central role in physiological functions. For example, matrix metalloproteinases (MMPs), one of the components of SASP, may play a positive role in the context of liver fibrosis and wound healing by contributing to reducing fibrotic plaques in the extracellular matrix(ECM) and fibrotic tissue remodelling. Growth factors including vascular endothelial growth factor (VEGF) and platelet-derived growth factor AA (PDGF-AA) are secreted from senescent cells in SASP form at the site of injury and they are regarded as key factors to induce angiogenesis, wound contraction during wound healing and fibrotic reduction[35]. For instance, Krizhanovsky et al (2008) [36]showed that senescent cells derived from activated hepatic stellate cells (HSC) in murine liver treated with CCl4 (induce fibrosis in experimental animal) plays a key role to limit liver fibrosis. In mice without key senescence regulators (p53⁻-mice), HSCs constantly proliferated which led to severe liver fibrosis. HSCs produced extracellular matrix-degrading enzymes and secrete cytokines which resulted in improving immune surveillance and consequently facilitated fibrosis resolution. Senescence was also induced in cultured primary human activated HSCs by treatment with a DNA damaging agent, etoposide, or replicative exhaustion, and senescence was confirmed by accumulated SA-β-gal activity plus acquired senescence-associated heterochromatic foci within several days after etoposide treatment. The results of RT-PCR analysis showed increased expression of extracellular matrix-degrading enzymes such as MMP1, MMP13, MMP10, and MMP12 and decreased expression of extracellular matrix components such as collagens type I, III, IV, and fibronectin which are constituents of the fibrotic scar, in

senescent HSCs compared to growing cells (p<0.001). So, these data showed that following chronic liver damage, senescent HSCs limit the fibrotic tissue accumulation by producing MMPs which have fibrolytic activity and inhibit fibrogenic factors production, helping the fibrosis resolution[36].

Factors secreted by senescent cells can influence surrounding cells and tissue microenvironment in a paracrine fashion to promote tumour progression and exacerbate senescence during ageing or in the course of persistent damage[37, 38]. IL-6, IL-8, GROα, IGBP-7, and TGF-B are among the specific SASP components which can reinforce and spread the senescence phenotype in a paracrine manner to neighbouring cells. For instance, SASP which was developed by human fibroblast strains after induction of senescence by ionising radiation induced an epithelial-mesenchymal transition (EMT) in two nonaggressive human breast cancer cell lines when they were cultured together for 7 days. These data showed that human fibroblasts developed SASP slowly after induction of senescence (7-10 days) and spread the senescence phenotype to neighbouring non-senescent cells through secretion of IL-6, IL-8, IL-1β and TGFβ. Thus, senescent cells can promote malignant phenotype and inflammation in nearby cells through their paracrine mechanism which is related to their SASP factors [38].

In summary, senescence can be transmitted to normal cells through SASP components which act as signalling molecules in an autocrine or paracrine manner. These components can act on nearby cells by the auto/paracrine pathway to initiate the maintenance of senescence or escape, immune system activation or suppression, and induction of tumorgenesis or suppression. All the mentioned SASP effects are dependent on the temporary or permanent presence of senescence cells. The short-term presence of senescent cells can exert some beneficial impacts on the organism when they are promptly removed by immune system cells and inhibit the accumulation of damaged cells within the tissue. However, the negative effects of SASP are associated with the accumulation of senescent cells and subsequently the continuous secretion of SASP as a result of ageing and decline of immune clearance efficacy. This leads to the spread of premature senescence to surrounding cells and disruption in the functioning of tissue and manny physiological processes (figure 1.3)[33, 35].
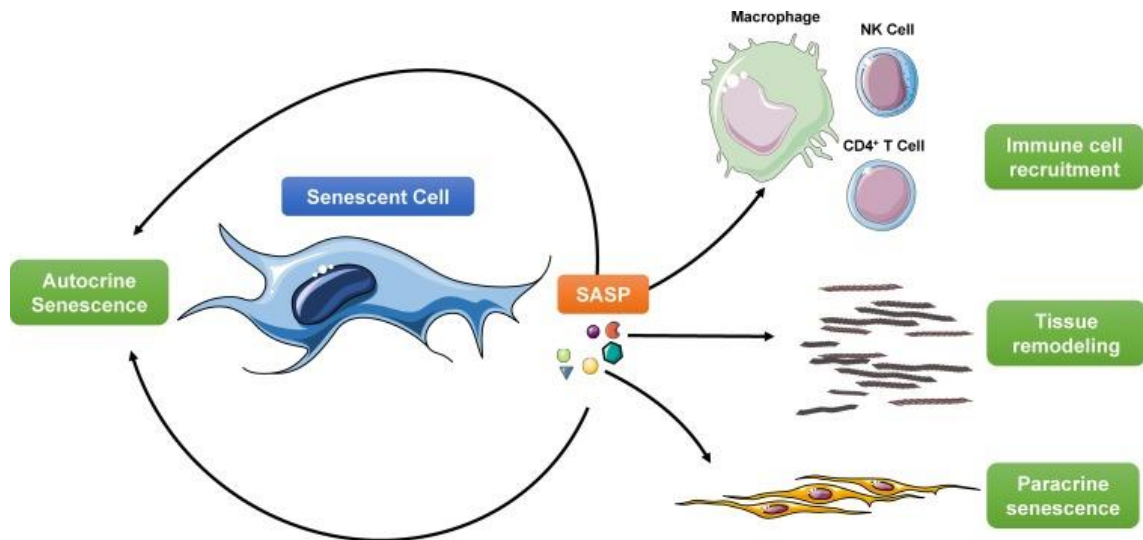
Figure 1.3. The SASP factors can reinforce or induce senescence growth arrest within cells in an either autocrine or paracrine manner. These factors attract immune cells including macrophages, natural killer cells (NK), neutrophils and T cells to clear the senescent cells within the tissue and consequently leading to tissue repair. Also, secretion of MMPs and VEGF can help tissue remodelling and reduce fibrosis. The paracrine activity of senescent cells can cause and spread the cellular senescence in normal neighbouring cells leading to chronic inflammation [33].

Although senescent cells usually display a SASP and express a wide range of pro-inflammatory factors, upregulation of cell surface molecules is the other feature which distinguishes senescent cells from proliferating cells. For example. For exmple, In a study by Kim et al (2017)[39] showed that DPP4 (dipeptidyl peptidase 4) was uniquelly present in the the surface of senescent cells but not proliferating cells. The DDP4 levels were significantly increased in the membrane fraction of human diploid senescent fibroblasts but not dividing fibroblasts. ICAM and uPAR/CD87 are the other cell surafce molecules which upregulated on the senescent cell membrane. The presence of DPP4 and other ligands on the surface of senecsent fibroblasts make them suitable targets for elimination by NK and CD8+ T-cells of the immune system[39]. In addition, The SASP phenotype can be enhanced by the upregulation of cell surface molecules which are only expressed on the surface of senescent cells. It has been shown that cell surface molecules including SCAMP4, CD36, and NOTCH1 which were highly expressed on the surface of human fibroblast senescent cells promoted the secretion of SASP and increased the level of proinflammatory cytokines and SASP

components. Therefore, these cell surface molecules can play a key role in the recognition of senescent cells by the immune system by inducing the secretory phenotype of senescent cells and secretion of proinflammatory factors which leads to the elimination of senescent cells by immune cells[40, 41].

1.2.5 Effects of cellular senescence and its reversal/removal

Accumulation of senescent cells in various tissue and organs during ageing can promote tissue degeneration and disrupt tissue structure and functions because of the factors they produce and secrete. However, it has been reported that the elimination of senescent cells resulted in increased longevity and reduced the occurrence of age-related diseases [42, 43]. For example, BubR1H/H mice, a transgenic mouse model, had a significantly short lifespan and showed different age-related phenotypes, including infertility, lordokyphosis, sarcopenia, cataracts, fat loss, cardiac dysrhythmia, stiffening or hardening of the vessel wall and impaired wound healing. The number of p16Ink4a cells which cause a range of ageing symptoms increased remarkably in certain tissues including adipose tissue, skeletal muscle, and the eye. Whereas, removing of p16Ink4a-expressing cells or senescent cells upon treatment with senolytic drug significantly delayed or prevented the development of age-associated phenotypes in tissues with elevated senescence markers. The development of lordokyphosis (a measure of sarcopenia onset in this model) and cataracts were delayed after the elimination of p16Ink4a-positive senescent cells by senolytic treatment compared to non-treated cells. So, these data showed that cellular senescence can cause age-related dysfunctions in genetically engineered mice models and clearing of senescent cells prevented tissue degeneration, delayed age-related phenotypes, and extended health span of mice [42].

Metabolic alterations such as an increase in mitochondrial metabolism were observed and reported in senescent cells. Data on metabolic changes associated with cellular senescence have shown that mitochondrial dysfunction, characterized by high production of ROS, occurs as a result of deterioration in mitochondrial oxidative phosphorylation (OXPHOS) during the early stages of cellular senescence [44]. OXPHOS is composed of five multi-subunit enzymes or respiratory chain complexes (complex I to V) that produce an electrochemical transmembrane gradient in the mitochondrial inner membrane to synthesis

cell energy in the form of ATP by complex V. Also, OXPHOS is the main source for ROS generation such as superoxide and hydrogen peroxide because it utilises 85-90% of the oxygen consumed by the cell. Mitochondrial DNA (mtDNA) is highly susceptible to any upregulation of ROS production in senescent cells due to co-location near the site of ROS production and lack of DNA repair enzymes. mtDNA can be damaged as a result of ROS upregulation in senescent cells and this leads to further impairment of mitochondrial OXPHOS function, thus releasing more ROS and reducing ATP production. Therefore, in senescent cells, mitochondrial ROS can exacerbate cellular senescence by causing more DNA damage and DNA damage response (DDR) leading to the initiation and maintenance of the senescent phenotype [44, 45].

A study by Passos et al (2007)[46] revealed significant mitochondrial dysfunction in senescent human fibroblast cultures as well as changes in gene expression patterns indicative of enhanced retrograde signalling. Senescence was induced in MRC5 fibroblast cells by H_2O_2 at 400 µM concentration for 30 minutes and the metabolic function of treated cells was compared with non-treated fibroblasts to assess whether mitochondrial dysfunction is related to fibroblast senescence. In senescent cells, mitochondria produced elevated levels of superoxide compared to young and non-treated fibroblasts ($p<0.01$). In addition, mitochondrial membrane potential decreased significantly in senescent fibroblasts ($p = 0.008$) which is often indicative of mitochondrial DNA (mtDNA) damage. Different enzymes associated with major functions in mitochondrial metabolism including glucose metabolisms such as HK2, PDP2, and PDK4, and lipid metabolisms such as CPT1A, PTE1, and FABP4 were up-regulated. So, increased mitochondrial ROS production in parallel with a breakdown of membrane potential and up-regulation of genes involved in glycolysis, and other mitochondrial functions occurred during senescence of human MRC5 fibroblasts. These results provide supporting evidence that cellular senescence promotes mitochondrial dysfunction characterized by increased production of reactive oxygen species.[46]

1.2.6   Biomarkers of cellular senescence

There is no single marker that can specifically define cellular senescence. So, multiple validation markers are required to confirm senescent phenotype. In addition to stable cell

cycle arrest and the SASP, many other phenotypic alterations happen in senescent cells upon exposure to different stressors. For example, senescent cells display an enlarged and flattened morphology, develop lysosomal compartments, and undergo chromatin remodelling and epigenetic alteration compared to growing or non-senescent counterparts[47].

The stable growth arrest is one of the most defining features of senescent cells and it is characterised by cell cycle regulators including p53, p21, p16, and a decrease in phosphorylated pRB. These protein markers increased significantly in different strains of fibroblasts including WI38, IMR-90, MRC5 and NHDF once senescence was recognised and confirmed [48]. Activation of p53 and p16^{INK4a}/Rb tumour suppressor networks govern the senescence growth arrest. The activation of the p53/ p21 pathway was observed in replicative senescence [49], DNA damage response (DDR)-induced senescence, oxidative stress-induced senescence [50] and oncogene-induced senescence (OIS)[50]. In a study by Chen et alt al in 199[51], human fibroblasts (IMR-90) were treated with sublethal doses of H_2O_2 for 2 h and as a result, H2O2 at 150uM concertation induced senesce-like growth arrest in fibroblast. One day after removing treatment, the p53 and p21 levels increased considerably in growth-arrested cells and an average of 3.5-fold elevation in p53 was observed in treated cells after 20 -24 h removing H_2O_2.

Induction of p53 can induce a quiescent state (transient cell cycle arrest) and activate DNA repair processes in the presence of temporary stress and then cells can resume the cell cycle after the resolution of the stress. So, these protein markers RB and p53, are also present in other forms of cell cycle arrest, such as quiescence [22].

P16Ink4a/RB pathway is usually activated by persistent stress or further signals which contribute to a long-lasting and irreversible arrest. In addition, replicative senescence, ROS-induced senescence, and OIS can activate the p16Ink4a/RB pathway but this pathway is not activated during DDR-induced senescence. It has been suggested that induction of p21^{CIP1} participated in the onset of senescence and its expression is not necessarily preserved in senescent cells, whereas p16^{INK4a} plays a larger role to maintain the permanent growth arrest and senescent state[52]. In agreement with this, the upregulation of p21 was observed in IMR90 human fibroblasts which were serially passaged to reach their senescence state. P21 was only present in newly senescent cells and then disappeared while

36

these cells were stained negatively for p16. However, the level of p16 increased after IMR90 cells entered the senescence and remained elevated for at least 8 weeks [49]. Therefore, p16 can be used as an excellent biomarker for senescent cells as it exists in different regulated phases of senescence. It is recommended that multiple markers including p16, p21, p53 and pRB should be explored to get more decisive information on the senescent cell cycle arrest [49].

Cell cycle arrest can be also further assessed through assays that measure cell proliferation or DNA replication. To assess the DNA synthesis in replicating cells, labelling techniques including the incorporation of 5-ethynyl-2'-deoxyuridine (EdU) or BrdU into the DNA are carried out to measure the fraction of growing cells which entered the S phase. As senescent cells are characterised by the incapacity of DNA synthesis and loss of replicative ability, they display a reduction in the incorporation of the mentioned modified nucleotides. The number of unlabelled (senescent) cells or the incorporation of these nucleotides can be detected by immunocytochemistry assay or flow cytometry analysis. In addition, immunostaining of cell proliferation marker Ki67 which is highly expressed during all phases of the cell cycle except G_0 can be performed to distinguish senescent cells and growing cells[52].

In addition to the mentioned protein markers, senescent cells are characterised by flattened and enlarged appearance with irregular-shaped nuclei. A study by Schneider et al in 1976 [53]showed that the volume of human fetal lung fibroblast cells (WI-38) at early passage (19 CPD) increased from 1930±20 μm^3 to 2655±234 μm^3 in senescent cells (39CPD). Also, macromolecular contents including cellular RNA and protein contents were increased significantly (~110 and 80 % respectively) in senescent cells compared to young cells.[53] Consistent with this result, an age-related increase in mean cell mass was observed in human fibroblast cells (IMR-90) at the late passage number. The mean cell size at early passage (28) increased from 35.4 to 67.6 by passage 53[54]. So, senescent cells can be identified by their enlarged appearance. However, this marker cannot be used as a senescence marker for all cell types as T cells are exempted from the size alterations [55].

Apart from morphological changes in senescent cells, an irregular nuclear envelope and destabilisation of the nuclear integrity were identified in senescent cells as a result of reduced nuclear lamin B1. Lamin B1 (LB1) is a main structural protein of the nucleus which

37

covers the inner surface of the nuclear envelope and contributes to the size, shape, and stability of the nucleus [56]. The loss of lamin b1 has been detected as a senescence-associated biomarker in culture and in vivo when primary human fibroblasts lost their lamin b1 after undergoing senescence. Lamin B1 loss occurred when human fibroblasts (HCA2, WI-38, IMR-90, BJ strains were made replicative senescent by the repeated subculture, or they were senesced by exposure to 10-Gy ionizing radiation. LaminB2, protein levels declined markedly (>4-fold) in several fibroblast strains induced to senesce by different stimuli in response to direct stimulation of either the p53 or pRB pathways. Thus, downregulated levels of lamin B1 can be served as a general marker to identify senescent cells within culture or tissue samples [57].

An increase in cell volume and protein content in senescent cells is accompanied by an increase in nuclear size or irregularities and increased lysosomal content. Increased levels of SA-β-gal activity is one of the most used markers to detect senescent cells in culture or tissue samples. SA-β-Gal is an essential hydrolase enzyme catalysing the hydrolysis of B-galactosidase into monosaccharides under controlled PH conditions only in senescent cells. The SA-β-gal activity is measured by colourimetric assay and 5-bromo-4-chloro-3-indolyl-β-d--galactopyranoside (X-Gal) which is the substrate for SA-β-gal, is catalysed by SA-β-gal to produce an insoluble blue precipitate in senescent cells. Thus, this assay is considered a good technique to measure the increased expression and activity of these lysosomal enzymes or proteins in senescent cells[52].

It has been shown that the SA-β-gal activity is dependent on the age of tissues, and it is also related to the senescent phenotype and increased frequency in aged tissues. For example, Goberdhan and co-workers 1995 [58] showed that different human cells expressed a beta-galactosidase after senescence in culture. More than 50% of human fibroblast strains including HCA2 (neonatal foreskin) and WI-38 (fetal lung) were stained positively for lysosomal β-gal upon senescence in culture or late passage numbers (after 8-10 PD). At the same time, the cells were not labelled positively with [3H] thymidine. In addition, the SA-β-gal was only detectable in senescent cells, and it was absent in pre-senescent and quiescent fibroblasts and keratinocytes even 7 days after quiescence induction. They also reported the age-related increase in this marker in skin samples from human donors aged 20-90 years. Several SA-β-gal positive cells were observed in samples from old donors (aged>69) which

suggests the induction of SA-β-gal is associated with physiological age and it can serve as a biomarker of ageing [58].

It is important to note that the SA-β-gal is immediately not detectable after the onset of senescence and there is a significant delay in the detection of SA-β-gal and entry into senescence. For example, Cho et al showed that the expression of SA β-Gal activity requires a lag of a few days after the onset of senescence. Senescence-associated cellular changes including cell volume, cell cycle-regulated proteins (p21 and p53 levels), mitochondrial content, and SA β-Gal activity were measured in MCF-7 cells (human breast cancer line) after exposure to 0.25 µM Adriamycin for 4h. The level of p21 and p53 and the mitochondria content increased within the first 24 h upon treatment compared to non-treated cells. In contrast, the number of SA β-Gal positive cells increased in a sigmoidal curved fashion with a delay of 2 to 3 days and then was followed by a continuous increase (an 8-fold increase over baseline) 6 days after treatment, and then it reached the highest level (14-fold increase) at day 8 post-treatment. Thus, in contrast to the other markers, the β-galactosidase activity remained low until day 3 demonstrating that the expression of SA β-Gal activity needs an induction period after the entry of the cell into senescence [59].

Chromatin condensation with the formation of heterochromatic foci known as senescence-associated heterochromatin foci (SAHF) is a pivotal marker of senescence. SAHF are specialized domains of facultative heterochromatin which involve suppressing and silencing proliferation-promoting genes such as E2F-regulated genes in the senescent cell. These foci can be detected by fluorescent techniques using DAPI staining and immunofluorescence to localise SAHF components such as macroH2A, H3K9Me2/3, and HP1 proteins. These primary antibodies can be used to identify SAHF by immunofluorescence. Different senescence inducers cause the formation of SAHF, including activated oncogenes such as H-RASG12V and BRAFV600E [60, 61], telomere attrition [62], chemotherapeutics such as etoposide [62] and bacterial toxins [63]. Human primary fibroblasts (BJ and MRC-5) and keratinocytes formed SAHF in response to senescence induced by replicative senescence or premature senescence by etoposide, doxorubicin, hydroxyurea, and bacterial intoxication. So, the detection of SAHF can be regarded as a marker in the field of senescence to detect these distinct alterations in heterochromatin in senescent cells [63].

In summary, senescent cells can be identified and characterised based on their phenotypical features and expression of multiple biochemical markers. However, there is no single and specific marker to confirm senescence and all the mentioned markers are not present in all senescent cells. Therefore, to establish a senescent phenotype, it is important to evaluate different markers besides cell growth arrest. General biomarkers of cellular senescence and the detection techniques are listed in table 1.1.

Table 1.1 Biomarkers of cellular senescence and detection techniques (ICC: immunocytochemistry assay, IF: immunofluorescence, IHC: immunohistochemistry, WB: western blot) [47, 64, 65].

Hall mark of senescent cells	Marker	Expected change after senescence induction	Detection method
Lack of DNA synthesis	BrdU and EdU	↓	Staining incorporation (EdU and BrdU labelling kit), IF
Loss of proliferation	Ki67	↓	ICC/IF, IHC
p53-p21 activation	p53, p21	↑	ICC/IF, IHC, WB, PCR
p16-pRB activation	p16INK4a, pRB	↑	ICC/IF, IHC, WB, PCR
Morphology, cell volume	Cell size	Enlarged and flattened, Increase in volume	Light microscopy, flow cytometry
Increase in lysosomal content and activity	SA-β-galactosidase	↑	Enzymatic staining
DNA damage	ATM, ATR, γH2AX	↑	IF
SAHFs formation	DAPI/Hoechst 33342	↑	IF
Nuclear membrane	Lamin B1	↓	IF, WB, qPCR
SASP	IL-6, IL-8, CXCR2, IGF2	↑	ELISA, WB

1.3. Senescence in the liver

1.3.1 Structure of the liver

The liver is the largest internal organ, accounting for approximately 2% to 3% of average body weight and has two blood supplies one venous and one arterial. The portal vein which carries blood from the spleen, pancreas, and intestines contributes about 75% of blood volume to the liver. This blood is rich in nutrients and other absorbed molecules but is relatively poor in oxygen content. The hepatic artery, a branch of the celiac trunk from the abdominal aorta contributes approximately 25% of the blood volume entering the liver. This blood is nutrient poor but provides oxygenated blood to the liver. Blood from the portal veins and hepatic artery ultimately flows through liver sinusoids before draining into the systemic circulation via the hepatic venous system[66].

80% of the liver is made up of parenchymal cells called hepatocytes. These are the primary functional cell of the liver and line the tissue surrounding the liver sinusoidal capillaries draining into the central vein for a key role in metabolic functions. Their role includes bile formation, albumin synthesis, and the further metabolism of molecules transported by the blood to the liver [67]. Non-parenchymal cells of the liver include cholangiocytes (2–3 %), liver sinusoidal endothelial cells (2.5 %), Kupffer cells (2 %), and hepatic stellate cells (1.4 %). Kupffer cells are liver-specific macrophages that have close contact with stellate cells and hepatocytes. These cells are a source of pro-inflammatory cytokines and chemokines and play a key role in the inflammatory response, eliminating foreign pathogenic molecules by phagocytosis of bacteria, bacterial endotoxins, viruses, and endogenous or foreign proteins [67]. Hepatic stellate cells (HSCs) are pericytes located in the space of Disse in close contact with hepatocytes and sinusoidal endothelial cells. HSCs are in the quiescent state under normal conditions but are activated in response to extracellular signals from fibrotic stimuli such as hepatitis, inflammation, and liver damage. These activated cells secrete extracellular matrix (ECM) molecules including collagen fibres in response to injury to create scar tissue and a fibrotic environment in the space of Disse and protect the liver from further damage. However, persistent HSC activation can result in chronic fibrosis and cirrhosis[66].

41

1.3.2 Senescence in parenchymal liver cells

Cellular senescence has been associated with loss of regenerative capacity in chronic liver disease. Cellular senescence has been demonstrated in epithelial (hepatocytes and cholangiocytes) and non-epithelial liver cells (hepatic stellate cells and immune cells) leading to negative effects on cell viability and tissue repair under pathological conditions [68].

Hepatocytes have significant regenerative potential and can restore up to 80% of liver tissue loss after tissue necrosis caused by toxic substances or partial hepatectomy. Under normal conditions and in the absence of liver injury, very few hepatocytes are in the cell cycle. The majority are in a quiescence state known as the G0 phase [69]. Hepatocytes do not proliferate in this state but remain metabolically active. However, after a liver injury, for example following toxin exposure, viral infection or hepatectomy, hepatocytes exit quiescence (G0) and re-enter the cell cycle from the G0 state to the G1 phase to compensate for the loss of liver tissue. This can occur within seven to ten days. Further progression towards the G1/S cell cycle is dependent on growth factor stimulation to overcome the mitogen-dependent restriction point (RP) in mid-late G1. This restriction point is controlled by tumour suppressor retinoblastoma protein pRB to check if the cellular environment supports proliferation. In the absence of growth factor stimulation, normal adult hepatocytes return to the G0 state, in *vivo* condition [69].

A complex network of endocrine, paracrine, and autocrine signals, including hormones, growth factors (Hepatocyte growth factors HGF and epidermal growth factor EGF), cytokines (IL-6 and TNF-α) and bile acid are involved in hepatocyte cell cycling. Once hepatocytes pass the G_1 restriction point (R point), they do not require growth factors to transit into the S phase and they can proliferate irreversibly. From this point onwards, the cell cycle is progressed to M-phase autonomously, driven by the activation of a series of structurally related serine/threonine protein kinases and cyclin-dependent kinases (CDK) to proliferate and restore liver mass. Once the liver mass is adjusted pre-hepatectomy size, hepatocyte cell proliferation is terminated under the control of a suppressor of hepatocyte proliferation such as transforming growth factor-beta (TGF-*β*) and activin A as well as extracellular matrix-driven signals (figure 1.4)[70, 71].
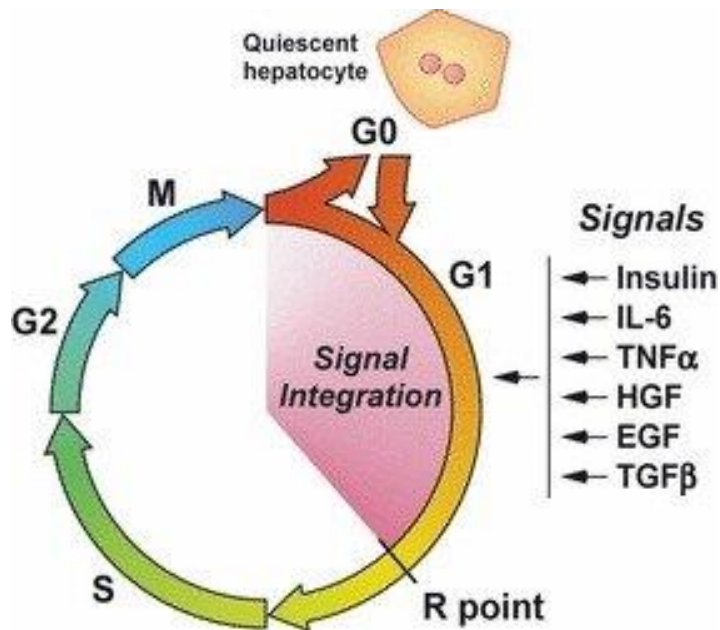
Figure 1.4. **Hepatocytes cell cycle during liver regeneration**. The regenerative process in the liver is initiated upon liver injury or tissue loss. Then, quiescent hepatocytes exit the G0 state and enter the G1 phase of the cell cycle to proliferate and restore the lost liver mass. Multiple signals are integrated with the G1 phase to orchestrate the regenerative process and induce hepatocyte proliferation within the liver [71].

A study by Koniaris and et al in 2003 [72] showed that hepatocyte proliferation was stimulated after 2/3 surgical removal of the liver lobes in a normal mouse model and resulted in a gradual liver mass restoration. After 70% partial hepatectomy, hepatocytes were the first cells to exit the resting state G0, enter the G1 phase of the cell cycle, and then traverse to the S phase for DNA synthesis. The first peak of DNA synthesis was observed in hepatocytes at 24h after hepatectomy and approximately 50 % of cells were labelled positive with 3H-thymidine, while non-parenchymal cells initiated DNA synthesis at 40 h after hepatectomy. The data also showed that the mass of the liver remnant increased to constitute 45% and 70% of the original liver weight 24 and 72 hours after the hepatectomy and also liver mass reached its original weight pre-operation 2 weeks after partial hepatectomy. Thus, the liver exhibits a high regenerative capacity which is accomplished by the ability of hepatocytes to re-enter the cell cycle and divide to replace the damaged tissue [72].

43

It is well-established that hepatocyte proliferation can replace damaged tissue following mild damage or after induction of liver regeneration. However, this is not the case when the degree of injury to the liver is severe or chronic. Hepatocytes cannot undergo cell division indefinitely in the presence of persistent damage during chronic and severe liver disease. Chronic liver diseases happen gradually and damage the liver over years. During chronic liver injury and activation of processes leading to liver cirrhosis, human hepatocytes are frequently stimulated to proliferate due to continual persistent waves of liver destruction and regeneration. These result in critical telomere shortening and replicative senescence [73, 74]. In a study by Dewhurst et al in 2020 [74], the relation between hepatocellular telomere length and the number of senescent hepatocytes was evaluated in liver samples at mild and severe fibrosis stages to see whether the limitation of hepatocyte regeneration is triggered by telomere shortening in cirrhotic livers. Telomere shortening and replicative senescence were specifically found in hepatocytes in the cirrhotic liver. Telomere length was measured in 76 cirrhosis samples induced by different chronic liver diseases including viral hepatitis, toxic liver damage (alcoholism), autoimmunity, and cholestasis and telomere length was compared to non-cirrhotic samples. The results showed that the mean telomere restriction fragments (TRFs) were significantly shorter in cirrhotic livers than with non-cirrhotic samples (P<0.0001). The TRF length range was 5.7–9.5kb and 7.5–11.5 kb in cirrhotic and non-cirrhotic samples, respectively. In addition, 41 of 49 cirrhosis samples (84%) were stained positive with β-Gal-positive cells, while only 1 of 15 control samples (7%) was positively labelled with β-Gal. The data showed that telomere length was significantly shorter in samples with severe fibrosis than in samples with milder fibrosis (P<0.0001), at telomere shortening, is accelerated following continuous liver damage and concomitant regeneration in chronic liver diseases and induced replicative senescence specifically in hepatocytes leading to termination of liver regeneration (figure 1.5)[74].
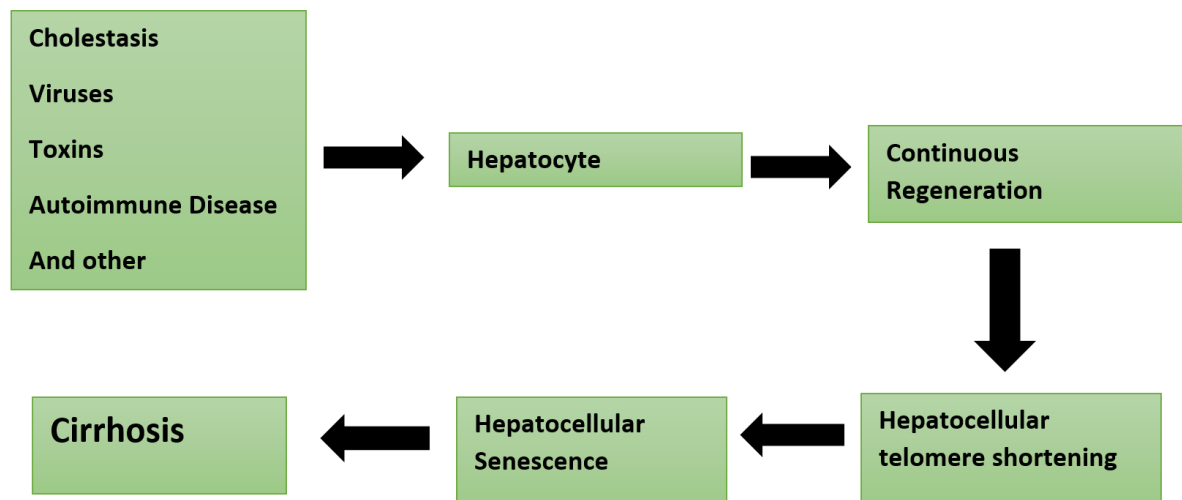
Figure 1.5. **The telomere hypothesis of cirrhosis**. In chronic liver disease, continuous liver damage and concomitant regeneration accelerate telomere shortening, specifically in hepatocytes finally culminating in senescence and cessation of regeneration. Continuous liver damage at this point triggers the activation of stellate cells and fibrotic scarring [74].

In addition to severe liver damage, ageing is the other factor that can cause an increase in the number of senescent hepatocytes. An increase in the number of senescent hepatocytes was reported in a study by Wang et al in 2014 [75] when they measured the biomarkers of senescence in normal mouse liver over 18 months of age. Hepatocyte senescence was characterised by loss of proliferation capacity, increased expression of SA-β-gal activity, accumulation of γ-H2A.X-positive hepatocytes, and increased levels of cell cycle inhibitors such as p21 and p16. Percentages of SA-β-gal-positive and γ-H2AX-positive hepatocytes increased from $1.37 \pm 0.64\%$ and $1.73 \pm 0.23\%$, respectively in 2-month-old mice to $40 \pm 4.6\%$ and $42.67 \pm 3.51\%$ at 18 months of age. Also, the protein levels of p21 and p16 increased significantly in 18-month-old mice compared to 2-month-old mice ($p<0.05$). Evidence that the proportion of senescent hepatocytes in the liver of mice increases with age has also been replicated in human studies. Enlarged human hepatocytes were observed in healthy liver tissue from 55- to 65-year-old individuals compared to younger adults from 21 to 30 years old. Also, approximately 69 and 72 % of old human liver sections were stained positively with SA-β-gal and γ-H2A.X, respectively, whilst only $8.2 \pm 1.87\%$ and

45

8.6 ± 1.61% of liver tissues were stained positively with SA-β-gal and γ-H2A.X, respectively in younger adults [75]. Thus, both continuous proliferative stimulus to the liver as a result of disease, injury or ageing causes an increased population of senescent hepatocytes with a subsequent impact on regenerative potential.

1.3.3 Senescence in non-parenchymal liver cells

Senescence in non-parenchymal liver cells may also occur because of ageing and chronic inflammation associated with tissue damage. The existence of cholangiocyte senescence in several biliary diseases including primary sclerosing cholangitis (PSC), primary biliary cirrhosis (PBC), and biliary atresia (BA) has been described [76-78]. In a study by Tabibian et alt al in 2014 [76], the pro-inflammatory activity of cholangiocytes and markers of cellular senescence were measured in the livers of patients with PSC, PBC, hepatitis C, and in healthy individuals to investigate whether cholangiocytes in the PSC liver display the features of cellular senescence and SASP. This study reported that cholangiocytes in the PSC liver showed the biomarkers of cellular senescence including increased expression of cell cycle inhibitor (p16^{INK4a}), histone γH2AX foci, and decreased level of cell proliferation markers. *In vivo*, the level of p16^{INK4a} mRNA expression was significantly higher in PSC cholangiocytes compared to PBC (3.1-fold, P<0.01), HCV, and normal liver tissue samples (both >20-fold, P < 0.01). Also, the percentage of γH2A.x foci-positive cholangiocytes were significantly greater compared to the other 3 conditions (P < 0.01). Cholangiocytes in the PSC liver were negative for cell proliferation marker Ki-67, consistent with senescence. In addition, four known SASP components including IL-6, IL-8, CCL2, and PAI-1 were significantly expressed in PSC cholangiocytes compared to PBC, HCV, and normal liver (p < 0.01). A cholangiocytes co-culture model was developed in the same study to assess whether senescent human cholangiocytes can induce senescence in bystander cholangiocytes as a result of their secretory activity. They demonstrated that bystander cholangiocytes had significantly increased expression of SA-β-gal when exposed to senescent cholangiocytes directly treated with H_2O_2 or LPS over 10 days (p<0.05). In summary, the findings of this study demonstrated that cholangiocytes in PSC displayed features and markers which were consistent with the senescence phenotype. Increased expression of SASP proteins by senescent cholangiocytes also supported the concept that

46

these cells can contribute to the progressive inflammation and hepatobiliary injury seen in PSC [76].

Liver progenitor cells (LPCs) are defined as a stem cell population within the liver that express markers for both hepatocytes and cholangiocytes including α-fetoprotein (AFP), cytokeratin 19 (CK19), and epithelial cell adhesion molecule (EpCAM). These cells are activated and differentiate into hepatocytes and cholangiocytes during extensive liver injury to regenerate the liver tissue. However, it has been reported that LPCs lose their proliferative capacity during ageing. A study by Cheng et al in 2017 [79] showed that LPCs in old mice lost their activation and proliferation upon liver injury as a result of excessive ROS and chemokine production by activated hepatic stellate cells during ageing. LPC activation and proliferation were measured in young (2 months old) and old mice (24 old months) fed with a choline-deficient, ethionine-supplemented (CDE) diet to induce liver damage. The expression of LPC-related markers, such as EpCam, CD133, and AFP was only increased in the livers of young mice (P < 0.05) after the CDE diet. Old mice had significantly lower numbers of proliferative markers including Ki67 and cyclin E1 after the CDE diet feeding (P < 0.05), suggesting that the activation and proliferation of LPCs in old-DDC mice were decreased compared to that of young mice. In addition, a significant increase in neutrophil infiltration, together with high levels of MDA (a marker of oxidative stress and hepatic lipid peroxidation) were observed in the livers of old mice compared to young mice (p<0.01). The study also showed that the expression of chemokines such as CXCL1 and CXCL7 from hepatic stellate cells was responsible for the migration of neutrophils in mice. The mRNA levels of CXCL1 and CXCL7 were upregulated in the livers of old mice compared to young mice. CXCL7 was particularly upregulated indicating that CXCL7 production from hepatic stellate cells could be a key factor inducing neutrophil infiltration leading to the negative regulation of LPC response in older mice. A significant number of H2AX positive LPC cells in old mice confirmed DNA damage in LPCs, suggesting that neutrophils inhibited LPC activation and proliferation through oxidative stress and induction of senescence in LPCs in old mice as a result of chemokine production from activated hepatic stellate cells during ageing, leading to impairment in liver regeneration [79]. These findings indicate that decreased LPC activation and proliferation impairs liver regeneration during ageing as a result of induction of senescence in LPCs.

1.4. Senescence and liver disease

1.4.1 Liver disease

Liver failure happens when liver function is diminished to the point where vital metabolic, synthesis and detoxification functions are critically diminished. During liver failure, progressive deterioration of hepatocyte function results in the accumulation of lethal toxins and un-metabolised substances in the blood and body tissues. Hepatotoxic compounds gradually saturate the detoxification functions of the liver causing further tissue damage via hepatocellular apoptosis or necrosis [80]**.**

Accumulation of liver toxins in the systemic circulation of patients with liver failure is one of the reasons which can cause further functional damage leading to life-threatening complications. These include hepatic encephalopathy (HE), coagulopathy, jaundice, cholestasis, and sepsis. The mortality rate associated with severe liver failure is substantial. More than 500 million people suffer from chronic liver disease globally and it causes 2% of all deaths. Liver transplantation is the only definitive cure. However, an increasing number of patients each year may die whilst waiting for a suitable donor organ to become available[1]. In the United States, more than 20% of patients with end-stage liver disease are on the waiting list to receive a transplant and the number of patients waiting for a liver transplant is much higher than the number of available organ donor (figure 1.6).). Apart from the scarcity of organ donors, surgical risk and the requirement for life-long immune suppression are the limitations associated with liver transplantation.

The growing organ shortage
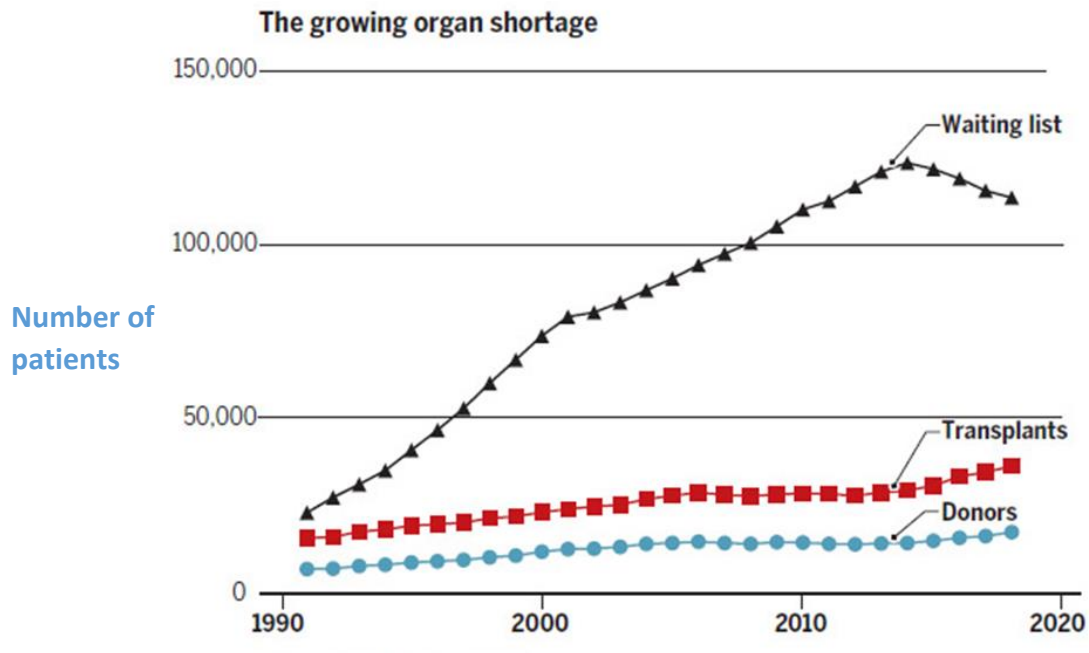
Figure 1.6. The gap between the number of patients waiting for liver transplantation and the number of donors in the United States from the years 1990 to 2020 [81].

The spectrum of liver injury is wide, depending on the cause, but all result in the onset of liver fibrosis first and eventually cirrhosis if not successfully treated. Liver fibrosis develops as a consequence of both inflammatory and non-inflammatory damage. In case of death of small group of hepatocytes and preservation of reticulin framework, the liver can regenerate without any scar formation. However, more excessive damage with the destruction of hepatocytes and collapse of reticulin fibres will initiate fibrosis. Hepatic stellate cells (HSCs) play a key role in the development of liver fibrosis. These cells can transform into myofibroblasts and produce collagen and an abnormal quantity of ECM components which leads to the formation of pericellular and perisinusoidal fibrosis around individual hepatocytes. This process led to the obliteration of fenestration in liver sinusoids and deterioration of nutrients exchange between sinusoidal lumen and hepatocytes. As a result, the fibrosis aggregates and becomes more compact [82].

In the presence of long-term or chronic state of liver cells or hepatocytes destruction and inflammation, the liver can become seriously scarred and damaged to the point where it is no longer reversible. This process is called cirrhosis. Because it is usually irreversible,

49

cirrhosis is often referred to as "end stage" or "late stage" liver damage. This process can lead to disruption of liver architecture due to the fibrotic tissue deposition at the extracellular matrix and formation of widespread nodules and vascular reorganisation which block the blood supply and nutrient exchange between sinusoid and hepatocytes which cause hepatocyte damage or death. The main clinical outcomes of cirrhosis are impaired liver function, jaundice, fluid accumulation in the abdomen (ascites), portal hypertension and development of hepatocellular carcinoma (HCC)[83].

The primary causes of liver injury and the onset of liver fibrosis and then cirrhosis are excessive alcohol consumption, obesity and viral hepatitis and are described in the following sections.

1.4.2 ALD and NAFLD

Alcohol-related liver disease (ALD) happens as a consequence of excessive alcohol consumption (more than 14 units of alcohol per week). A direct relationship exists between the quantity of alcohol consumed and ALD risk. According to the WHO, ALD accounted for 3.3 million deaths in 2012 and approximately 7,700 people in the UK die each year due to this disease [84]. Heavy alcohol consumption can lead to three stages of damage. Fatty liver or steatosis is the earliest response to high alcohol consumption, and it is characterised by fat accumulation within hepatocytes. Fatty liver may cause no damage and it can be reversed by stopping or reducing drinking. However, steatosis can progress to steatohepatitis leading to liver inflammation and then to fibrosis Hepatic fibrosis initially begins with active pericellular fibrosis which may develop into cirrhosis. Liver cirrhosis is characterised by excessive liver scarring, vascular and architectural alterations, which may result in liver cancer and/or liver failure [84].

Non-alcoholic fatty liver disease (NAFLD) represents a spectrum of liver disorders which is characterised by macro vesicular steatosis in more than 5% of hepatocytes in the absence of alcohol overconsumption. Approximately 20 to 30% of patients with NAFLD develop non-alcoholic steatohepatitis (NASH) which is a more progressive and severe form of NAFLD and is defined by liver inflammation, and hepatocellular ballooning and eventually progress to fibrosis, cirrhosis, and hepatocellular carcinoma. The prevalence of NAFLD is about 25% in

the general population and it is expected to be the most common cause of cirrhosis and liver transplant over the next decades. Metabolic syndrome, type 2 diabetes (T2D), obesity and dyslipidaemia are the common risk factors for NAFLD. The mechanisms leading to NAFLD are not fully understood. The two-hit model is the most widely supported theory to explain NAFLD pathogenesis. In this model, the first hit is defined by hepatic triglyceride accumulation or steatosis which exposes the liver to injury mediated by 'second hits', such as inflammatory cytokines, mitochondrial dysfunction, and oxidative injury. This in turn leads to steatohepatitis and/or fibrosis which can directly cause toxicity by increasing oxidative stress and by activation of inflammatory pathways (figure 1.7) [85, 86].

There are few treatments available for patients with NAFLD. Current treatments primarily concentrate on lifestyle changes to improve the metabolic parameters which contribute to disease progression including a healthy diet, weight loss when needed, and regular exercise. In addition to lifestyle modification, some clinical trial data suggested that antioxidants such as vitamin C and E, and pioglitazone (anti-diabetic medication to treat type 2 diabetes) may be beneficial in non-diabetic NASH patients. However, these treatments have not yet shown substantial evidence of benefit. Liver transplantation remains the only definitive treatment option for end-stage cirrhosis[85].
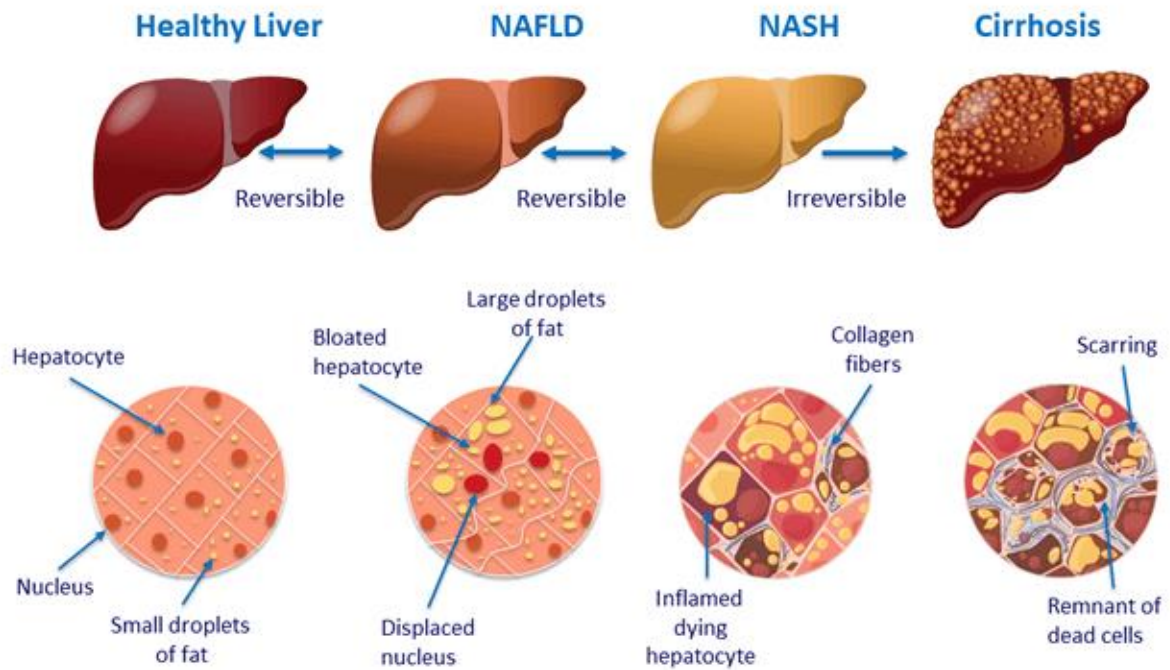
Figure 1.7. NAFLD is divided into two types; simple fatty liver or NAFLD, in which fat droplets are formed within hepatocytes (steatosis) and some of them become large enough to cause hepatocytes to swell up with fat and push the nuclei to the edge of the cell. After enough excess fat has accumulated in the liver, chronic inflammation, and hepatocytes death result in the process of steatosis and inflammation which is referred to as steatohepatitis in the absence of alcohol. This process is called non-alcoholic steatohepatitis (NASH). Chronic and continuous hepatocyte damage and death can lead to the formation of fibrosis. Eventually, excessive scar formation will result in loss of liver function a state known as cirrhosis [87].

1.4.3   ALF AND ACLF

Acute liver failure (ALF), also known as fulminant hepatic failure, is a rare and critical condition with a high mortality rate ranging from 40 to 90%. It can rapidly progress to multi-organ failure and death. This disease is characterised by a rapid loss in hepatocyte function followed by jaundice, encephalopathy, coagulopathy, cerebral edema, renal failure, and infection in mostly young patients without pre-existing liver disease. ALF affects approximately 2000 patients annually in the United States and accounts for about 7% of liver transplants annually. The major cause of ALF in developing countries is acute viral

infections from hepatitis A, B, and E. However, many ALF cases in Europe and the United States are mostly due to drug-induced liver injury or paracetamol-induced hepatotoxicity[88]. N-acetylcysteine (NAC) is an effective treatment for paracetamol-induced hepatotoxicity and also can be beneficial to treat non-paracetamol-induced ALF which may improve survival in patients with low-grade encephalopathy. Specific antiviral therapy including ganciclovir is required if a viral case is identified. Patients with ALF usually require admission to the intensive care unit (ICU) and receive medical therapy to control encephalopathy and cerebral edema. These treatments include intracranial pressure monitoring, hyperventilation, hypothermia, ammonia lowering strategies and administration of antibiotics to prevent and treat infections. However, there is no treatment for the overall ALF condition other than transplant [89].

Acute liver deterioration in patients with chronic liver disease or prior decompensation of cirrhosis is called acute-on-chronic liver failure (ACLF) which results in irreversible liver failure. The concept of ACLF was first used in 1995 to describe a condition in which two types of injuries happen in the liver simultaneously, one chronic and the other acute. Different definitions have been introduced by several expert groups including the American Association for the Study of Liver Diseases (AASLD), European Association for the Study of the Liver (EASL), and Asian-Pacific Association for the Study of the Liver (APASL). The definition suggested by the AASLD and EASL groups is: "acute deterioration of pre-existing chronic liver disease usually related to a precipitating event and associated with increased mortality at 3 months due to multi-system organ failure". In contrast, experts from APASL introduced another definition for this disease "acute liver injury manifesting as jaundice (serum bilirubin ≥5 mg/dL) and coagulopathy (INR ≥1.5 or prothrombin activity of <40%), complicated within 4 weeks by ascites and/or encephalopathy in a patient previously diagnosed or undiagnosed chronic liver disease"[90]. So, in general, ACLF is a syndrome that can develop in patients with previously diagnosed or without chronic liver diseases including cirrhosis and it is characterised by acute hepatic decompensation which leads to liver failure (jaundice) and multi-organ failure[90]. The trigger of ACLF is not identifiable in 40 to 50% of patients with ACLF. Active alcoholism, chronic viral hepatitis, and bacterial infections are the most reported triggers of underlying chronic liver disease in ACLF. Systemic inflammation caused by infection, or an acute hepatic injury plays a key role in this disease development.

53

Rapid deterioration of liver function and rapidly evolving multi-organ failure is associated with increased mortality within a period of 28 days and up to three months from onset. Currently, there is no specific treatment available for patients with ACLF except for liver transplantation and therefore, management of ACLF is mainly based on general supportive treatment, prevention, and treatment of complications, and supportive therapy of organ failures in the ICU setting. In general, it is particularly challenging to treat patients with ACLF because the precipitating event is unknown in most cases. es. s. Patients with ACLF require rapid evaluation for liver transplantation (figure 1.8) [90, 91].
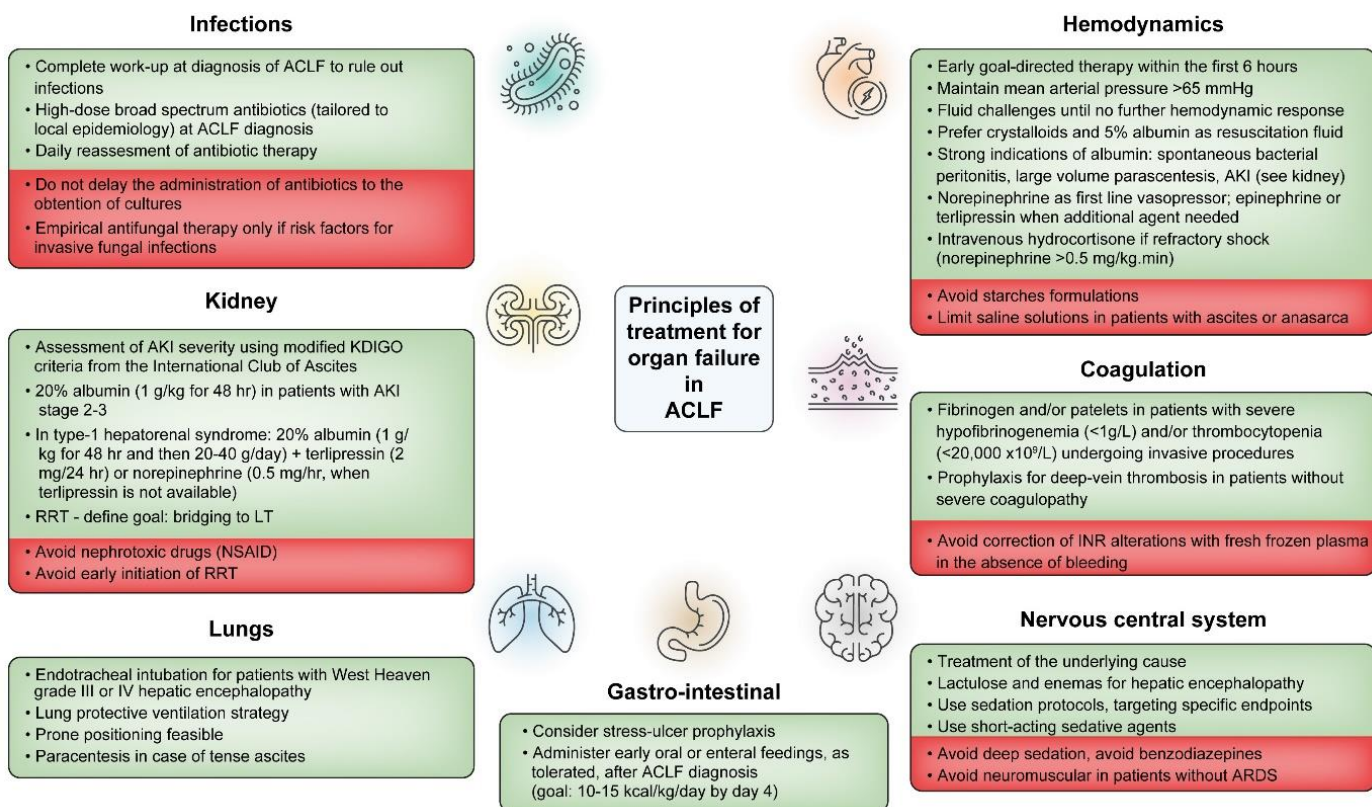
Figure 1.8. Principles of treatment of organ failure in ACLF[90].

1.4.4. The role of senescence in chronic liver disease

An increase in the proportion of senescent hepatocytes and their accumulation has been demonstrated in diverse chronic liver diseases [5, 6, 92, 93]. Further, these studies reported that hepatocyte senescence is closely associated with increased fibrosis stage, impaired hepatic function, and an adverse outcome in chronic liver disease. A study by Aravinthan et al. in 2012 [5] demonstrated the relationship between cellular senescence and adverse

clinical outcome in NAFLD. Cellular senescence biomarkers including telomere length, cell cycle phase markers, and nuclear area were assessed in the liver sections of 70 patients with NAFLD and 60 control samples. The results showed that hepatocyte telomere length was lower in patients with NAFLD compared with controls which were independent of age in either group (553 vs. 1053, p <0.0001). The biomarkers of cellular senescence including p21 and γ-H2AX protein expressions were increased significantly in hepatocytes in NAFLD compared with the normal liver (p = 0.001 and p = 0.01 respectively). In addition, hepatocyte p21 expression (56% vs. 22.6%, p <0.0001) and hepatocyte nuclear area (p = 0.006) were significantly higher in patients with diabetes mellitus and those with worsening fibrosis stage than in patients without diabetes mellitus and improved fibrosis stage. This association was independent of age and sex of patients demonstrating that hepatocyte p21 expression correlated with fibrosis stage and diabetes mellitus. During the 67-month follow-up period, patients with a higher number of p21 positive hepatocytes and larger nuclear area were linked to adverse liver-related outcomes, such as hepatocellular carcinoma, liver transplant, or liver-related death. In summary, the results of this study showed that the proportion of senescent hepatocytes increased in the liver biopsies taken from patients with NAFLD and also that there was a positive association between senescent cell accumulation, fibrosis stage and disease progression [5].

Hepatocyte senescence may be linked to liver dysfunction in chronic liver disease through a change in hepatocellular function following induction of senescence and a subsequent decline in liver function. A study by Aravinthan in 2013 [6] showed hepatocyte senescence is associated with alterations in gene expression, impaired hepatic function, and adverse liver-related outcomes. In this study, induction of senescence in HepG2 cells was performed through oxidative stress with 0.5 mM H_2O_2 in a culture medium for 1 hour, and the gene expression of control and treated HepG2 cells were compared with patients with liver cirrhosis who underwent liver transplantation. Gene expression of major cell cycle inhibitors including p53, p21, and p16 was up-regulated significantly in H_2O_2 - treated HepG2 cells compared to untreated cells and over 90% of H_2O_2 -treated cells stained positively for p21 and SA-β-gal. Also, IL-8 gene expression was up-regulated in treated cells compared to control cells. IL-8 secretion in the medium was increased from 500 pg/ml to about 1400 pg/ml in H_2O_2 -treated HepG2 cells. So, cellular senescence was confirmed in H_2O_2-treated

HepG2 cells which showed the combination of the presence of SA-β-gal, cell cycle arrest along with elevated levels of IL-8 in conditioned media. Senescent cells showed that 354 genes had significant differential expression (p <0.01) compared to control cells. Among 354 genes, 266 genes associated with cell cycle inhibitors including p21, p15, TGFβ1, TP53INP1, PLK2, and SFN were up-regulated. While 88 genes which are involved in cell cycle progression including CDK1 and Cyclin B2 were downregulated in senescent cells. Those genes which were up-regulated in HepG2 senescence were also up-regulated in liver cirrhosis samples. 406 genes including P16, P21, and P53 (known to be involved in cellular senescence) and SASP genes (IL-8, IL-6) were upregulated in liver tissue from patients with cirrhosis compared to the normal liver [6]. Thus, these results confirmed the senescence-related gene expression in human liver tissue from patients with cirrhosis and the expression of potent cell cycle inhibitors such as p16, p21 and p53 confirmed cell cycle arrest and senescence of hepatocytes in chronic liver disease. This study also showed significant alterations in synthetic functions of senescent hepatocytes. Hepatocyte synthetic function including levels of α-fetoprotein (15000 to 2000 KC/L), fibrinogen (from 120 ng/ml to less than 50 ng/ml) and retinal binding protein productions (400 to 100 ug/ml) were significantly reduced in the conditioned media of senescent HepG2 cells compared to the control cells. These observations suggest that senescent HepG2 cells have impaired synthetic function in *vitro* explaining a close relation between hepatocyte senescence and manifestations of chronic liver disease including impaired synthetic function. In conclusion, an association between hepatocyte senescence and manifestations of chronic liver disease at the level of gene expression was demonstrated. Further, a potential relation between hepatocyte senescence and liver dysfunction and adverse liver-related outcome seen in chronic liver disease was shown in this study [6].

It was found that the presence of alcohol-related liver disease (ALD) and cirrhosis was significantly correlated with increased numbers of senescent hepatocytes. The result of immunohistochemical staining showed that hepatocyte cyclin A (S phase) and PH3 expression (M phase) were lower in patients with ALD cirrhosis compared to the regenerative liver (p<0.001) and p21 was highly expressed in hepatocytes in ALD compared to the regenerative liver (33.6% vs 5.6%, p<0.0001). The proportion of hepatocytes that expressed p21 increased significantly in patients with advanced fibrosis stages (p<0.01). 80%

of hepatocytes were stained positively with p21 at fibrosis stage 4 while 20% of hepatocytes were stained with p21 at fibrosis stage 1. Also, hepatocyte p21 expression correlated positively with prothrombin time (p=0.0003) and an inverse correlation with serum albumin (p=0.03) in patients with ALD cirrhosis. These results indicate a strong correlation between increased p21 expression and increased fibrosis stage and liver dysfunction in ALD cirrhosis and that hepatocyte senescence plays a key role in ALD [92].

Senescent hepatocytes may contribute to the pathogenesis of chronic liver disease by adopting a feature of secretory phenotype known as SASP in which the production of inflammatory cytokines, chemokines, and proteases is upregulated and can modify the tissue microenvironment. To study the pathogenic effects of senescence in chronic liver disease, a *vitro* model of oxidative stress-induced senescence in the human hepatocyte cell line was designed and senescence was induced in HepG2 by exposure to 300 µmol/L H_2O_2 for 48 hours. An increase in secretory activity of hepatocytes was observed after induction of senescence. Senescent hepatocytes produced a high level of proteins which likely contribute to hepatocyte SASP compared to the control cells on a per cell basis (mean 4.6-fold increase per cell, *P* = 0.06). Gene expression of *SAA4*, *ECADH*, *IL32,* and *IL8* (typical SASP component) was significantly increased in senescent hepatocytes 8 days after treatment (P<0.05). Also, senescent hepatocytes enhanced chemokines production including CCL20 (known as liver activation regulated chemokine), CXCL16, and fibrinogen. A significant increase in migration of inflammatory human macrophages in the senescent hepatocyte-conditioned medium was observed compared to control (P = 0.022) which can cause pro-inflammatory microenvironment and pathogenesis in chronic liver disease. As a result, senescent cells can develop fibrogenesis and the pathogenesis of chronic liver disease through the recruitment of inflammatory cells, especially macrophages [93].

1.4.5   The possible pathway of cellular senescence in liver fibrosis and cirrhosis

Despite the convincing evidence for senescence of hepatocytes and cholangiocytes, the mechanisms that drive the evolution of senescence in chronic liver disease remain controversial. Replicative senescence has been considered the basis for hepatocyte

senescence in chronic liver diseases and is also linked to progressive fibrosis and the development of cirrhosis. Replicative exhaustion is usually caused by telomere attrition from repeated cell division during the long-term process of cell death and regeneration in hepatitis C virus (HCV)-related chronic liver injury. Based on the finding of the study by Sekoguchi ad et al in 2007 [94], telomere shortening was specifically observed in hepatocytes, not other cell types during the development of chronic liver injury stages and subjects that were positive with HCV had shorter hepatic telomeres than healthy controls (p<0.001). Hepatocytes with shorter telomere length showed the morphological signs of cellular senescence including the increase in both DNA content and nuclear size and the relative telomere intensity reduced with increasing nuclear size. In addition, the relation between telomere length and degree of fibrosis was assessed in patients with chronic viral hepatitis and data showed that relative telomere intensity was significantly decreased in HCV-positive patients with severe fibrosis than in patients with no or mild fibrosis (p<0.0001). This data indicates that telomere shortening is closely associated with hepatic fibrosis. Serum ALT and Ki-67 levels are considered a marker of regenerative proliferation, these two markers were measured in this study to see whether telomere shortening progresses more rapidly in tissues with active cell turnover. The telomere length in patients with high serum ALT (>100IU/L) was significantly shorter than in patients with ALT lower than 100 IU/L (P value=0.0018) and patients with high Ki-67-PI (higher than 3%) had lower relative telomere intensity than the patients with low Ki-67-PI (<3%) (p<0.001). Therefore, telomere shortening was accelerated in tissues with active cell-cycle turnover because of frequent cell divisions in tissue from HCV-positive patients. Based on this observation, this study suggested that the gradual and progressive telomere shortening is the primary reason for cellular senescence in HCV-related hepatitis which is happened following elevated cell-cycle turn-over or continuous cell division[94].

In the same study, markers associated with oxidative stress such as hepatic 8-OHdG expression, hepatic iron loading, and serum ferritin levels were also measured to study the relation between ROS levels and telomere shortening in tissues of HCV-related chronic liver injury. The results of this study demonstrated that 8-OHdG-positive hepatocytes had significantly shorter telomeres than 8-OHdG-negative hepatocytes, in particular at the severe fibrosis stage (p<0.05). Also, relative telomere intensities were significantly lower in

patients with high serum ferritin levels (>250 ng/ml) and patients with iron loading than in control patients (p= 0.01). These results demonstrated that a higher level of ROS was associated with shortened telomeres and this trend was more evident at the severe and late fibrosis stage supporting the hypothesis that oxidative stress plays a key role to accelerate premature senescence, especially in the advanced stage of fibrosis [94]. In summary, this study showed that replicative senescence is the primary mechanism for hepatocyte cellular senescence in HCV-related hepatitis which is happened following the gradual and progressive telomere shortening in cells with elevated cell-cycle turn-over. However, in addition to the cell-cycle-dependent telomere shortening or replicative senescence, telomeres can be damaged and shortened by oxidative stress independent of the number of cell replications. In other words, replicative senescence can be induced prematurely before telomeres become critically short [94].

A study by Moustakas et al in 2021 [95] reported that hepatic senescence occurred in NAFLD independent of age and that it may be linked to stress-induced senescence. Hepatic senescence was measured in two models of diet-induced NAFLD in non-aged mice including a high-fat diet (HFD) caused obesity in mice and a non-obese NAFLD model. Mice were fed a high-fat, choline-deficient, low-methionine diet (HFD-CD) and compared with control mice having a normal diet (ND). SASP-related genes including monocyte chemoattractant protein-1 (MCP-1), matrix metalloproteinase 3 (MMP3), and Plasminogen activator inhibitor-1 (PAI-1), TNF-α, and IL-6 were upregulated in both HFD, and HFD-CD mice compared to the ND control. Senescence was confirmed in both models by increased expression of p16, p21, and p53 genes. Only the increased expression of p16 in HDF and p16 and p53 in HFD-CD reached significance compared to the control group (p<0.05). Also, the result of immunohistochemistry showed that the majority of cells in the liver were stained positively with GL13 in both models compared to normal diet-fed ones (statistically was not significant). The findings of this study also showed that the induction of senescence in NAFLD was not associated with replicative or premature replicative senescence because the telomere length and the percentage of global DNA methylation were not changed in both NAFLD models compared to control, while the levels of malondialdehyde (MDA), as an indicator of oxidative stress were upregulated significantly in both treated groups (p < 0.05). Therefore, the results of this study suggest that hepatic senescence can happen

independently of age and also senescence can increase the risk of NAFLD emergence, even in non-aged organisms. NAFLD-related senescence happened as a result of stress-induced, rather than telomere-dependent or replicative senescence. Telomere length did not change in this model and telomere shortening was not involved in NAFLD development in non-aged models [95].

Using genetically engineered mouse models, a study by Ferreira-Gonzalez et al in 2018 [96]discovered that senescent cholangiocytes induce profound alterations in the cellular and signalling microenvironment, TGFβ production, and induction of senescence in surrounding cholangiocytes and hepatocytes via the secretion of paracrine factors. Cellular senescence was initially confirmed by increased expression of p21, p16 ($p < 0.01$), and γH2A.X ($p < 0.001$) in cholangiocytes and hepatocytes of primary sclerosing cholangitis (PSC)/ primary biliary cirrhosis (PBC) human biopsies compared to control samples. This provided evidence that cellular senescence is an essential feature of PSC/PBC. Then, a mouse model of biliary disease based on the conditional deletion of Mdm2 in bile ducts under the control of the Krt19 cholangiocytes promoter was developed to study the mechanisms of biliary senescence in the liver. In this model, deletion of Mdm2 which is a key negative regulator of p53, resulted in p53 and p21 protein expressions in cholangiocytes and further cell cycle arrest indicated via negative Ki67 staining. The induction of cellular senescence in cholangiocytes was also confirmed by the expression of other markers including 53BP1, γH2A.X, and DCR2. In addition, while p53 expression was only limited to cholangiocytes, p21-positive and HNF4α-positive hepatocytes were detected in this model. These senescent hepatocytes also expressed other markers of senescence including 53BP1, γH2A.X and DCR2 while maintaining Mdm2 expression suggesting that the senescence induced in hepatocytes is probably p53-independent and was triggered by paracrine activity from the cholangiocytes. Also, p27 which is usually activated by transforming growth factor β (TGFβ), was highly expressed in both cholangiocytes and hepatocytes ($p<0.01$). To confirm whether cholangiocytes induce senescence in a paracrine manner in surrounding hepatocytes, the most notable components of the SASP were measured in bile ducts from induced mice. The results showed that the mRNAs encoding SASP proteins had a significantly increased expression of TGFβ1 ($p = 0.0007$) and TGFβ2 ($p = 0.0047$) in bile ducts. Increased expressions of other SASP factors such as NF-κB ($p = 0.0132$) and IL1-α

(p = 0.0160) were also observed in bile ducts from treated mice. Activation of the SASP in bile ducts and production of TGFβ by cholangiocytes caused a reduction in total liver proliferation (less than 1% Ki67 positive cells) and increased number of p21 and p27 positive-hepatocytes (p<0.01) supporting the hypothesis that senescence spreads from cholangiocytes to the surrounding cells via the secretion of paracrine factors and it is TGFβ-dependent [96].

In summary, cellular senescence can have either beneficial or detrimental effects on the liver. However, this opposing role of senescence in the liver depends on the liver cell type and the pathological state of the liver. For example, the process of cellular senescence in HSCs is beneficial for the liver as these cells play a key role in maintaining tissue homeostasis and fibrosis resolution. HSCs involve in the fibrosis process and wound healing as they transdifferentiate from quiescent to activated HSCs in response to inflammatory and injury signals produced by damaged hepatocytes and biliary cells. These cells are responsible for the deposition of ECM and secrete collagen and tissue inhibitors of metalloproteinases (TIMP) to fill the wound in the liver tissue. Upon completion of fibrotic response, activated HSCs are removed by apoptosis or undergo replicative senescence to be later removed by immune cells. In the absence of tumour suppressor proteins such as p53 and p16 and cellular senescence, HSCs become continuously activated and continue to ECM deposition resulting in excessive liver fibrosis and cirrhosis. The clearing of HSCs is an important part of fibrosis resolution[97].

In contrast, in cirrhotic conditions, cellular senescence in parenchymal cells including hepatocytes is detrimental and has a significant role in the progression of chronic liver disease towards cirrhosis and HCC. This detrimental effect of hepatocytes is mainly associated with procarcinogenic effects through their secretory activity. The secretion of proinflammatory cytokines and chemokines by senescent hepatocytes can cause the induction of senescence in the neighbouring cells and affect the proliferation of surrounding parenchymal or non-parenchymal and stem cells[97]. Telomere shortening following repeated cell proliferation has been determined as the main reason for hepatocyte senescence in chronic liver disease. However, the results of some studies placed more emphasis on stress-induced hepatocyte senescence [98, 99]. Some studies have shown that telomeric and non-telomeric DNA damage happens through common cellular stressors such

61

as oxidative stress and that this may cause telomere-dependant and telomere-independent cellular injury ([figure 1.9](#)). In conclusion, stress-induced and replicative senescence are both responsible for cellular senescence in the parenchymal (hepatocytes) and nonparenchymal compartments.
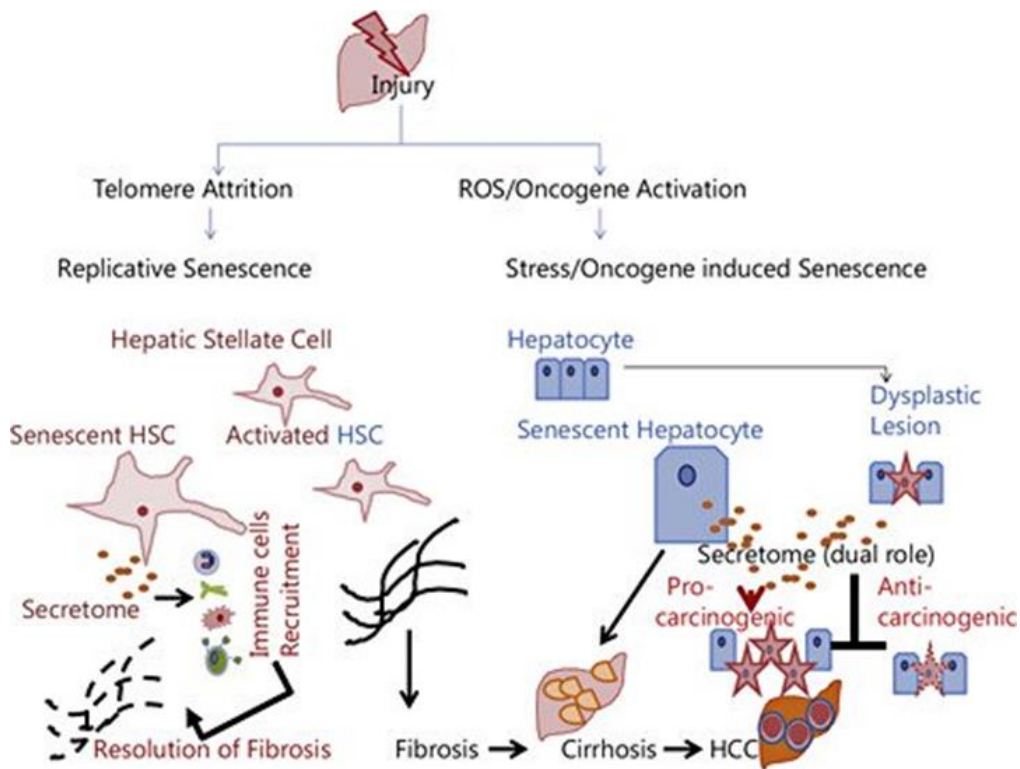
Figure 1.9. Both replicative senescence and stress-induced, or premature senescence appears to be involved in cellular senescence chronic liver disease. Induction of SASP inactivated HSCs is beneficial for ECM degradation and clearing of activated HSCs from the site of liver injury and fibrosis resolution. The secretory activity of senescent hepatocytes may have an anticarcinogenic effect by blocking the proliferation of injured liver cells in the early stage of liver diseases. However, in the later stage of disease progression, senescent hepatocytes secrete elevated levels of proinflammatory cytokines and chemokines such as CCL2 and TGFβ which can act as a procarcinogen and develop the conversion of non-senescent cells to senescent cells in a paracrine manner leading to fibrosis progression and cirrhosis[97].

1.4.6 Liver toxins and senescence

Hepatocyte function is compromised during acute liver failure or chronic liver disease, which progresses leading to toxin accumulation and the presence of un-metabolised substances in patient blood circulation. Components of plasma from patients with acute liver failure (ALF) with evidence of cytotoxic effects include ammonia, lactate, bile acids, bilirubin, bacterial lipopolysaccharide, and cytokines IL-6, TNF-αand IL-1β[100-102]. Evidence indicates that senescence plays a role in the development of liver disease, causing alterations in hepatocyte metabolic and synthetic functions. However, the role of liver toxins in the plasma of patients with advanced liver disease on the induction of hepatocyte senescence is poorly understood.

Bile acids are endogenous compounds that may be increased up to 100 times the normal concentration in patients with chronic liver disease and it is believed that they have a key role in liver injury by inducing apoptosis or necrosis of hepatocytes[103]. The role of bile acids in the induction of senescence is unknown. However, there is some indication that bile acids can promote permanent cell cycle arrest and impaired hepatic function. These compounds can promote ROS generation through impairment of respiration and electron transport in hepatic mitochondria and cause mitochondrial dysfunction, thereby inducing oxidative damage and hepatocyte senescence. It has been shown that bile acids can potentially affect the replicative process by inhibiting DNA synthesis. Modification of DNA synthesis has been observed in rat hepatocytes in primary culture after 6 hours of treatment with bile acids in unconjugated and tauroconjugated form including cholic acid (CA) and ursodeoxycholic acid (UDCA) at 10 to 1000 μM concentrations. The unconjugated form of bile acid reduced hepatocyte viability significantly at 1000μM concentration (P<0.05). However, treatment with tauroconjugated forms such as CA and UDCA did not affect cell viability at 10 to 500μM concentrations. Thus, unconjugated bile acids induced a significant, concentration-dependent toxic effect in comparison to the conjugated form [104]. This concentration (1000 μM) is even higher than the level of bile acids in liver diseases which is about 13 μM [105]. Thymidine incorporation into DNA was significantly reduced after treatment with a 200μM tauroconjugated form of bile acids (P<0.05). While treatment of hepatocytes with tauroconjugated form at 200μM concentration had no significant effect on cell viability. So, hepatocytes remained viable after treatment with

conjugated form bile acids, but they could not proliferate due to a lack of DNA synthesis. These results suggest that reduced hepatocyte proliferation following bile acid treatment is not dependent on a decrease in hepatocyte viability. It indicates that bile acid may inhibit DNA synthesis and proliferation by inducing senescence in certain cell types. [104]. In summary, bile acid accumulation in patients with liver disease can negatively affect liver regeneration through inhibition of DNA synthesis and induction of permanent cell growth arrest (senescence) in hepatocytes.

Unconjugated bilirubin (UCB), an endogenous metabolite of heme oxidation, can have cytotoxic properties at high concentrations and induce apoptosis in cells. The physiological concentration of bilirubin is about 0.01–10μM [106]. An elevated concentration of bilirubin can generate oxidative stress and induce cell toxicity by induction of DNA damage. A study using a mouse model of neonatal hyper bilirubinemia (12μM) in *vivo* showed that the level of phosphorylated histone (γH2AX), which is a specific molecular marker for monitoring DNA damage, increased significantly in the cerebellum of hyper bilirubinemic mice (P<0.01). This result showed that bilirubin caused damage to DNA during severe neonatal hyperbilirubinemia suggesting that neurotoxicity in *vivo* can be associated with bilirubin-induced DNA damage. Bilirubin at a high concentration (>20μM) can cause DNA damage in the cerebellum due to oxidative stress which results in severe neurological damage and death. Incubation of SH-SY5Y cells with 140 nM free bilirubin concentration (equivalent to 30μM unconjugated bilirubin) for 48 hours resulted in a significant increase in *γ*H2AX signals confirming bilirubin-induced DNA damage in cultured cells as observed in *vivo* (*P* < 0 01). Further, an increase in intracellular ROS levels was reported upon bilirubin exposure leading to DNA damage and decreased cell survival. In summary, bilirubin at high concentrations can cause irreversible neurological damage and death by induction of oxidative stress and subsequently DNA damage which is caused by elevated ROS levels [107].

Bilirubin can also affect tumour cell lines and immortalised cell line growth by inducing cell cycle inhibitors. Different tumour cell lines including HRT‑18 (colon cancer), PANC‑1 (pancreatic cancer), HepG2 (hepatocellular cancer), MKN45 (gastric cancer) and NIH/3T3 were treated with bilirubin at 5, 25, 125 μM concentrations for 48 hours. A significant reduction in proliferation even at the lowest dose (5 μM) was observed in HepG2 and

64

NIH/3T3 cells (P <0.05). In other cell lines, proliferation was significantly inhibited at 25 and 125 µM doses (P<0.001). Tumour cell line HRT‑18 was arrested at the G0/G1 phase of the cell cycle after 24 hours of treatment at a concentration of 25µM. These results indicated that there were fewer cells in G2 after bilirubin treatment compared to non-treated cells (P< 0.05). A sustained increase in p53 and p27 expression was also seen after bilirubin treatment (25µM) at the 24 to 36-hour time points. Consistent with these results, Rb phosphorylation was suppressed in the presence of bilirubin after 24 and 36 hours. Rb was hypophosphorylated, which results in the inability of the cells to pass the restriction point in late G1 and thus prevents them from entering the S phase. Bilirubin inhibited tumour cell line proliferation in *vitro* via induction of tumour suppressor proteins including p53, p27 and hypophosphorylation of the Rb. Evidence suggests that the cell growth inhibitory effect of bilirubin occurs because of interruption of the cell cycle and induction of senescence [108].

1.5   Liver replacement strategies and senescence

1.5.1   Liver support devices

Liver transplant remains the only treatment for liver failure despite decades of research into alternative strategies to address the shortage of transplantable organs and potentially bridge patients to transplantation or temporarily support native liver function allowing it to recover. Extracorporeal liver support systems have been developed to help remove toxins and metabolites from the patient's blood through non-biological hemofiltration as a bridge treatment before liver transplantation[3]. However, extracorporeal support systems cannot replicate liver function effectively including synthetic and regulative functions and currently there is no evidence of significantly improved survival rates in patients with liver failure after treatment with liver assist devices[3].

In early development, most liver support devices were only able to remove selected hepatic toxins from the patient's blood. It was thought that the removal of toxins from the patient's plasma would enhance the clinical state of the patient. Initial detoxification devices used absorbents (charcoal and resin) for absorption of these molecules and dialysis to remove a limited amount of water-soluble toxins from whole blood or plasma[109]. However, further studies showed that the clinical features of hepatic failure were associated with more

complex biochemical abnormalities [110]. Substances including small molecular weight toxins, mediators of inflammation, endotoxins, and cell growth inhibitors accumulate in the blood and cause neurological disorders, prevent hepatocyte function, and inhibit liver regeneration. Many of these toxins are protein-bound toxins that cannot be removed by traditional liver support devices. The list of main toxins which are processed by the liver is shown in table 1.2. Therefore, new liver assist devices developed based on the concept of blood purification and these devices focus on removing all substances accumulating in the patient's blood during liver failure[111]. Artificial liver support devices and bio artificial liver support devices, incorporating a cell component, are two major groups of liver support devices.

Table 1.2. List of liver toxins [112].

Toxin	Examples
Small water-soluble molecules	Ammonia, creatinine, phenylalanine, tyrosine
Albumin-bound molecules	Bile acids, bilirubin, metabolites of aromatic amino acids, tryptophan, Indoxyl sulphate, fatty acids, heavy metals

Artificial liver support devices are non-cell-based devices that have been developed to remove toxins and metabolites from a patient's blood through blood detoxification. In the early developments, artificial systems using the principles of haemodialysis or hemofiltration combined absorption and filtration processes for the removal of a limited amount of water-soluble toxins including ammonia. More efficient artificial detoxification systems were developed to control and eliminate albumin-bound toxins by the addition of albumin to the dialysate and the use of large-pore filters [113, 114]. Molecular Adsorbent Recirculating System (MARS), the Single-Pass Albumin Dialysis system and the Fractionated Plasma Separation and Adsorption system (Prometheus) are the most known artificial liver devices.

MARS, an extracorporeal liver support device was developed by Gambro in 1993 to treat patients with acute liver failure. This system consists of two circuits: the blood circuit and the secondary circuit containing albumin with a charcoal column, an anion exchange resin column, and a dialysate circuit. In the blood circuit, the patient's blood passes through the high flux dialysis filter with a membrane molecular weight cut off of 50 kDa. A second circuit containing 600 ml of 20% albumin acts as the dialysate in the secondary MARS circuit. Albumin-bound toxins from the patient's plasma can cross the membrane and bind to the albumin within the MARS circuit. In this system, water-soluble toxins are subsequently removed via a low-flux dialyser connected to the secondary circuit and the regenerated albumin is ready to accept new toxins from the patient blood circuit when passing the membrane again [115, 116].

MARS, like other artificial support systems, has some advantages and disadvantages. The MARS device effectively removed free bilirubin and bilirubin bound to albumin. For example, a significant decrease in albumin-bound substances including bilirubin (18%) and bile acids (44%) was observed in 15 patients after 6 h treatment. However, a significant reduction in platelets (15.4%) and prolongation of coagulation tests (-21%) were documented during extracorporeal therapy [117]. In another study, 24 patients with severe liver failure and multiple organ dysfunction syndromes (MODS) were treated with MARS for 6-24 h. A marked reduction of bilirubin and bile acids (54.8% and 22.5% respectively) together with significant removal of cytokines including g TNF-alpha, IL-6, IL-8, and INF-gamma was reported in this study after MARS treatment (p<0.01) [118]. In contrast, another study showed no effects on cytokine removal after a total of 269 MARS treatments in 64 patients with acute-on-chronic liver failure (ACLF)[119] These studies showed that the MARS system was effective in short-term removal of the albumin-bound substances, however, it does not show a significant effect on survival. Long set-up times (6-10 hours), hypoglycaemia, coagulopathy, bleeding, and sepsis is other reported issues associated with the MARS system [113].

Prometheus system is based on fractioned plasma separation, adsorption, and haemodialysis. Dialysis and adsorption in this system can remove albumin-bound and water-soluble toxins like other extracorporeal liver support systems. In this system, the patient's plasma which contains albumin flows through a membrane with a molecular weight cutoff

close to 300KDa, and plasma is perfused through two columns containing various adsorbents where protein-bound toxins are cleared. The purified albumin is re-infused into the blood circuit and then blood passes through a high flux filter to eliminate water-soluble toxins. Both MARS and Prometheus systems have been effective and beneficial to eliminate albumin-bound substances such as bilirubin or bile acids. However, the Prometheus system provides maximum water-soluble toxin clearance compared to MARS because of the presence of a flux dialyser in the blood circuit which improves more water-soluble toxin detoxification [120]. 12 patients with acute or acute-on-chronic liver insufficiency were treated with the Prometheus system. A significant reduction was observed in the circulating levels of soluble interleukin (IL) 2 receptor ($p < 0.001$), total bilirubin, and ammonia ($p<0.05$). The total survival rate was 41.6% after 30 days [120].

Single pass albumin dialysis (SPAD) is a simple and easy method for blood purification because this system only requires standard dialysis equipment and has a similar proposed function to that of the MARS device. However, in SPAD, the albumin solution is added rather than recycled [113]. A study by Sponholz et al in 2016 6 [121] showed that MARS and SPAD were equally efficient to reduce plasma bilirubin levels in 32 patients. Bilirubin levels were reduced to -68 µmol/L and -59 µmol/L after treatment with MARS and SPAD, respectively. However, other paraclinical parameters include serum bile acid (39 µmol/L), albumin-binding capacity (+10%), creatinine (24 µmol/L) and urea levels (0.9 mmol/L) were affected by only MARS. Neither MARS nor SPAD effectively removed cytokines in this study [121]. Artificial liver support treatments are limited in efficacy and provide no long-term survival benefit in large multi-centre randomised clinical trial data [115]. All mentioned artificial systems focus on detoxification, but to support the failing liver function some return of the synthetic and metabolic function of the liver is required [122].

Bioartificial livers (BALS) have been developed to overcome the limitations associated with non-biological devices and to replace the metabolic activities of the liver as a bridge to transplant or organ recovery after liver decompensation. Bioreactors containing porcine or human hepatocytes are used in bioartificial livers to provide biotransformation and synthetic liver function [122]. Patient blood or plasma is filtered through a device containing hepatocyte cells which acts as an artificial liver to replace failing liver function. Biologic liver support systems combine the synthetic and regulatory function of the liver cells with the

detoxification of patient plasma [122]. Several types of bioartificial systems have been developed which are different in their cell-housing mechanisms containing hollow fibre-based, multilayer membrane-based, scaffold-based, and perfused bed design systems. Among these housing mechanisms, hollow fibre-based BAL systems have been the most extensively tested in clinical trials [123].

Extracorporeal liver assist device (ELAD) is the only BAL device utilizing human hepatoblastoma cell lines (C3A). The ELAD system has four hollow fibre cartridges filled with 100g of C3A cells which have reduced tumorigenic potential with high production of albumin and alpha-fetoprotein. The hepatocytes are housed in the extra capillary space of a hollow fibre open membrane with a molecular weight cut-off of 70 kDa preventing the passage of hepatocytes and separating cells from immunoglobin and leukocytes to avoid immune rejection. Small particles such as synthesised proteins and protein-bound toxins can cross the barrier between plasma and hepatocytes. The patient's blood is initially separated into plasma, and then plasma is passed through a charcoal unit and an oxygenator unit before entering the bioreactor. In the first pilot controlled clinical trial, 24 patients with acute liver failure were randomly allocated to ELAD hemoperfusion or standard therapy group (control). Hemodynamic stability was maintained in both groups. The overall survival rate for the patients treated with ELAD was 78% (7 out of 9 patients) and in the control group was 75% (6 out of 8 patients). No evidence of significant improvement in survival rate was reported[124]. After this study, a modified ELAD with a higher membrane cut-off (120 kDa) and four cartridges with 100 g of C3A in each were used to treat patients with fulminant hepatic failure. 5 patients were treated with this device, and they all successfully bridged to transplantation and 80% of patients (4 of 5) survived the 30-day endpoint[125]. The latest controlled randomised clinical trial was performed on 203 patients with severe alcoholic hepatitis 96 patients were treated with ELAD, and 107 patients received standard of care treatment only (SOC) for 3 to 5 days continuously. There was no difference in overall survival between ELAD and SOC groups (51% vs 49.5%). The death rate was reported at 47.9 % for the ELAD-treated group and 47.7% for patients who received SOC treatment only. The study failed to evidence the beneficial effect of ELAD on survival rate in patients with end-stage liver disease [126].

The HepatAssist BAL device was developed by Demetriou et al in 1986[127]. The patient's plasma is perfused through a bioreactor which is in a hollow fibre configuration containing $5-7 \times 10^9$ cryopreserved porcine hepatocytes on the external part of the membrane. The patient's plasma is firstly separated and then passed over a charcoal absorber for detoxification before entering the bioreactor unit. After that, treated plasma and the blood cells are reconstituted and returned to the patient. In a phase, I multicentre clinical study, 39 patients with ALF were treated with the HepatAssist device and 32 patients were bridged to liver transplantation (LT) successfully and 6 patients recovered without LT. The survival rate was 90% after one month of treatment. A randomised, multicentre controlled trial was then performed in 171 patients with fulminant and subfulminant hepatic failure which demonstrated the safe use of this device. However, no significant difference in survival rate between the BAL group and the control group treated with SOC was observed (71% vs 62%) (p=0.26)[128].

The modular extracorporeal liver support (MELS) device consists of different extracorporeal therapy units including the cell module, detox module and dialysis module. The cell module in this system is a multicompartment bioreactor loaded with primary human liver cells obtained from discarded liver and it is also composed of three polyether-sulphone (PES) hollow fibre membranes with a 400 kDa cut-off organised in a 3D network to separate plasma and hepatocytes. A detox module is a detoxification unit which enables albumin dialysis for removing albumin-bound toxins [129]. In phase I uncontrolled clinical trial study, eight patients were treated with MELS. Bioreactors were loaded with 1.8 to 4.4×10^{10} of porcine primary hepatocytes to treat ALF patients throughout 8 to 46 hours of treatment. 91 to 98% of the cells remained viable during the treatment and no complications were reported. All patients were bridged safely to transplantation with a 100% survival rate after at least 3 years.

MELS and AMC-BAL (AcademischMedisch Centrum Bioartificial liver) systems have similar cell performance, but porcine cells have direct contact with the patient's plasma in the AMC-BAL system to allow optimal mass transfer and direct oxygenation of hepatocytes. Four different porcine hepatocyte-based BAL systems including BLSS, MELS, AMC-BAL and TECABALSS/HBAL were tested in phase I and II clinical trials for treating patients with ALF [127, 130]. Many clinical data in these systems were associated with neurological state

improvement with minimal reduction of serum bilirubin and arterial ammonia [130, 131]. However, adverse effects such as bleeding complications, hemodynamic instability [130] and thrombocytopenia [132] have been noted in these studies. A major concern in using porcine hepatocyte-based devices is the danger of immunological responses and risk of zoonotic infections coupled with the current lack of efficacy in human trials. At present, trials related to AMC-BAL have been stopped because of physiological cross-species incompatibilies of porcine hepatocytes with human tissues and other logistical problems associated with the use of porcine cells in this system [127]. Lack of ammonia and total bilirubin elimination were also concerns associated with the mentioned devices and these devices have yet to show substantial data demonstrating patient survival benefits (figure 1.10) [4].

In summary, bioartificial liver support devices could potentially either bridge patients to transplantation or temporarily support native liver function allowing it to recover. However, there are some limiting aspects related to BALs that need to be considered to produce a fully functional and clinically effective device. These include a lack of an ideal cell source and sustained hepatocyte function over the required treatment period in these systems. The loss of viability and functionality of hepatocytes during treatment is currently problematic.
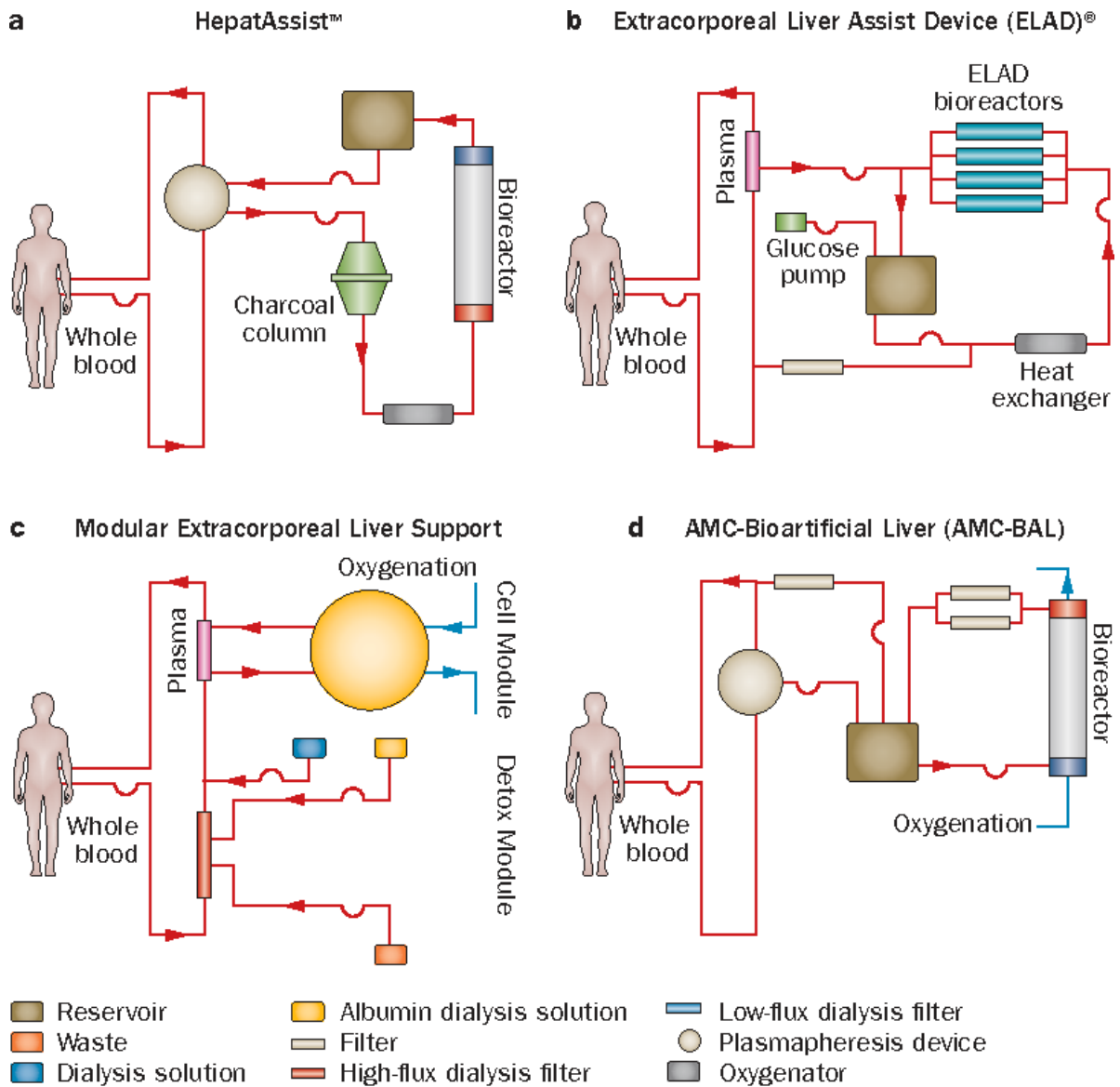
Figure 1.10. Bioartificial liver support devices. (a) HepatAssist™ system, (b)Extracopropeal Liver Assist Device (ELAD), (c) Modular Extracorporeal Liver Support (MELS), (d) Academic Medical Center Bioartificial Liver (AMC-BAL)[133].

1.5.2 The application of immortalised cell lines in BAL

Cell type plays a key role in bioartificial liver treatment, and the efficacy of BAL devices relies on the bioactivity of cells in a bioreactor. Diverse liver cell sources include primary human cells, primary porcine hepatocytes, human hepatoblastoma and tumour-derived cell lines (C3A). These cells have been used in the bioartificial liver as a biological component to perform synthetic functions including metabolic, detoxification and biliary excretion and

regulatory function [115]. Human primary hepatocytes which can be isolated from the human liver are ideal for BAL systems. The utilisation of primary hepatocytes in the BAL system resulted in no or low immunological responses. However, it is complex to source primary human liver cells and isolates enough cells with the sustained functional capacity to provide a feasible BAL system [115]. Low availability and poor proliferation capacity of human primary hepatocytes limited their application in the clinic. Also, a significant loss of viability and low capacity for attachment to matrices are two fundamental issues associated with cryopreserved human hepatocyte cells. Xenogeneic cells are more easily available than primary human cells, but the risk of infection and metabolic compatibility exists with these cells. Primary porcine hepatocytes are commonly used in AMC-BAL and HepatAssist systems for preclinical and clinical evaluation. Although porcine hepatocytes are easily available, the risk of immunogenicity and infection may limit the clinical application of these cells in BAL systems [134, 135].

To overcome the limitations associated with primary human and porcine hepatocytes, alternative cell sources of proliferating cells such as liver-tumour-derived cell lines, immortalised hepatocytes or liver stem cells have been developed. This development addressed minimal immunogenicity, no risk of Xeno-zoonosis, and improved cell proliferation [135].

Several hepatic cell lines are available which are directly derived from liver tumour tissue or from primary hepatocytes *in vitro.* The application of tumour-derived cell lines including HepG2 in the BAL system is considered an alternative treatment for primary cells. HepG2 is a hepatoblastoma-derived cell line isolated in 1975 from a 15-year-old male with hepatocellular carcinoma. Cells have an unlimited life span, high availability and epithelial-like morphology. It should be noted that HepG2 cells have been selected due to their albumin-synthesising capacity, but the ammonia detoxification capacity, urea production and drug metabolic functions are poor because they lack urea cycle enzymes and have a limited number of mitochondria [136]. C3A cell lines, a clonal derivative of HepG2, which have reduced tumorigenic potential with high production of albumin and alpha-fetoprotein were used in the ELAD device in non-controlled clinical trials. For example, in a study by Yang et al [129], C3A cells were co-cultured with human placental mesenchymal stem cells to better resemble the complicated environment of the liver and maintain hepatic functions

73

in *vitro* in a three-dimensional fluidized bioreactor. The albumin synthesis and CYP1A2 activity were significantly increased after treatment. However, urea synthesis was not improved in this study. Therefore, the application of HepG2/C3A cells in BAL devices has been limited because of insufficient functionality. In addition, a detachment of C3A cells from the ELAD system and the risk of metastatic spreading following their escape from the system to the bloodstream has been considered a theoretical concern [135].

Immortalised hepatocytes have been developed to overcome the limitations associated with primary human and porcine hepatocytes and liver-tumour-derived cell lines. Immortalised human hepatocytes are usually derived from healthy primary hepatocytes using a defined immortalisation strategy. Immortalisation strategies have been applied in human hepatocytes to generate hepatocyte cell lines with extended replicative capacity, maintaining detoxification function and protein expression at the same level as that in primary human hepatocytes[137] [138]. There are different methods for immortalisation of primary hepatocyte cells in culture conditions, but the most frequently used methods are overexpression of viral oncogenes, expression of human telomerase reverse transcriptase (hTERT), or a combination of both [139]. The expression of viral oncogenes including adenoviral E1A/E1B genes, the simian virus 40 large T antigen (SV40 Tag) and the human papillomavirus 16 (HPV16) E6/E7 genes have been used to establish hepatocyte-derived cell lines (Table1). Immortalisation by viral genes was achieved by inactivation of the tumour suppressor genes (p16/pRB and p53) that induce a replicative senescent state in cells. Reactivation of telomerase through the expression of telomerase reverse transcriptase protein (TERT) is another approach for immortalisation to overcome telomere-dependent senescence [139]. Immortalisation techniques allow cells to proliferate by overcoming the predicted number of divisions known as the Hayflick limit and senescence. However, chromosomal abnormalities, phenotypic changes and tumorgenicity associated with immortalisation techniques have remained controversial issues [140]. Characteristics of the available immortalised hepatic cell lines for bioartificial liver system application are shown in table 1.3.

Table 1.3. Characteristics of immortalised hepatic cell lines

Cell line	Immortalisation strategy	Functionality	Ref
HHL(−5/−7/−16)	Adult hepatocytes Retroviral vector HPV16 E6/E7	• Contained markers of hepatocyte and biliary phenotype (CK7/8/18/19). • Expressed CYP450 protein at levels comparable to Huh-7 and HepG2 cells. • Produced ALB, though at lower levels than Huh-7 and HepG2 cells. • Stained negative for AFP and did not display elevated nuclear expression of p53 protein. • Possessed active gap junctions. • Respond to INF-α stimulation by upregulation of major histocompatibility complex I and II • Exhibited, in contrast to the Huh-7 and HepG2 cells, increased capacity to bind recombinant hepatitis C virus-like particles.	[141, 142]
cBAL111	Fetal hepatocytes Lentiviral vector hTERT	• Expressed high mRNA levels of immature markers, GST-Π and AFP, and very low mRNA levels of mature markers, ALB, A1AT and TF. Transcript levels of HNF4 α increased after prolonged culturing. • Stained positive for GS, ALB, CK18, CK19, vimentin and the progenitor cell marker CD146 but displayed CK18 in a pattern characteristic of dedifferentiated human hepatocytes • Produced urea and ALB, though at lower levels than mature human hepatocytes. • Possessed the ability to differentiate into functional hepatocytes once transplanted in *vivo*, without the occurrence of tumour formation	[143]
HepLL	Adult hepatocytes Lipid-mediated gene transfer (lipofectamine reagent) SV40 Tag	• Displayed morphologic characteristics of liver parenchymal cells. • Expressed HNF4, HBCF-X, GST-n and ALB mRNA as well as ALB and CYP2E1 protein but no ASGP mRNA. • Stained positive for human hepatocyte special antigen but negative for AFP.	[144]

76		• Secreted ALB and urea at levels not significantly different from primary cultured human hepatocytes. • Synthesized glycogen. • They were not tumorigenic after transplantation into SCID mice. • Possessed a good potential for regeneration and active metabolic function in recipient organs	
C3A	clonal derivative of Hep G2	• High albumin production, high production of alpha-fetoprotein (AFP) and ability to grow in glucose deficient medium. • The C3A cells confirmed their ability to produce urea and ammonia, and also to some extent to remove an overdose of ammonia loaded in the supernatant.	[145]
		• The ammonia detoxification capacity of C3A is poor rendering its limited application in BAL and there has been no further clinical research in the last few years	
NHBL2	derived from well-differentiated hepatocellular carcinoma tissues	• possessed the capacity of synthesizing albumin and CYP2E1 and quantitative analysis showed that the albumin synthesis ability of NHBL2 was comparable to C3A while urea production was highly abundant in NHBL2 compared with that of C3A • Albumin, CK18 and CYP2E1 were extensively expressed in NHBL2 • Expressed AFP, genes related to bioconversion and metabolism (CYP3A4, CYP3A5, GST-α, CPS-1) • urea production in supernatant from NHBL2 cells was significantly higher compared with that from C3A cells • positively expressed CK18 indicating the epithelial tissues origin of this cell line	[137]
HepLi5	Established via transfection of Simian virus 40 large T antigen (SV40 LT) into primary human hepatocytes	• Subcutaneous injection of HepLi5 cells into nude mice did not induce tumours within 3 months. • Expressed human blood coagulation factor x (HBCF-x), glutamine synthetase (GS), glutathione S-transferase (GST), and albumin mRNA. It also expressed human CYP450 mRNA including CYP-3A5, CYP-2E1, CYP-2C8-19, and CYP3A4 • Albumin secretion and urea production in HepLi5 cells significantly increased at 20 days after large-scale culture (16.6 and 36.2 % respectively)	[138]

1.5.3 Liver cell lines and senescence

The development of hepatic cell lines *in vitro* has achieved significant attention for fundamental and applied research and screening purposes. Applied cells in BAL and hepatocyte transplantation must maintain their performance after exposure to the patient's plasma, especially in BAL devices where hepatocytes have direct contact with plasma [146]. However, plasma from both healthy donors and acute liver failure (ALF) patients is known to induce intracellular lipid accumulation and a decrease in hepatic functionality of primary hepatocytes and hepatic cell lines in BALs [147, 148]. For instance, Hepa-RG cells, a valuable biocomponent of a BAL, were negatively affected by exposure to both ALF-rat plasma and healthy plasma. Plasma was derived from healthy rats and ALF rats and then HepaRG cells cultured in a monolayer were exposed to the plasmas for 16 h. The ALF plasma contained increased levels of ammonia (1.24mM), total bilirubin (>15μM), aspartate aminotransferase (AST >6000 u/L) and lactate dehydrogenase (LDH >3000U/L). Exposure to both plasmas elevated cell leakage (2.5-fold), the formation of lipid droplets and decreased transcript levels of various hepatic genes including CPS (encoding the first enzyme of the urea cycle), GS and CYP3A4 (max 40-fold) (57). Urea cycle activity and ammonia elimination decreased markedly after exposure to ALF plasma ($p < 0.05$). Therefore, HepaRG cell functions were adversely affected by both ALF and healthy plasma [148].

The effect of porcine ALF plasma and healthy human plasma on hepatic differentiation and functionality of HepaRG cells was also studied to investigate whether plasma induces toxicity against these cells. HepaRG cells were cultured in monolayers and laboratory-scale BALs after 16h exposure to both plasmas. Plasma-induced damage occurred and was associated with rapid activation of NF-κB target genes. Sixteen hours of exposure to healthy human plasma did not affect cell viability. However, hepatic gene-transcript levels decreased significantly ($p < 0.05$) and dose-dependently within four hours of exposure to both plasmas. In addition, upregulation of pro-inflammatory genes including CCL20, EGR1, IL-6, and IL-8 happened after a one-hour exposure to human plasma which was associated with upregulation of the pro-inflammatory NF-κB signalling pathway. Hepatic gene transcript levels including *CYP3A4*, hepatic nuclear factor 4 Alpha (*HNF4A*) and arginase 1 (*ARG1*) were decreased by 17±2%, 7±2% and 5±2% respectively for four hours of exposure to human plasma. Also, after 16 hours of exposure to human plasma, hepatic functionality

such as ammonia elimination and CYP3A4 activity reduced by 48±21% and 29±7% compared to control cultures, respectively. The reduction in hepatic gene transcript levels and functionality was accompanied by upregulation of pro-inflammatory cytokines and was closely related to the upregulation of the pro-inflammatory NF-κB signalling pathway which has a role in the induction of SASP phenotype and promotion of senescence. Therefore, plasma can negatively affect hepatic functions in *vivo* conditions which can be associated with induction of senescence following early NF-κB activation. ALF plasma also exerted more toxic effects and altered gene expression when compared to healthy plasma [146].

The effect of ALF plasma on porcine hepatocyte viability and function in the AMC-BAL system was investigated in a study by Abrahamse et al in 2002[149]. Hepatocytes were isolated from resected pig livers and then transferred to the bioreactor of the AMC-BAL system to treat anhepatic rendered pigs for 24 hours. Hepatocyte viability and function including LDH leakage, ammonia clearance, urea synthesis, ethoxycoumarin O-deethylase (ECOD) activity and pseudocholine esterase production were measured before and after the 24h treatment with ALF plasma (group I) and were compared with control groups (group II) including bioreactors which were incubated with growth medium for a similar period of 24h treatment. No significant differences in cell count and viability of group I and group II have been observed post-treatment. However, ammonia clearance from hepatocytes that were used to treat anhepatic pigs reduced significantly after treatment compared to the control group (P<0.05). Also, after treatment, urea synthesis rate was significantly lower compared to the pre-treatment urea synthesis rate (P < 0.05) but there were no significant differences in ammonia clearance between group I and II post-treatment. ECOD activity of hepatocytes in the bioreactors of group I were completely abolished after treatment of anhepatic pigs. While the ECOD activity of hepatocytes in bioreactors of group II did not change after the 24 h culturing period. Pseudocholine esterase production from hepatocytes in both bioreactors did not change significantly before and after treatment. The findings of this study clearly showed a reduction in porcine hepatocyte function in bioreactors after exposure to plasma of pigs with induced ALF [149]. However, this study did not suggest any mechanisms by which reduced hepatocyte function may have occurred following exposure to the patient's plasma within the BAL system.

1.6. Summary

1.6.1 Knowledge gap

It has been shown that hepatocyte senescence is linked to liver dysfunction in chronic liver disease through changes in hepatocellular regenerative capacity and function. Progressive accumulation of senescent hepatocytes can disturb hepatic function leading to decompensation and progression of changes leading to liver cirrhosis. In patients with acute or acute chronic liver failure, the loss of detoxification, synthesis and metabolic processing normally carried out by hepatocytes leads to complications associated with toxin accumulation. Liver dialysis and bio-artificial liver strategies have been developed for detoxification and to incorporate hepatocyte-specific processing, respectively. However, no devices have provided a clinical survival benefit to date. A severe decline in hepatocyte function has been observed in monolayer and BAL cultures of hepatocytes after exposure to ALF plasma. Evidence from studies exposing hepatocytes to toxin-containing ALF plasma suggests that there is a cytotoxic effect on liver cells in addition to a disturbance in the cell cycle and a reduction in cell function. These alterations in hepatocyte function within BAL systems may be associated with cytotoxic compounds accumulating in blood during ALF. This may lead to induction of senescence or cell death after exposure to perfused liver toxins. These changes induced by senescence should be considered a critical factor in mediating device failure by negatively affecting hepatocyte function within a BAL bioreactor after exposure to perfused liver toxins. However, no studies have directly investigated the impact of senescence on reduced BAL hepatocyte function over time or whether senescence suppression strategies may be incorporated to improve bioartificial liver function by using senescence inhibitor compounds.

1.6.2 Hypothesis

This study hypothesises that senescence compromises the growth and functional capacity of hepatocytes within a BAL prototype device after exposure to liver toxins through a mechanism that can be inhibited using antioxidants and senescence inhibitor compounds.

1.6.3 Aim

This study aims to investigate the role and significance of hepatocyte senescence in bio-artificial liver failure using a hepatocyte-loaded macroporous cryogel prototype device. It will then consider routes to protect hepatocytes against senescence-associated through the protective effect of antioxidants and senescence inhibitor compounds.

1.6.4 Objectives

To address this aim, the study objectives are to:

1. Characterise a suitable hepatocyte cell line to study the impact of liver toxins and establish a suitable cell model to study hepatocyte senescence
2. Develop methods for induction of senescence and characterise senescent cells
3. Develop tests to assess the impact of senescence on key metabolic functions
4. Assess the effect of liver toxins treatment on induction of senescence in tumour-derived hepatocytes
5. Synthesise a cryogel matrix to establish a 3-dimensional BAL model to study the effect of senescence on hepatocyte proliferation and function
6. Use the BAL bioreactor as an in *vitro* model of liver failure to assess induction of senescence and its role in declining device function
7. Evaluate the effect of and mechanisms by which senescence inhibitor compounds may reverse bio-artificial liver prototype failure

Chapter 2 Methods

2.1 Cell culture

The HHL cell lines were provided as a kind gift from Dr Nathan Davis with the production described [141]. The HHL-7 cell line was cultured in high glucose (4.5 g/L) Dulbecco's modified Eagles' medium (DMEM) (Thermo Fisher, UK) with 10% (v/v) foetal bovine serum (FBS) (Thermo Fisher, UK), 1% (v/v) MEM non-essential amino acid (NEAA) (Thermo Fisher, UK) and 1% (v/v) penicillin/streptomycin P/S, (Thermo Fisher, UK) in a 37°C humidified incubator with 5% CO_2.

Human liver hepatocellular carcinoma HepG2 cells were purchased from the American type of culture collection (ATCC). The cells were cultured in Eagle's Minimum Essential Medium (MEM) (Thermo Fisher, UK) supplemented with 10% (v/v) FBS and 1% NEAA (v/v) in a humidified incubator with 5% CO_2 at 37°C. NIH-3T3s were cultured in high glucose DMEM with 10% FBS and 1% P/S. The media was changed every alternate day and cells passaged at 70% confluency. The cells were washed with phosphate-buffered saline (PBS) (Sigma, UK) and passaged using standard trypsinisation by the addition of 4mL (0.25%) Trypsin-EDTA (Thermo Fisher, UK), neutralisation by the addition of 8 mL fresh media and centrifugation for 5 minutes at 1500 g. Following centrifugation, (Thermo Fisher, UK) supernatant from the cell pellet was aspirated. The pellet was resuspended in the 1mL of the medium. After determining the cell number, a new flask was reseeded using a volume of 10-15 mL and a cell concentration of 5 x10^5 cell/mL. Cells were incubated at 37°C with a CO_2 level of 5%. For use in subsequent experiments HHL-7, HepG2 and NIH-3T3 cell lines were seeded at the required concentrations in duplicate per experimental repeat and incubated at 37°C in a humidified incubator with 5% CO_2 for 24 hours before use.

2.2 Establishment of the 3-D static model
2.2.1 Cryogel synthesis

- **Synthesis of poly (HEMA-co-MBA) and poly (HEMA-co-PEGDA) cryogels**

Cryogels made of 2-hydroxyethyl methacrylate (HEMA) (Sigma, UK) and cross-linked with Polyethylene glycol diacrylate (PEGDA) (Sigma, UK) or N, N'-Methylenebis (acrylamide) (MBA) (Sigma, UK) were synthesised for use as a cell scaffold for bioartificial liver application

following the method developed in a previous study using the principles shown in figure 2.1 [150]. Briefly, 0.891 mL of monomer HEMA and 0.266g of cross-linker MBA was dissolved in 20 mL of deionised (DI) water in a conical flask and the solution was degassed with nitrogen gas or a vacuum pump for 10 minutes to remove the soluble oxygen. The cryogel was produced by free-radical polymerisation catalysed by N, N, N', N'-Tetramethylethylenediamine (TEMED) (Sigma, UK) and ammonium persulfate (APS) (Sigma, UK). After adding 20 µL of TEMED (first initiator) the solution was cooled in an ice bath for 15 minutes. 20 mg of APS, the second initiator was added to the solution and the reaction mixture was stirred for 30 seconds. A volume of 2 mL was immediately pipetted into a 9 mm inner diameter glass tube. The solutions were frozen in an ethanol cryobath at -12°C for 18 hours. The cryogel columns were thawed at room temperature, washed with 500 mL of DI water and stored at 2-8 °C for further use.

Poly (HEMA-co-PEGDA) cryogels were synthesised according to the protocol defined above using 0.891 mL of HEMA and 0.237 mL of polyethene glycol diacrylate (PEGDA) dissolved in 20 mL of DI water.

Figure 2.1. schematic representation of cryogel synthesis [151].

- **Post-synthesis modification of HEMA-PEGDA and HEMA-MBA cryogels with alginate**

 HEMA-MBA and HEMA-PEGDA cryogels were put in an aqueous solution of 0.1M glutaraldehyde (Sigma, UK) and 0.1M HCl (Sigma, UK) and incubated with agitation for 2 hours. After washing the cryogels three times in DI water, they were put in a 1% alginate %w/v (Sigma, UK) solution and incubated overnight at room temperature with agitation.

83

Finally, cryogels were washed 3 times with water and stored in DI water at 2-8 ˚C for further use.

- **Alginate cryogel preparation (HEMA-PEGDA and HEMA-MBA cryogels with alginate) and seeding of HHL-7 cells**

Alginate cryogel discs (3x9 mm height by width) were prepared and incubated in glycine solution (Sigma, UK) overnight (0.5 M glycine in 0.1 M sodium phosphate buffer). Cryogels were washed in DI water three times, sterilised in 70% ethanol for 5 minutes and washed with sterile PBS three times. The cryogels were placed in the wells of a 48-well plate and sterilized with UV light (Fisher Scientific, UK) for one hour on each side. The cryogel discs were incubated with 500 µL of DMEM media supplemented with 10% FBS at 37˚C for 24h. HHL-7, HepG2 and 3T3 cells were grown on each cryogel in duplicate per experimental repeat and incubated at 37˚C in a humidified incubator with 5% CO2 for at least 24h. Experiments were repeated in triplicate.

2.3 Establishing a cell model for induction of hepatocyte senescence
2.3.1 Immunocytochemistry assay (ICC) to establish HHLs and HepG2 phenotype

The characterisation of novel human hepatocyte lines (HHLs) derived from the healthy human liver was analysed by ICC assay for the presence of parenchymal and non-parenchymal phenotype markers. HHL5, HHL7, HepG2 and 3T3 cell lines were plated in triplicate on autoclaved sterilised round glass 8mm coverslips (Fisher Scientific, UK) at a concentration of 10^5 cell/mL and grown to near confluence for 24h. Negative controls including no primary antibody were included. The coverslips were washed with PBS, fixed with the addition of methanol-acetate (Sigma, UK) (mixture of 1:1 ratio) and incubated at room temperature for 5 minutes. The coverslips were washed with PBS twice and stored at 2-8 ˚C with wash buffer (0.1%BSA in PBS 1X) for 24h. The coverslips were placed in a humidifying chamber and incubated at 4°C overnight with 0.5 mg/mL of each primary antibody including anti-human cytokeratin 7 (Invitrogen, UK) and anti-human cytokeratin 8 (Invitrogen, UK) containing 1% bovine serum albumin (BSA) (Sigma, UK) as a blocking agent. The coverslips were washed in three changes of PBS and incubated in a 2 µg/mL solution of secondary antibody (Goat anti-mouse IgG H&L-Alexa Flour 488, Invitrogen, UK) at room

temperature for 4 hours in the dark. The coverslips were washed in PBS three times and mounted on glass slides with a drop of diamidino-2-phenylindole (DAPI) (Sigma, UK) solution. Stained cells were examined and imaged with a Zeiss laser scanning confocal microscope (Zeiss LSM-410, UK) using an excitation/emission wavelength of 495/519 nm for Alexa Fluor 488 and an excitation/emission wavelength of 405/488 nm to detect DAPI stained nuclei.

2.3.2 Hydrogen peroxide treatment

HHL-7. The HHL-7 cells were seeded on coverslips at a concentration of 10^5 cells/mL and cultured in the standard culture medium for 24 h before treatment. To determine the effect of oxidative stress on cellular senescence, human hepatocyte cells were treated with different doses of hydrogen peroxide (Sigma, UK) (100, 200, 300, 400, 500, 600μM) for 24 hours. The control HHL-7 cells were incubated in culture media alone. After each treatment, the cells were washed with PBS and allowed to recover in a standard culture medium for 24 h before further experimentation. Experiments were repeated in triplicate.

2.3.3 Mitomycin C treatment

The HHL-7 cells were trypsinised and seeded at a cell density 10^5 cells/mL on coverslips. For induction of premature senescence, HHL-7 cells at approximately 70 to 80 % confluency were treated with 1μg/mL mitomycin-C (Abcam, UK) for 24 hours and 10μg/ml mitomycin-C for 1 hour. Experiments were repeated in triplicate.

2.3.4 Etoposide treatment

The HepG2 cells were passaged by standard trypsinisation and seeded at a cell density 10^5 cells/mL on coverslips. For induction of premature senescence, HepG2 cells at approximately 70 to 80 % of confluency were treated with 10 and 20 μM of etoposide for 24 and 48 hours. Experiments were repeated in triplicate.

2.3.5 Liver toxin and cytokine treatment

The HepG2 cells were cultured in MEM supplemented with 10% FBS, 1%NEAA and 1% P/S in a humidified incubator with 5% CO_2 at 37°C. HepG2 cells were seeded on 2-dimensional coverslips and 3-dimensional (3D) alginate cryogel surfaces at 1×10^5 cells/mL concentration and treated with liver toxins and cytokines at the concentrations shown in table 2.1 for 6h. The control cells were incubated in standard culture media alone. After 6 hours, the cells were washed with PBS once and allowed to recover by incubation in a culture medium overnight. Experiments were repeated in triplicate.

Table 2.1. List of toxins used for treatment and their concentrations

Toxins	Concentration (mg/mL)
Creatinine (Sigma, UK)	0.2
Bilirubin (Sigma, UK)	0.1
Sodium chenodesoxycholate (C-Doca)(Sigma, UK)	0.4
Ammonia (Sigma, UK)	0.05
Urea (Sigma U5378, UK)	1.8
IL-6 (Abcam, UK)	1.0×10^{-6}
IL-8 (Abcam ab49839, UK)	1.0×10^{-6}
TNFα (BIOLEDGEN, UK)	1.0×10^{-6}

2.3.6 Cytokine treatment

HepG2 cells were seeded on coverslips in 6-well plates at 1×10^5 cells/mL concentration and incubated in a growth medium for 24h. After 24 h incubation, the medium was removed from each well and cells were treated with IL-6, IL-8 and TNF-α separately at 1 ng/mL concentration for 6h. Control cells were incubated in a standard growth medium only. Cells on coverslips were treated in duplicate with each cytokine. After 6 hours, the cells were

washed with PBS once and allowed to recover by incubation in a standard culture medium overnight. Experiments were repeated in triplicate.

2.4 Assays to assess the impact of hepatocyte senescence on metabolic function
2.4.1 Cell viability assays

- **MTT assay**

Cell viability was measured by thiazolyl blue tetrazolium bromide (MTT) (Abcam, UK) assay comparing 2-D and 3-D cryogel surfaces. A standard curve was used to establish a linear relationship between cell concentration and MTT absorbance values. To measure cell viability HepG2 and HHL-7 cells were seeded into the wells of 96 well plates (2-D surfaces) and onto alginate cryogels at 5×10^5 cells/mL concentration in duplicates. To optimize the cell seeding density for the MTT assay, a series of concentrations in 100 µL medium including $5 \times 10^5, 2.5 \times 10^5, 1.25 \times 10^5, 6.3 \times 10^4, 3.1 \times 10^4, 1.6 \times 10^4, 8 \times 10^3$ cell/well were set up by serial dilution in the wells of 96-well plate (Thermo Fisher, UK), and incubated for 24 hours. After 24 hours of incubation, 10µL of MTT solution (5mg/mL) was added to each well and incubated at 37°C (5% CO_2) for 2 hours until purple-coloured formazan product developed. At the end of the incubation, the medium was removed from each well and 100µL of Dimethyl sulfoxide (DMSO) (Thermofisher, UK) was added to each well to lyse the cells. The plate (Thermo Fisher, UK) was then left for 5 minutes in a plate shaker and the absorbance was measured by spectrophotometry at a wavelength of 570 nm.

In order to measure the cell viability on cryogels, after the extract incubation time, the discs were moved on a new well-plate and 50µL of MTT reagent in 500 µL phenol red-free medium was added to each well followed by a further 4 hours incubation at 37˚C in a humidified incubator with 5% CO2. At the end of the incubation, the medium was removed from each well and 500µL of DMSO was added to each well to lyse the cells. The plate was then incubated for 15 minutes and absorbance was read by spectroscopy at a wavelength of 570 nm.

- **Live and dead assay**

A live/dead cell viability assay (Thermo Fisher, UK) was also performed to visualize the presence of live and dead HepG2 and HHL-7 cells on the cryogel discs. To perform the assay, HepG2 and HHL-7 cells were seeded at a concentration of 5×10^5 cells/mL on HEMA-MBA-alginate cryogels. The cell-seeded cryogels were incubated at 37˚C in a humidified incubator with 5% CO_2 for 6 days. The medium was changed every 2 days. Before the assay, the polymers were washed with 500 µL PBS to remove or dilute serum esterase activity generally present in serum-supplemented growth media. The calcein AM and ethidium homodimer-1 reagents were mixed (1:1 dilution) and then diluted in DAPI with PBS (1:1 dilution). 100 µL of the working solution was added to each of the cryogel discs followed by visualisation using confocal microscopy. The excitation/emission filters were set at 494/517 nm to observe living, green fluorescent cells and at 528/617 nm to detect dead, red fluorescent cells.

2.4.2 Immunocytochemistry assay for Ki67 and p53 staining

Detection of Ki67 (Thermofisher, UK) and P53 proteins (Anti-P53 Antibody, Clone BP53-12, Sigma, UK) was carried out by immunocytochemistry (ICC). HepG2 cells were seeded at 1×10^5 cells/mL in a 6-well plate containing autoclave sterilised coverslips. Cells on coverslips were washed twice in 1mL of PBS and fixed with 3.7% v/v formaldehyde solution (Sigma, UK) for 10 minutes at room temperature, washed twice with wash buffer (3% BSA in PBS, w/v) and then permeabilised with 0.5% v/v Triton® X-100 (Triton, Sigma) in PBS. After three PBS washes, the cells were incubated with 1µg/mL Ki-67 monoclonal antibody and 5µg/mL of anti-p53 mouse monoclonal antibody at 4°C overnight. Then, cells were washed with wash buffer 10 times and incubated with 1µg/mL Goat anti-Mouse IgG (H+L), Superclonal™ recombinant secondary antibody, Alexa Fluor 488 (Thermofisher, UK) at room temperature for 4 hours. The nuclei stained with DAPI and visualised using a confocal microscope and filter were set for Alexa Fluor 488 with an excitation/emission wavelength of 495/519 nm and excitation/emission wavelength of 405/488 nm to detect DAPI stained nuclei. The percentage of Ki67 and p53-positive cells were quantified by counting the number of Ki67 or p53 positive cells (green stained) as a proportion of total blue stained, DAPI positive cells. Experiments were repeated in triplicate.

88

2.4.3 EdU incorporation assay

The Click-iT EdU Alexa Fluor 488 imaging kit (Thermofisher, UK) was used according to the manufacturer's instructions. Treated HHL-7 and HepG2 cells were allowed to recover for 24 hours in DMEM or MEM containing 10% FBS, 1% MEM Non-essential amino acids solution and 1% penicillin-streptomycin in a 37˚C humidified incubator with 5% CO2. Cells were incubated with 10 µM (5-ethynyl-2'-deoxyuridine (EdU) for 3 h. Cells were then rinsed with medium and fixed using 3.7% v/v formaldehyde for 10 min. Cellular membranes were permeabilised using 0.5% Triton-X-100 v/v in PBS for 20 min. Cells were then washed twice with PBS and treated with 50µL of the Click-iT reaction cocktail for 30 min. 500 µL of Click-iT® reaction cocktails contain 430µL 1X Click-iT® reaction buffer, 20µL CuSO4, 1.2 µL Alexa Fluor® azide and 50 µL reaction buffer additive. Following this reaction, cells were washed once with PBS and counterstained with 1 µg/ml Hoechst 3342 in PBS for 10 min. Fluorescence was measured using a confocal microscope. The excitation/emission filters were set at 495/519 nm to observe Alexa Fluor® dyes (green) and at 350/461 nm to detect Hoechst dye bound to DNA (blue).

2.4.4 RT-PCR assay

HepG2 cells at $1x10^5$ cells/mL concentrations were seeded into the wells of a 12-well plate and incubated at 37˚C, 5% CO_2 overnight. Etoposide treatment at a concentration of 10µM was added to each positive control well and incubated for 48h. Negative control cells were grown in media only. After 48 h incubation, the treatment was washed with PBS two times and trypsinised. The cell pellet was collected and stored at -80˚C until RNA extraction. The cell pellet was washed with 1ml of PBS and centrifuged at maximum speed for 30 seconds. 350µl of buffer RLT and 350µl of 70% ethanol (RNAeasy Mini Kit, Qiagen, UK) were added to the sample to provide conditions that improve the selective binding of RNA to the RNA easy Min Elute membrane. The sample was then transferred to the RNA easy Min Elute spin column. DNase and any contaminants were washed with 700µl of RW1 buffer and 500µl of buffer RPE respectively. Then, the total RNA was eluted in RNase-free water. The total RNA concentration and purity were measured by the Nanodrop machine (2000/2000C

Spectrophotometers, Thermo Scientific, UK) by the 260/280 nm absorbance ratio. The template RNA was subjected to Quantitect reverse transcription procedure for complementary DNA (cDNA) synthesis. The purified RNA sample was incubated in a gDNA wipeout buffer (Qiagen, UK) at 42˚C for 2 minutes to remove contaminating genomic DNA. The cDNA was synthesized by reverse transcription using a master mix (Qiagen, UK) (1µl of quantiscript reverse transcription, 2µl of quantiscript RT buffer and 1µl RT primer mix) according to the manufacturer's protocol. The entire reaction was kept at 42˚C for 15 minutes and then reverse transcriptase was inactivated at 95˚C for 3 minutes. Gene expression was measured on Rotor-Gene Q (Qiagen, UK) cycler according to the program outlined in the manufacturer's protocol using SYBER green master mix (Qiagen, UK). PCR was done in the condition of denaturation at 95˚C for 5min and combined annealing/extension at 60˚C for 10 S for 40 cycles. The primer sequence for real-time PCR is shown in table 2.2. Relative gene expression levels were calculated using the ΔΔCT method. Actin was used as an internal reference.

Table2.2 Primers for real-time RT-PCR

Target	Accession no	Forward primer 5'-3'	Reverse primer 5'-3'
P53	NM_138349	TAGTGTGGTGGTGCCCTATG	CACATGTAGTTGTAGTGGATGGTG
Albumin	NM_000477	59GCT GTC ATC TCT TGT GGG CTG T 3	59ACT CAT GGG AGC TGC TGG TTC 3

2.4.5 Measurement of albumin and urea level

The metabolic activity of HepG2 and HHL-7 seeded on 2-D and 3-D surfaces were determined by measuring the albumin secretion and urea synthesis. For two-dimensional (2D) cultures, HepG2 and HHL-7 were seeded into the wells of a 24-well plate (2D) at a final concentration of 5×10^5 cells/mL. Similarly, for 3D culture, the cell suspension was seeded on HEMA-MBA and HEMA-MBA-alginate at a final concentration of 5×10^5 cells/mL in duplicate and let to settle and adhere for 48 hours. The media was collected from each sample at

different time points and collected samples were immediately frozen and stored at -20°C before analysis. Medium without cells was used as a blank control.

The albumin concentration in the sample medium was measured by using the SimpleStep ELISA® kit (Abcam, UK), following the manufacturer's protocol. Briefly, 50µL of each sample and standard solutions were added to the anti-tag antibody pre-coated wells of a 96-well plate. Then, 50 µL of the antibody cocktail which contains capture and detection antibodies were added to each well and the plate was sealed and incubated for 1 hour at room temperature on a plate shaker set to 400 rpm. The wells were washed 3 times with 350 µL 1X Wash Buffer PT and then 100 µL of 3,3',5,5'-tetramethylbenzidine(TMB) substrate was added to each well and incubated for 10 minutes in the dark on a plate shaker at 400 rpm. After 10 minutes, a 100 µL of stop solution was added to each well and the plate was covered and incubated for 1 min in the dark on a plate shaker at 400 rpm. The absorbance was read on a plate reader at 450 nm. Absorbance readings were extrapolated by using the albumin standard curve obtained from 0 to 45 ng/mL concentration.

Urea concentration in media was measured using a Quantichrom Urea assay kit (Bioassay Systems DUR-100, US), according to the manufacturer's instructions. To stimulate urea production, each sample was treated with 1mM ammonium chloride (NH_4Cl), (Sigma 213330, UK) for 24 hours and then the medium was collected and stored at -20°C until analysis. Briefly, 50µL medium (blank), 50µL of 5 mg urea/dL (standard) and 50 µL of all samples were transferred in duplicate into 96 well plates. Then, a 200 µL working reagent containing 1:1 reagent A and reagent B (provided in the kit) was added to each well and incubated at room temperature for 20 minutes. The absorbance was then measured using a plate reader at 520 nm. The urea concentration in each sample was calculated following this equation:

$$Urea = \frac{OD\ sample - OD\ blank}{OD\ standard - OD\ blank} \times n \times [STD]$$

OD sample, OD blank and OD standard are the absorbance of sample, blank and standard respectively, n is the dilution factor and [STD] is 5 mg/dL for low urea-containing samples.

2.5 Assessing the impact of senescence inhibitor compounds on hepatocyte senescence

2.5.1 Dose-response curve of resveratrol

HepG2 cells were seeded on coverslips at 1×10^5 cells/mL concentration and cultured in the standard growth medium for 24 h in a humidified incubator at 5% CO_2 at 37°C overnight. Then, cells were treated with resveratrol (Sigma R5010, UK) at 2, 5, 10, and 25 μM concentrations in duplicate for 24h. The control cells were incubated in a standard culture medium alone. Experiments were repeated in triplicate.
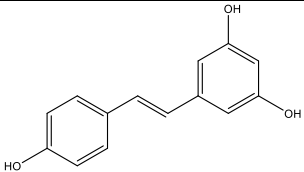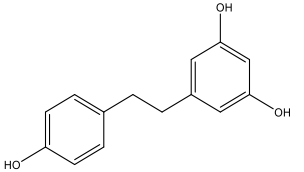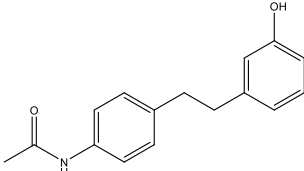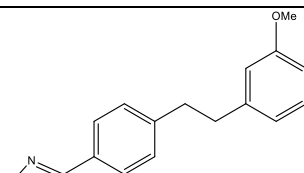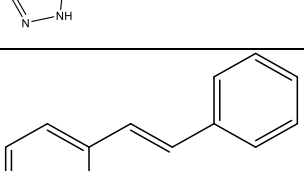
2.5.2 Treatment of HepG2 cells with Resveratrol and liver toxins

HepG2 cells were seeded on coverslips and cryogels at 10^5 and 5×10^5 cells/mL concentrations, respectively. They were pre-treated with resveratrol (RSV) at 2 and 5 μM concentrations in duplicate and incubated for 24h. After 24h, RSV treatment was removed from each well and then cells were treated with liver toxins and RSV at the mentioned dose for a further 6 h. Treatments were removed from each well after 6 h incubation followed by incubation in a standard growth medium only overnight. The control cells were grown in a growth medium only.

2.5.3 Treatment of HepG2 cells with Dihydroresveratrol, vitamin-C and resveralogues

Cells were seeded on a 2-dimensional (coverslips) surface at 10^5 cells/mL concentration and were pre-treated with resveratrol, dihydro-resveratrol, vitamin-C (Sigma, UK), V29 (E)-1,2-diphenylethene, V34 (E)-4-(3,5-dimethoxystyryl)benzonitrile and V31 (E)-N-(4-(3,5-dihydroxystyryl)phenyl)acetamide (table 3) at 5μM concentrations in duplicate for 24 h before being treated with liver toxins. After 24 h, the medium was removed from each well and cells were treated with a liver toxins cocktail and mentioned poly-phenolic compounds at 5μM concentrations for 6h. The control cells were incubated in culture media alone. After 6 hours, the cells were washed with 1mL of PBS once and allowed to recover with a complete culture medium overnight. Resveratrol-related compounds and their activities are listed in table 2.3.

Table 2.3. List of the resveratrol-related compound and their activities (rejuvenation: lifespan extension and ageing reversal)

Compound	Radical scavenging	SIRT-1 activity	Rejuvenation	Chemical structure
Resveratrol	+	+	+	
Dihydroresveratrol	+ (lower than RSV)	+	+	
V31	–	+	+	
V34	–	+	+	
V29	–	–	+	

2.6 Senescence and BAL design
2.6.1 3-D bioreactor model design

Bioreactors consisted of three glass tubes (9 mm diameter, 100 mm height) (Fisher Scientific, UK), which were linked with medium reservoirs via silicon tubes (Ismatec2-stop, 2.79 mm 6/pk, Germany). Each glass tube contained 10 layered HEMA-MBA-alginate cryogel discs (2 mm thickness) which were separated with 2 mm- height PLA 3-D printed spacers. The glass tubes were further closed and linked to the silicon tubes with 3-D printed

connectors made with PLA polymer. A multichannel peristaltic pump (Ismatec IP-N digital peristaltic pump 8-channel, WZ78010-11, Germany) was used to circulate the medium from reservoirs at a flow rate of 2 mL/min via silicon tubes connected to the chambers. The medium reservoirs were prepared by drilling plastic plugs to make two holes which house one inlet and one outlet for the silicon tube to maintain the medium circulation over chambers. The glass tubes, medium bottles and silicon tubes were sterilized by autoclaving before assembly. 20 mL of pre-warmed MEM medium was added to the medium reservoir and recirculated in the incubator at 37 °C and 5% CO2 (Figures 2.2 and 2.3).

2.6.2 HEMA-MBA-Alginate cryogel preparation and sterilisation

HEMA-MBA- alginate cryogels were cut to a 2 mm thickness. Discs were washed with DI water 3 times, sterilised with 70% ethanol for 15 minutes and washed with sterilised PBS 3 times. Then, they were sterilised under a UV lamp for 1 hour on each side. Each disc was incubated in medium (MEM with 10% FBS, 1% NEAA and 1% P/S) at 37°C and 5% CO_2 overnight.

2.6.3 Cell seeding on cryogels for multi-layered bioreactor

HepG2 cells were seeded at a concentration of 5 x 10^5 cells/mL on each cryogel and kept for 4 hours in the incubator to allow cells to adhere to the surface of cryogels.

2.6.4 Pre-treating with 5µM resveratrol

5µM resveratrol solution was prepared in a 20 mL medium and was added to the medium reservoir. The medium contained resveratrol recirculated in the chamber containing cryogels with cells in the incubator at 37 °C and 5% CO_2 for 24h.

2.6.5 Treating with liver toxins

After 24 h, the medium containing resveratrol was removed from the reservoir and cells were treated with liver toxins cocktail only and liver toxins plus resveratrol at 5µM

concentration for 6h. The control cells were incubated in culture media alone. The treatments were removed after 6 hours, and the cells in chambers were washed with 1mL of medium twice. 20 mL of growth medium was added into each reservoir and recirculated in the incubator at 37 °C and 5% CO_2 for a further 24 h. Experiments were repeated in triplicate.

2.6.6 Measuring cytokine levels

The concentration of IL-6, (BD Pharmingen, UK) IL-8 (BD Pharmingen, UK) and TNF-α, (BD Pharmingen, UK), were measured by ELISA assay according to the manufacturer's protocol. Briefly, the wells of a clear flat bottom 96-well plate were coated with the capture antibody diluted in coating buffer containing 0.1 M sodium carbonate at PH 9.5 and incubated at 4°C overnight. The well plates were washed 3 times with wash buffer (PBS with 0.05% v/v Tween) and then blocked with assay diluent (PBS with 10%FBS, PH7) for 1 h at room temperature. Standards were reconstituted in assay diluent to give the top concentration of 300pg/mL for IL-6, 200 pg/mL for IL-8 and 500 pg/mL for TNF-α. Serial dilutions of the standards were prepared. Samples for IL-6 and IL-8 were diluted 1:2. 100 µL of all samples and standards were added to appropriate wells and the plates were sealed and incubated for 2 hours at room temperature. Then, plates were washed with washing buffer 5 times and 100µL of working detector solution (detection antibody and streptavidin-HRP reagent) was added to each well. Plates were sealed and incubated in the dark for 1 h. Plates were washed with wash buffer 7 times and 100µL of tetramethylbenzidine (TMB) and hydrogen peroxide solution were added to each well. The plates were incubated in the dark for 30 minutes and then 50 µL of stop solution (1M H_3PO_4) was added. The absorbance was read at 450 nm using a plate reader (thermofisher, UK). Experiments were repeated in triplicate.
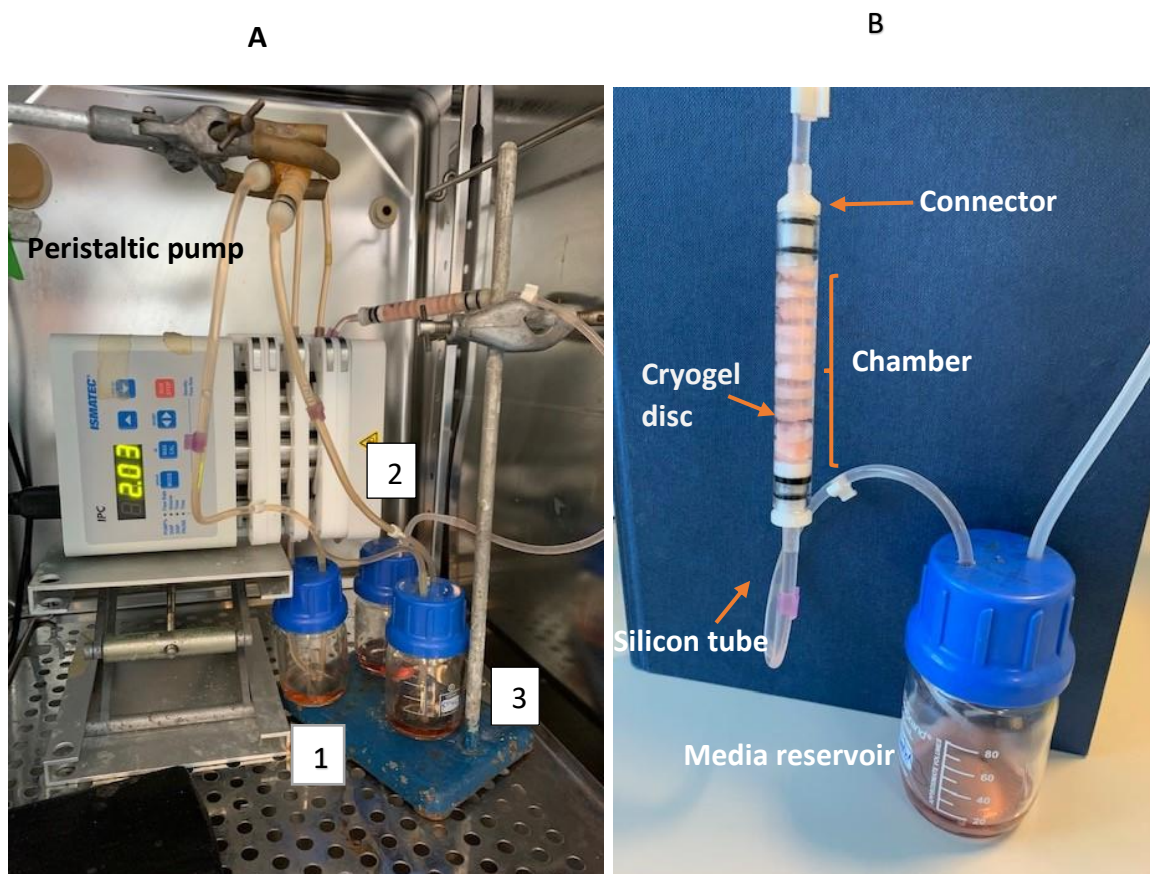
Figure 2.2. **A**. **bioreactor experiment set-up.** System 1 was composed of the HepG2 cells seeded in cryogels and incubated in a medium only. Cells in system 2 were pre-treated with 5µM resveratrol for 24 h and then treated with liver toxins plus resveratrol for 6h. HepG2 cells were treated with liver toxins only for 6 h in system 3. **B**. Multi-layered bioreactor consisted of 10 cryogels discs (2 mm thickness) which were separated with 3-D printed spacers. Cryogel discs and spacers were placed inside the 9mm glass tubes sequentially one after the other. The chambers were closed by 3-D printed connectors and connected to the silicon tubes.
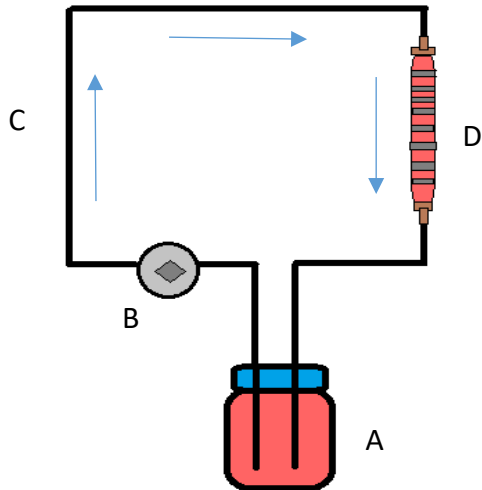
Figure 2.3. Schematic of the multi-layered bioreactor set-up. The components of the systems are: A) Medium reservoir, B) peristaltic pump, C) silicon tubes, D) Chamber.

2.7 Data and statistical analysis

All data were analysed using Graphpad Prism 5 software. MTT, ELISA, ICC and EdU assay data values from three different biological replicates were transformed into mean control ± standard deviation. Statistical analyses were performed using Bonferroni's multiple comparison test. Significance was detected at p-value of <0.05 (*), <0.01 (**), <0.001(***).

Chapter 3 Result

3.1 Hepatocyte cell line characterisation

3.1.1 Characterisation of HHL and HepG2 phenotype using immunocytochemistry

The presence of non-parenchymal and parenchymal phenotype markers in HHL-5 and HHL-7 grown on coverslips was assessed using immunocytochemistry (ICC). Their features were compared with established human hepatoma cell lines (HepG2) and non-liver cells (3T3). The expression profile of cytokeratin 7 (CK7) and CK8 are shown in figure 3.1. The parenchymal marker CK8 was present in all cell lines (HHL-5, HHL-7 and HepG2) except for the non-liver 3T3 fibroblast cell line. The non-parenchymal phenotype marker CK7 was found in HHL-5 and 7 but was absent from the HepG2 and 3T3. Therefore, HHL cell lines retained the expression of CK7 and CK8 and also maintained the primary hepatocyte phenotype.

CK7   CK8

A

B

C

D
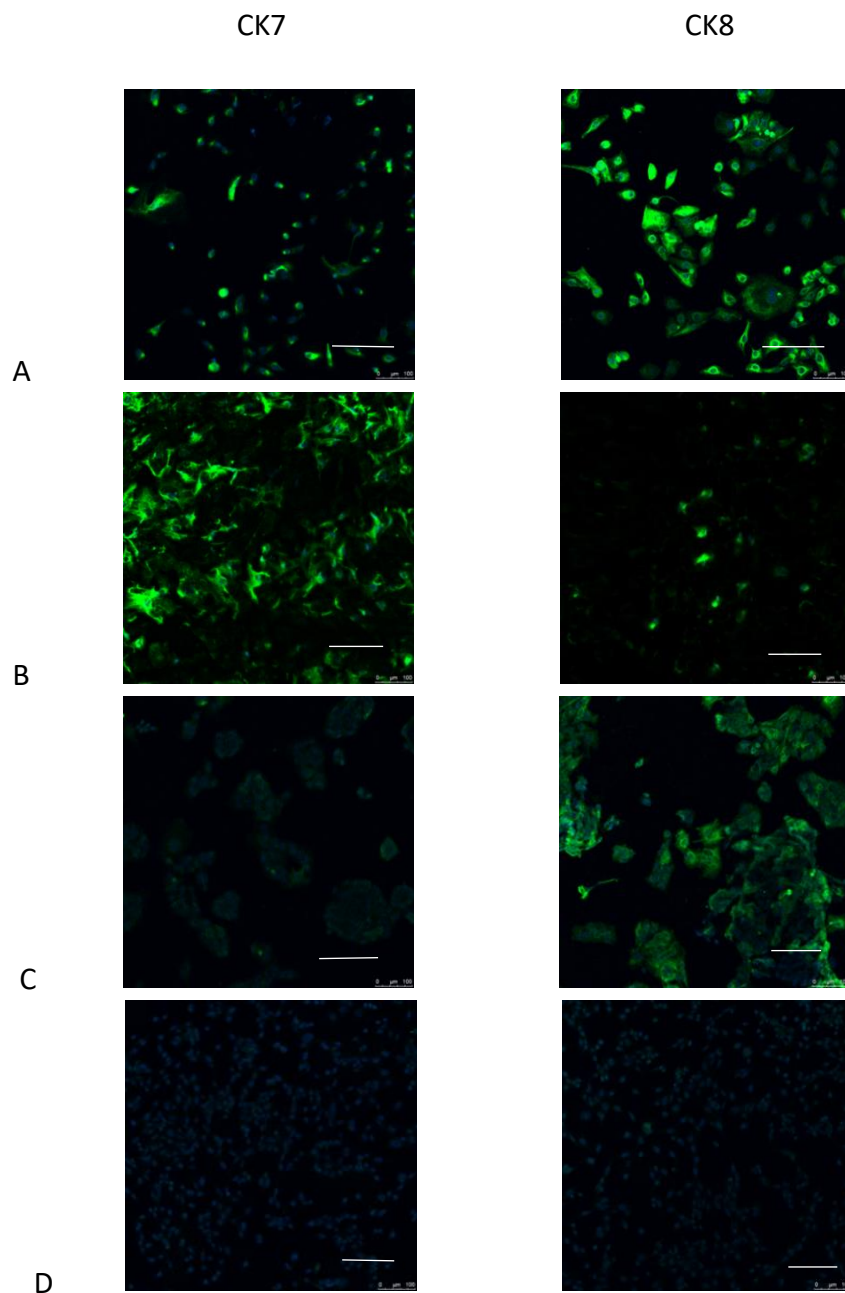
Figure 3. 1. Immunocytochemistry assay for the presence of parenchymal and non-parenchymal phenotype markers (CK7 and CK8) in liver cell lines. The HHLs, HepG2 and 3T3 cells were seeded at a concentration of 4.5 x 10^3 cell/mL and grown on cover slips for 24 h and then probed for the presence of CK7 and CK8. Scale bar 100 µm. (A: HHL-7, B: HHL-5, C: HepG2, D: 3T3).

3.2 Establishment of the hepatocyte matrix model

3.2.1 Measurement of HEMA-based cryogel biocompatibility

Figure 3.2 shows the cell viability and proliferation of HHL-7 cell lines seeded on HEMA-based cryogels after 24, 72h and 1-week incubation. This figure shows the conversion of MTT to formazan by cells is time-dependent. The longer incubation time resulted in more cell numbers adherent to all cryogels. After 72 h and 1 week of incubation, cell number in HEMA-MBA-alginate cryogels was significantly higher than in HEMA-MBA, HEMA-PEGDA-alginate and HEMA-PEGDA cryogels. After one week of incubation, the number of viable cells on HEMA-PEGDA cryogels was 0.89 ± 0.02 *10^4 cells/mL, and on HEMA-PEGDA-alginate cryogels was 4.2 ± 0.07 *10^4 cells/mL, on HEMA-MBA cryogels was 3.75 ± 0.4 x10^4 cells/mL and on HEMA-MBA-Alginate cryogels was 9.94 ± 0.3 *10^4 cell/mL. Cells in all mentioned cryogels were viable and able to proliferate over 7 days of incubation. However, the lowest cell number was seen on HEMA-PEGDA cryogels over one week period and the cell density in HEMA-PEGDA-alginate cryogels was significantly lower compared to HEMA-MBA-alginate (**$p<0.01$, figure 3.2). Therefore, HEMA-MBA-alginate cryogel was chosen for further experiments as it exhibited the highest cell viability at different time points.
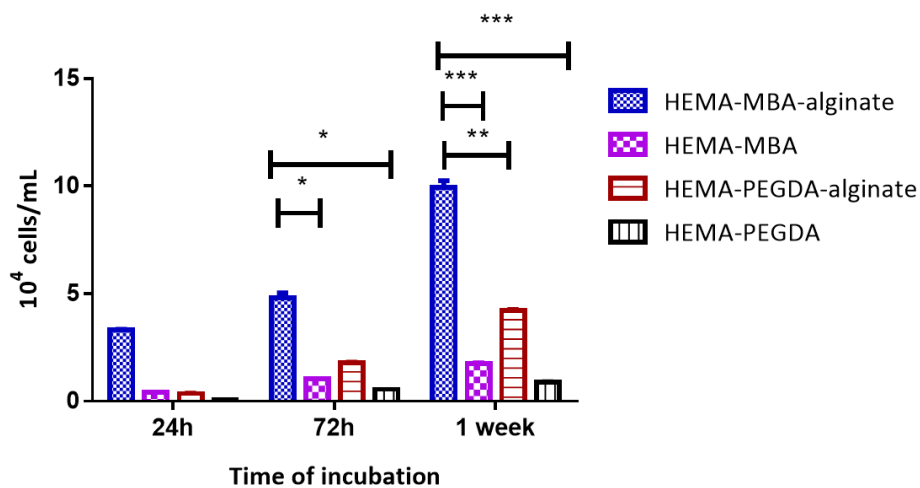
Figure 3.2. MTT assay of HHL-7 cells grown on HEMA-based cryogels after 24h, 72h and 1-week incubation. Values represent mean ± standard deviation (n=3). Data were compared using two-way ANOVA with Bonferroni post-test (*p<0.05, **p<0.01, ***p<0.001).

3.2.2 HepG2 and HHL-7 cell proliferation on HEMA-MBA-Alginate cryogels over time

HEMA-MBA-alginate cryogels supported the adhesion and proliferation of viable hepatocyte HepG2s and HHL-7s over an incubation period of 7 days (figure 3.3). A significant increase in hepatocyte cell number was measured for both hepatocyte cell types, increasing from 3.61 ± 0.31 to $10.0315 \pm 0.06 \times 10^4$ cell/mL for HHL-7 and 3.55 ± 0.05 to $10.0170 \pm 0.05 \times 10^4$ cell/mL for HepG2 from the 3 days to the 7-day time point. No significant difference in growth parameters between the HepG2 and HHL-7s was observed on the cryogels. Live-dead staining of both cell types grown for 7 days on the cryogel discs showed green fluorescent living hepatocytes growing across the surface of each cryogel disc and with the few number of dead cells labelled by red, ethidium homodimer-1 (EthD-1) fluorescence (figure 3.4).

102
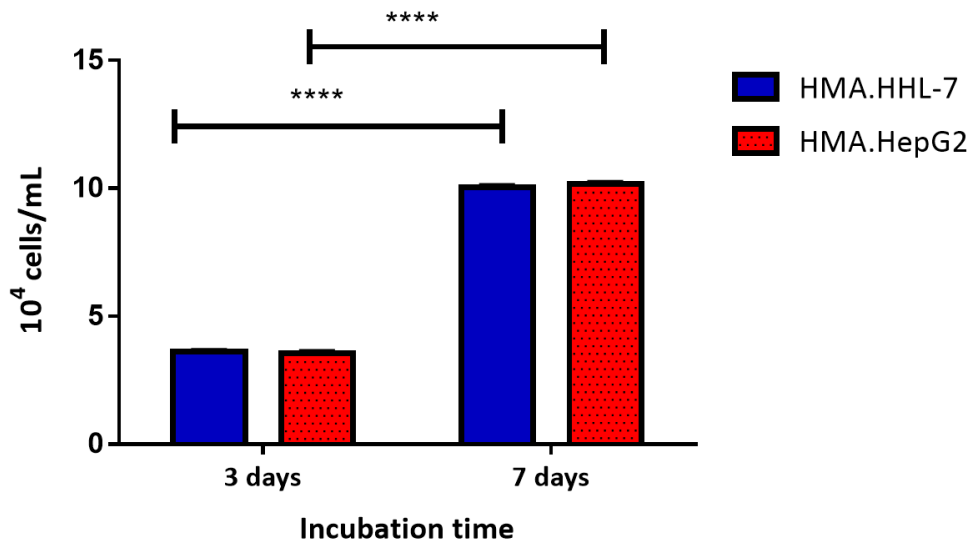
Figure 3.3. HepG2 and HHL-7 cells were seeded on HEMA-MBA-Alginate cryogels at 10^5 cells/mL density and incubated for 7 days. Cell viability was determined by the MTT assay after 3 and 7 days of incubation at 37˚C in a humidified incubator with 5% CO_2. Results are reported as mean ± SD (n=3). Statistical analysis was performed using a two-way ANOVA and Bonferroni post-test (****$p < 0.0001$). (HMA.HHL-7: HEMA-MBA-alginate seeded with HHL-7)

Live	Dead	Merged
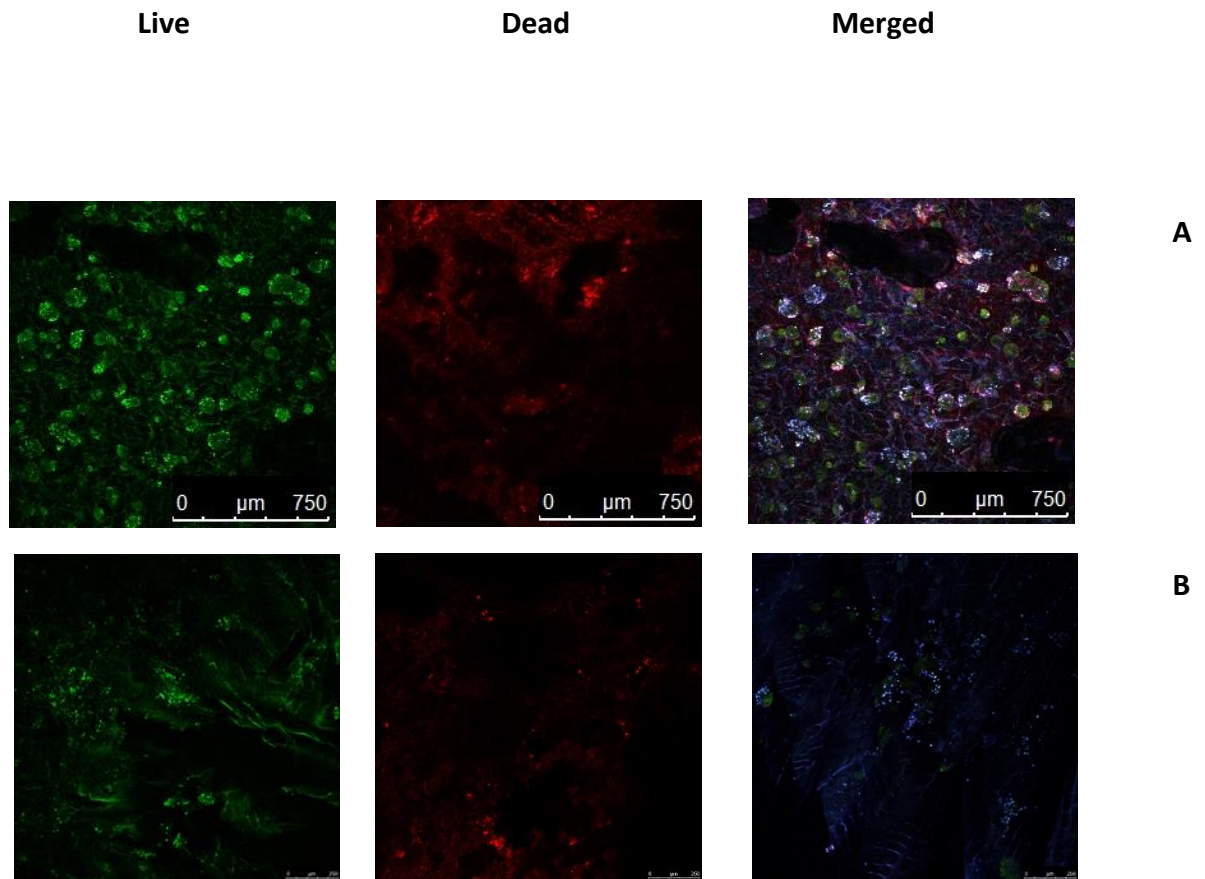
Figure 3.4. Live and dead staining of HHL-7 and HepG2 cells after being cultured on HEMA-MBA-Alginate cryogels for 7 days. Live cells were stained with Calcein-Am (green) and dead cells were stained with EthD-1 (red). The scale bar is 750µm. (A: HepG2, B: HHL-7)

3.2.3 Albumin synthesis by HHL-7 and HepG2 cells in 2-D and 3-D surfaces

Albumin secretion is an important index of functional activity in hepatocytes. Therefore, the total amount of albumin synthesis by HepG2 and HHL-7 cells was measured at 2-D and 3-D surfaces at different time points and is shown in figure 3.5. Secretion of albumin remained at higher levels when HepG2 and HHL-7 were cultured on HEMA-MBA-alginate (3-D surfaces) at every time point. HepG2 cells secreted albumin 70.57±8.52 and 73.03±5.78 ng/mL on 3-D surfaces over 3 and 7 days of incubation which was higher than on 2-D surfaces (6.81±0.92 and 61.56±0.12 ng/mL) at that time point. Albumin production by HHL-7 cells was significantly higher on the 3-D surface of the cryogel (13.77±2.54 and

104

74.25±11.63 ng/mL) compared to the 2-D surface of the coverslip (4.51±2.67 and 30.61±0.86 ng/mL) over 3 (p<0.05) and 7 days (p<0.001) incubation respectively. Figure 3.5 also shows HepG2 produced a higher level of albumin on both surfaces compared to that produced by the HHL-7 cells at the same period on day 3 and day 7 for the cell's growth on the 2D tissue culture surface.
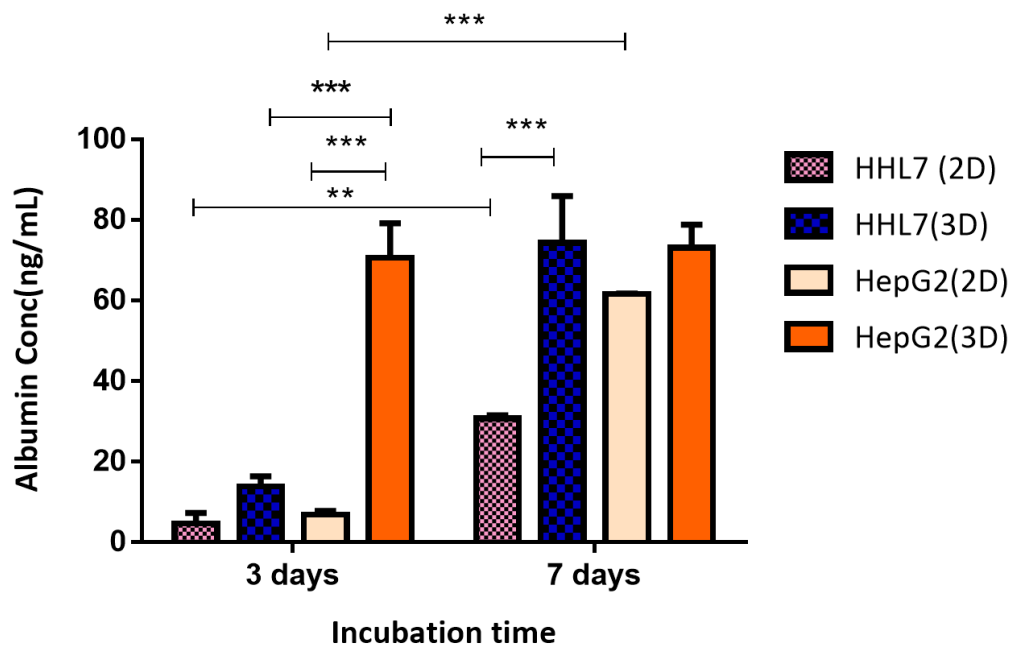
Figure 3.5. Secretion of albumin by HepG2 and HHL-7 cells cultured on HEMA-MBA-alginate (3-D surfaces) and 6-well plates (2-D surfaces) after incubation for 3 and 7 days. The concentration of the albumin in the sample was determined by interpolating the blank control subtracted absorbance values against the standard curve. Data represent the mean±SD from three independent cultures, n=3, statistical analysis was carried out using a two-way ANOVA with Bonferroni Post-hoc test (*p<0.05, **p<0.01), ***p<0.001).

3.2.4 Urea synthesis by HHL-7 and HepG2 cells in 2-D and 3-D surfaces

HepG2 and HHL-7 cell functionality was determined by the measurement of urea synthesis in the culture medium. Figure 3.6 shows that both cell lines possess the other important hepatocyte function, which is ammonia detoxification and converts it to urea after 24 h incubation with 1mM ammonium chloride. Urea synthesis for HepG2 and HHL-7 cell lines grown in 3-D surfaces (HEMA-MBA-alginate cryogel) was 3.29±0.08 and 2.96±0.02 mg/dL respectively and it was 2.67±0.01 for HHL-7 and 3.12±0.02 for HepG2 at 2-D surfaces. HepG2 and HHL-7 cell lines produced higher levels of urea at 3-D surfaces compared to 2-D surfaces. HepG2 cultured either on 2-D or 3-D surfaces had a better ability to synthesise urea compared to HHL-7. The difference was statistically significant ($p < 0.01$).
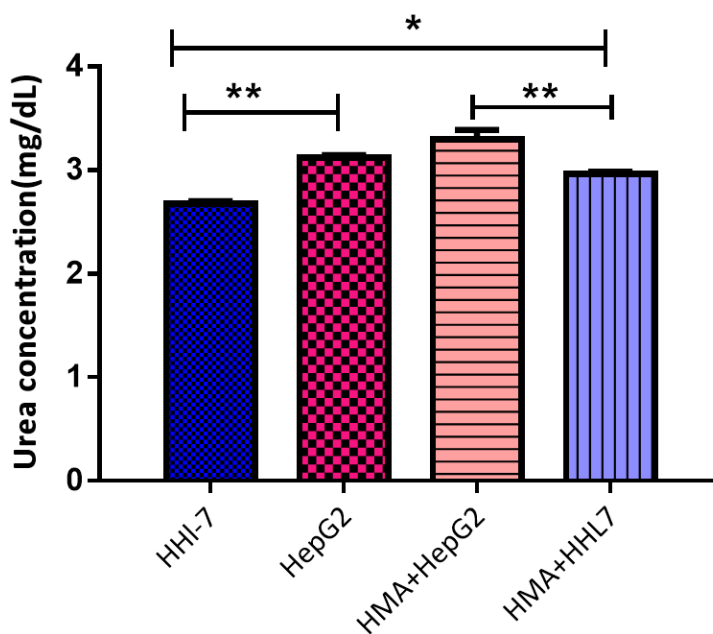
Figure 3.6. Synthesis of urea by HepG2 and HHL-7 cells cultured on HEMA-MBA-Alginate (3-D surfaces) and 6-well plates (2-D surfaces) after incubation for 3 days. The concentration of the urea in the sample was determined by interpolating the blank control subtracted absorbance values against the standard curve. Data represent the mean ± SD from three independent cultures and determinations. (*$p < 0.05$, ** $p < 0.01$)

3.3 Developing a model of hepatocyte of senescence
3.3.1 Induction of senescence in HHL-7 by hydrogen peroxide treatment

- **Hydrogen peroxide treatment reduced HHL-7 cell viability**

The effect of increasing H_2O_2 concentration on cell viability was measured using the MTT assay. MTT assay showed that H_2O_2 reduced cell viability at all tested concentrations on 2-D surfaces (figure 3.7). The percentage of viable cells was 36%, 29% and 18 % for cells treated with H_2O_2 at 100, 200 and 300 µg/mL respectively. A significant reduction in % cell viability occurred on exposure to an increasing concentration of H_2O_2 at all the concentrations used from 100-300 µM compared to the cell-only control (p< 0.0001, figure3.7). The cells viability was also reduced significantly at lower concentrations (20 and 50µM) after 24 h treatment with H_2O_2 (data not shown).
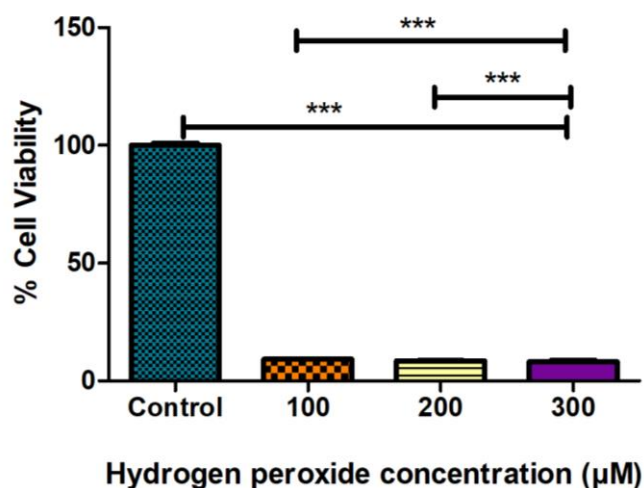
Figure 3.7. Effect of H2O2 on HHL-7 viability. HHL-7 cells were incubated with H_2O_2 at increasing concentrations (µM) for 24 h. Cell viability was then measured by an MTT assay 2 days after removing treatment. Data are expressed as the mean ± SD of two independent experiments (n=3) and were expressed as % of viability in comparison to control. Data were compared using One-Way ANOVA with Dunnet post-test (***p< 0.0001 compared with the control group).

- **H₂O₂ does not induce senescence in HHL-7 cells**

The effect of oxidative stress on proliferation-associated protein levels was determined by Ki67 staining with ICC assay. Confocal microscopic analysis in figure 3.8 shows the result of the Ki67 staining cells (green stained cells) in the treated and non-treated control cells. No change in Ki67 expression levels was observed after exposure to 10, 50 and 100 µM doses of H₂O₂ for 24 hours.
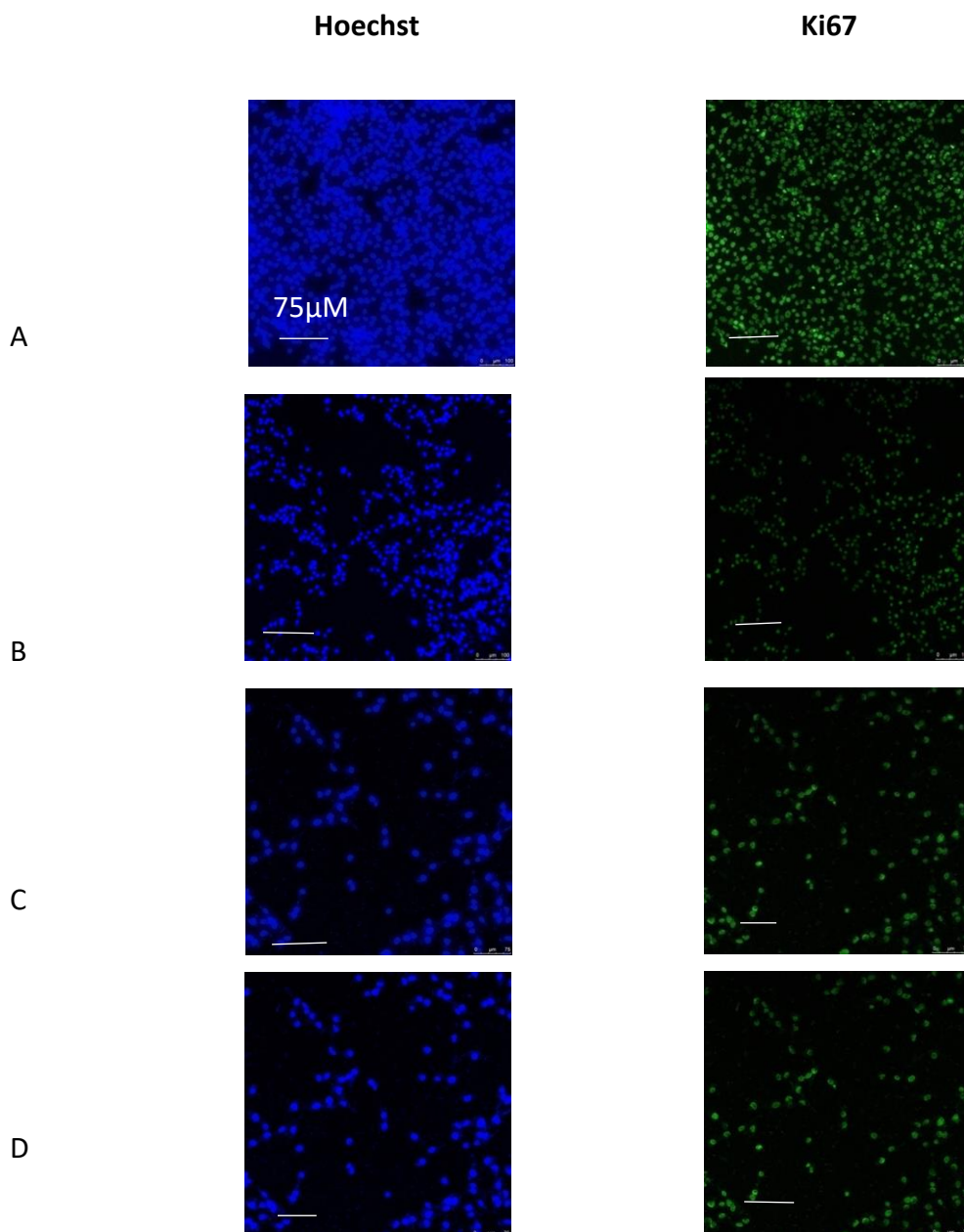
Figure 3.8. Effect of H_2O_2 on Ki67 expression in HHL-7 cells. HHL-7 cells were treated with indicated doses of H_2O_2 for 24 hours and ICC assay was used for Ki67 staining (green) with DAPI counter-staining for cell nuclei (blue). The scale bar is 75μm. (A: Control, B: 10 μM, C: 50μM, D: 100μM H_2O_2)

3.3.2 Induction of senescence in HHL-7 by mitomycin-C treatment

- **Mitomycin-C reduced HHL-7 cell viability**

The MTT assay was used to analyse the cell viability in the mitomycin C-treated cells (Mito-C). Figure 3.9 shows the HHL-7 cell number after removing the treatment. Exposure to 1 and 10 μg/mL of MitoC resulted in a significant reduction of the number of cells at each time point in comparison with the non-treated cells (figure 3.9).
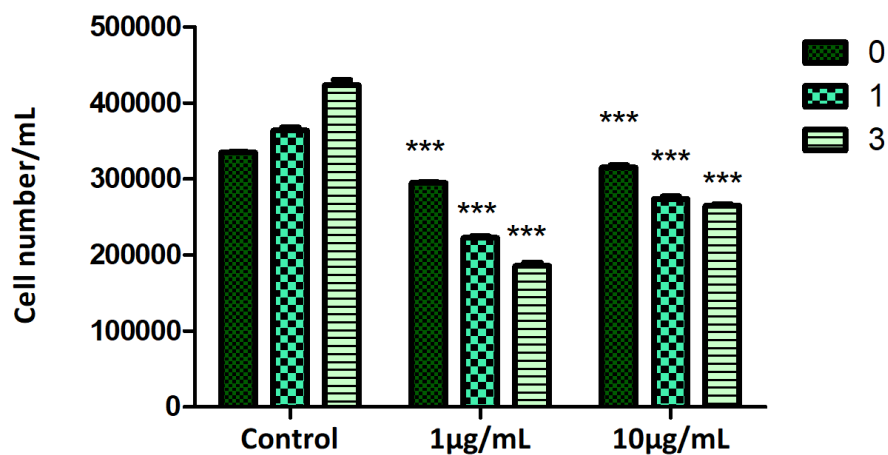
Figure 3.9. Effect of Mito-C on the cell viability of HHL-7s. The number of living cells was measured immediately after treatment (0), 1 and 3 days after treatment using MTT assay. Data were compared using two-way ANOVA with Bonferroni post-test (*p<0.05, **p<0.01, ***p value<0.001, **** p<0.0001 compared to control).

109

- **Mitomycin-C could not induce senescence in HHL-7 cell**

Figure 3.10 shows the percentage of EdU-positive cells after removing treatment. The percentage of EdU positive cells was about 93.5 % for control cells, 82.7 and 80.3 % at 1 and 10µg/mL concentrations of Mito-C after 24 and 1 h treatment respectively. There were no significant differences between untreated and treated cells. The percentage of EdU positive cells at both Mito- C concentrations remained high which means that this treatment appears to be insufficient to induce a permanent cell cycle arrest in HHL-7 cell lines.

A

B
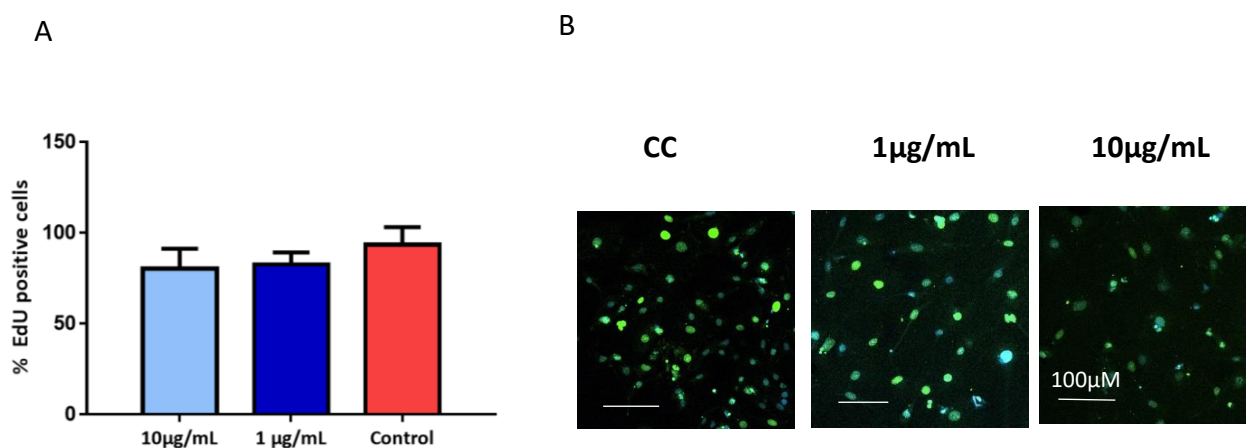
Figure 3.10. **A**. Control and Mito C- treated HHL-7 cells were incubated with EdU for 48 h one day after removing treatment and its incorporation was detected with ALEXA flour 488 (green). Cell nuclei stained with DAPI (blue). **B**. The results are expressed as the Mean ± SD of three independent experiments using One-Way ANOVA with Bonferroni's Multiple Comparison Test. (Scale bar 100µM)

3.3.3 Induction of senescence in HepG2 cells by etoposide treatment

- **Etoposide at low concentration was not toxic to the HepG2 cell**

The cell viability was measured by MTT assay immediately after removing treatment which showed a significant reduction of viable cells at 20 µM etoposide concentration at both time points ($p < 0.001$, figure 3.11). The percentage of viable cells after 24 and 48h was 100%±0.28 and 84%±0.2 in control cells, 98.8%±0.29 and 83.7%±0.21 in 10µM-treated cells, 71%±0.01

110

and 70%±0.024 in 20µM treated cells. Etoposide at 10µM concentration didn't affect cell viability after 48 h incubation compared to the control cell. Consequently, a threshold concentration of 10µM was chosen to treat cells for 48h and avoid cytotoxic damage.
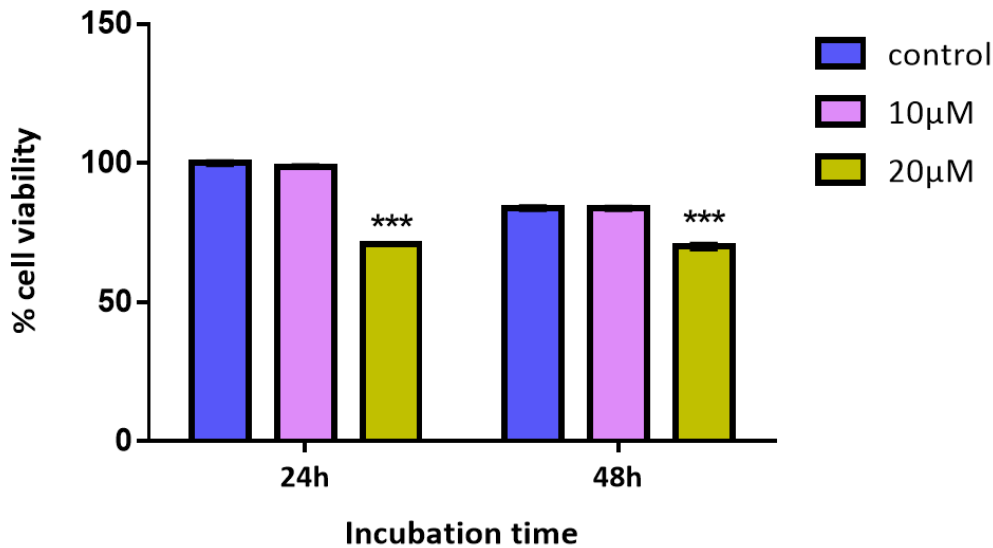
Figure 3.11. The viability of HepG2 cells was evaluated after etoposide treatment. The percentage of viable cells was measured immediately after removing treatment using an MTT assay. Results are reported as mean ± SD (n=3) using Two-way ANOVA Tukey's multiple comparisons tests (***$p < 0.001$ compared to control).

- **Etoposide treatment induces senescence in HepG2 cells**

I. **Reduction of EdU positive cells in etoposide-treated cells**

The incorporation of thymidine analogue into newly synthesised DNA was measured by EdU labelling assay. The percentage of EdU positive cells reduced significantly in HepG2 cells treated with etoposide at 10 and 20µM concentration after 48h treatment compared to the control cells ($P < 0.001$, figure 3.12). The percentage of EdU positive cells was 28.8± 3.2 in control cells, 19.69697±1.2 and 15.06849±1.7.6 in 10µM and 20µM etoposide-treated cells.
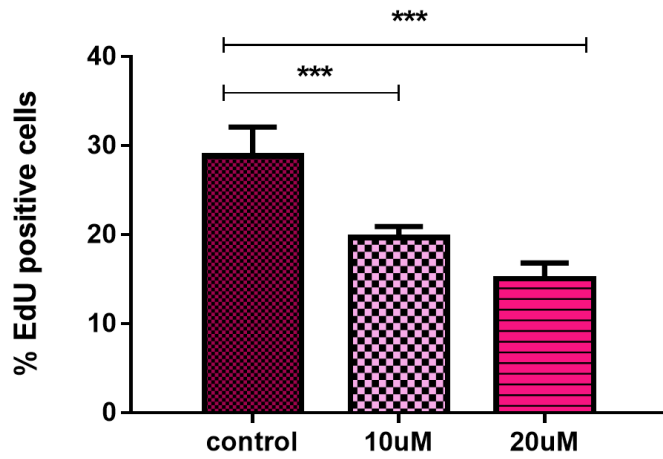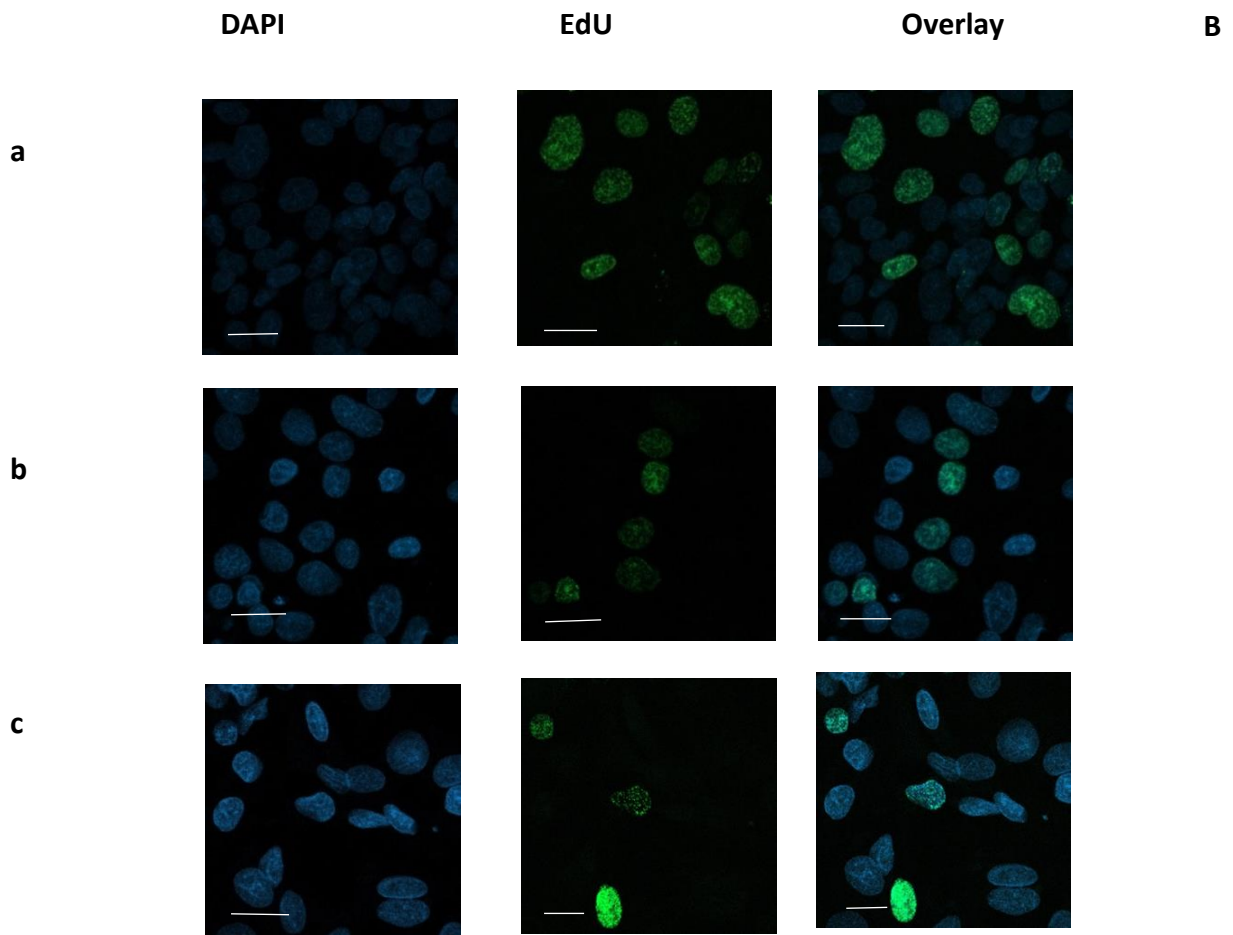
Figure 3 12. **A**. Effect of etoposide on the proliferation of HepG2 cells. The percentage of EdU-positive cells was quantified. The results are expressed as the Mean ± SD of three independent experiments (20 fields of view for each coverslip) using One-Way ANOVA with

Bonferroni's Multiple Comparison Test (***p< 0.001). **B.** Proliferating cells were labelled with EdU (green). Cell nuclei stained with DAPI (blue) (**a**: control, **b**: 10µM, **c**: 20µM). Scale bar 10µm

II. Reduction of Ki67 protein expression after etoposide treatment

To complement the measurement of the growth fraction, the expression of Ki67 was analysed using immunocytochemistry. Figure 3.13 shows the results of the Ki67 staining in treated and non-treated HepG2 cells. The percentage of Ki67 positive cells decreased from about 58% to 19% in etoposide-treated cells (p< 0.0001, figure 3.13).

DAPI   **Ki67**   **Merged**

CC
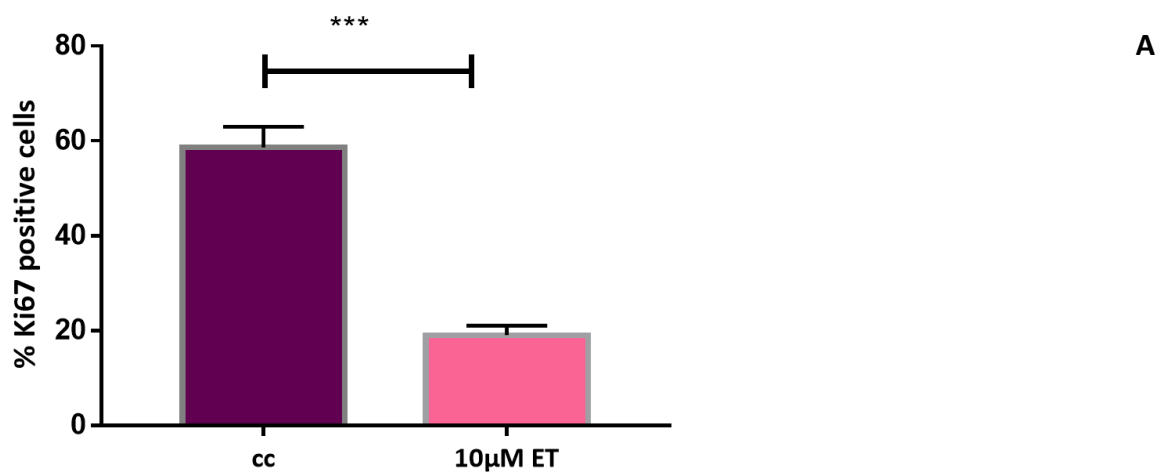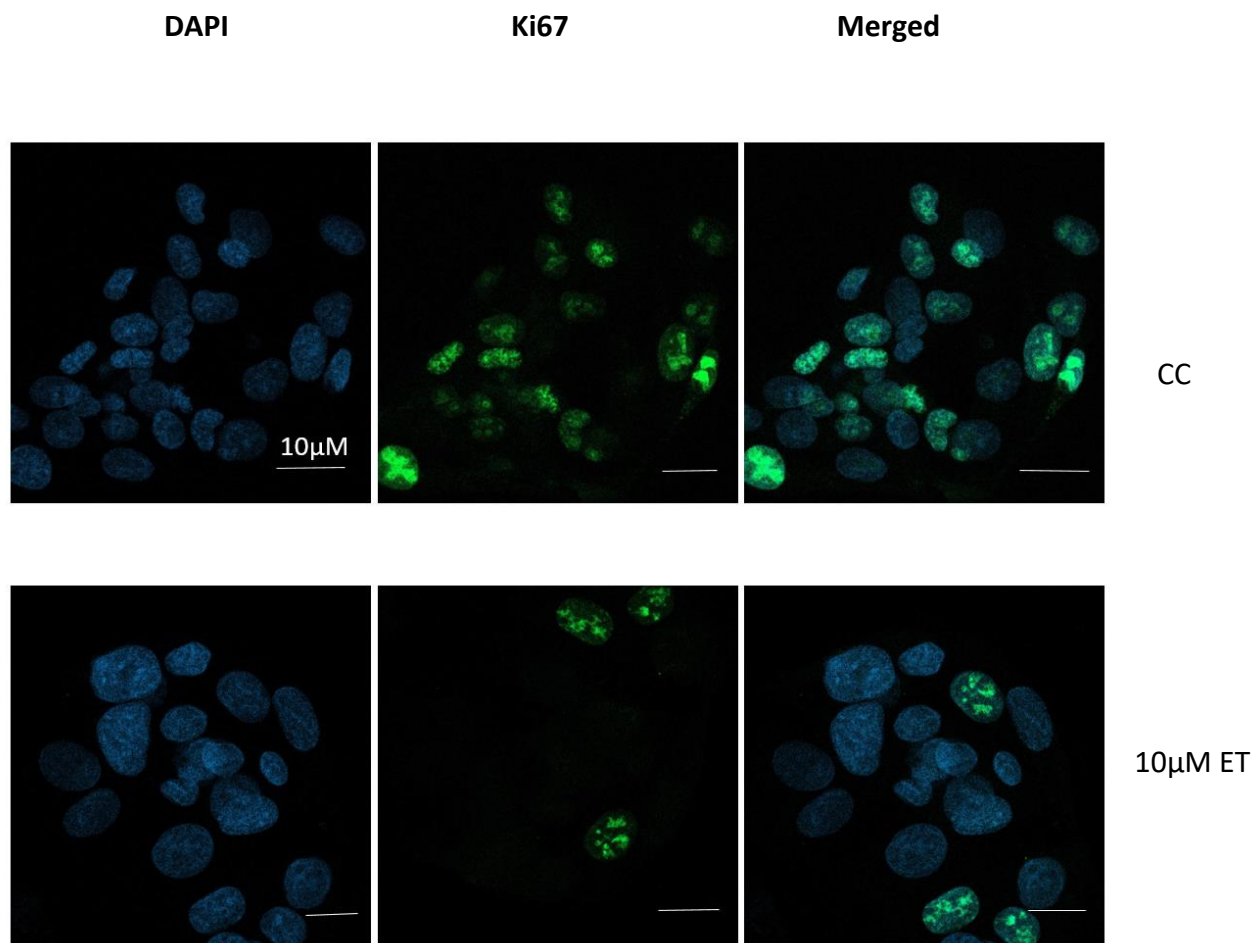
10µM ET

Figure 3.13. **A.** Expression of Ki67 antigen. HepG2 cells were treated with 10µM etoposide for 48 h. Ki67 staining was performed in duplicate and at least 100 cells were inspected to determine the percentage of Ki67 positive cells. The data are expressed as the Mean ± SD of three independent experiments using t Test (***p< 0.0001) n=3. **B**. Immunocytochemistry staining of Ki67. HepG2 cells were stained with Ki67 antibody (green) and DAPI was used to counterstain nuclei (blue) (CC: control, ET: etoposide). Scale bar 10µm.

III.   Increase of p53 protein expression after etoposide treatment

Activation of p53 protein in etoposide-treated cells is shown in figure 3.14. Figure 3.14A shows that 48% of treated cells with etoposide were stained positively for p53 and the level of p53 positive cells was much higher in treated cells compared to the control cells (p<0.0001). To confirm the immunofluorescence results for p53 staining, the level of p53 gene expression was measured by qRT-PCR. Figure 3.14C shows the comparison of p53 gene expression levels in treated cells versus control. The p53 gene expression in treated HepG2 cells was higher than in non-treated cells. However, the difference is not significant. Etoposide treatment affected the regulation of the p53 genes which resulted in higher p53 protein production compared to the control cells (figure 13.4C).

A

P53   Merged   DAPI

10µM ET

10µM

Control
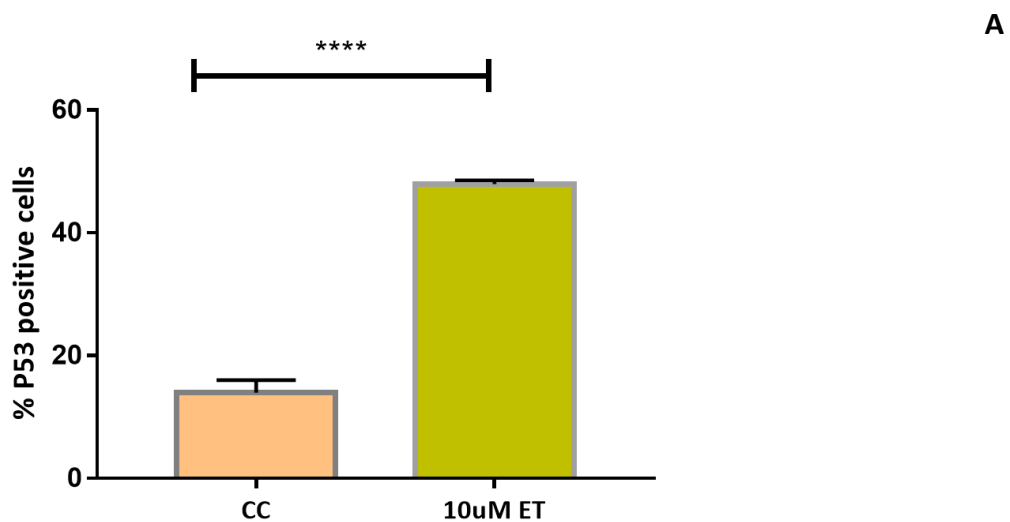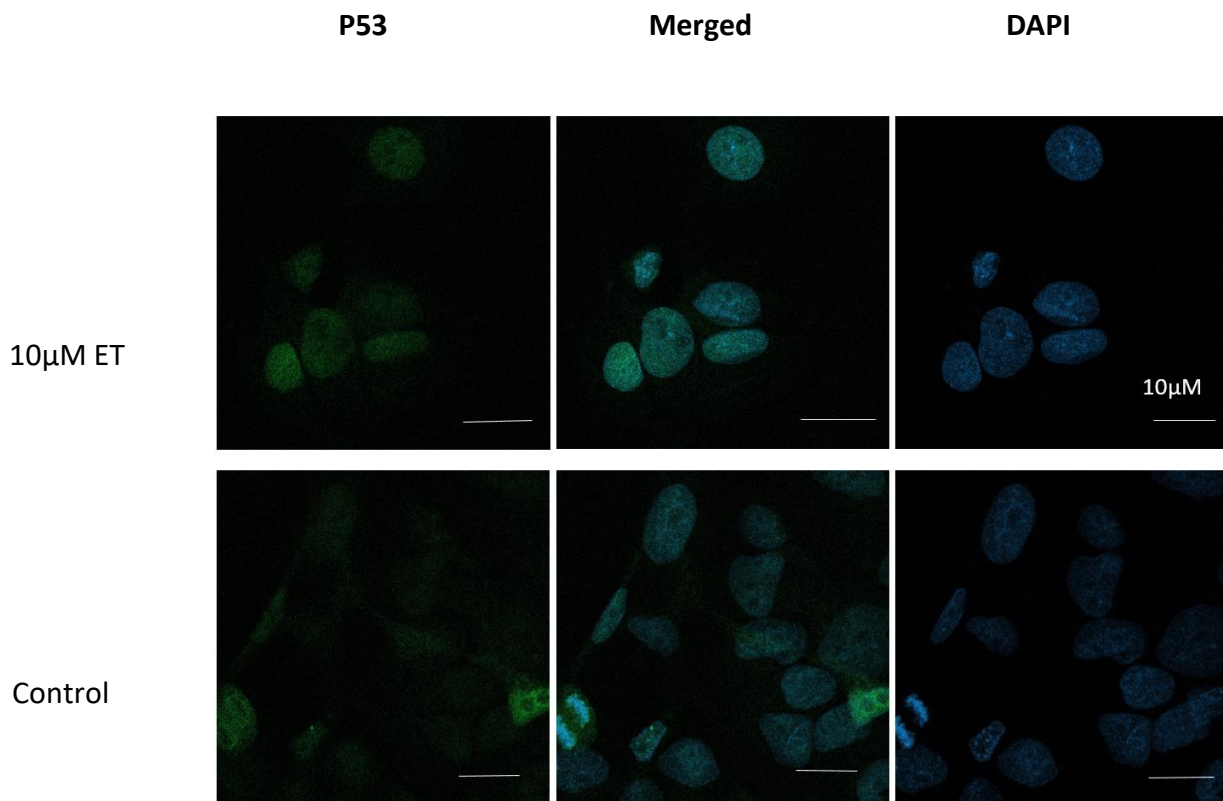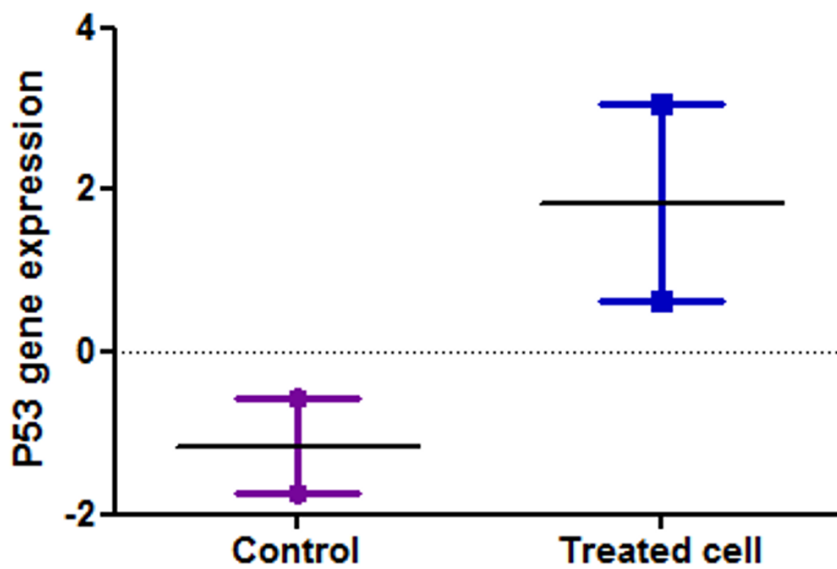
Figure 3.14. **A**. Quantification of P53 positive cells. P53 staining was performed in duplicate and at least 100 cells were inspected to determine the percentage of P53 positive cells. The

data are expressed as the Mean ± SD of two independent experiments using t Test (***p< 0.0001). **B**. Immunocytochemistry staining of p53. HepG2 cells were stained with p53 antibody (green) and DAPI was used to counterstain nuclei(blue) (ET: etoposide). Scale bar 10µm.**C**. Effect of etoposide treatment on P53 protein expression in HepG2 cells. The expression level of P53 in treated and non-treated HepG2 cells was analysed by qRT-PCR. The expression of actin was used as an internal control. Transcripts were normalised to actin and are shown as fold change over control levels.

3.4 Senescence alters key parameters of normal liver functions including albumin synthesis and urea production
3.4.1 Reduction of albumin synthesis in etoposide-treated cells

For evaluation of the functional capacity of senescent hepatocytes, albumin synthesis was measured in treated and non-treated HepG2 cells with 10µM etoposide. As HepG2 was successfully grown in HEMA-MBA-alginate cryogels with high cell viability, the total amount of albumin secretion by HepG2 cells was measured at 2-D (well plate) and 3-D surfaces (HEMA-MBA-alginate) in senescent hepatocytes and then compared with non-treated HepG2 cells. Figure 3.15 shows a decrease in albumin synthesis in etoposide-treated cells at 3-D (HM-alginate/HepG2+ET) (p<0.05) and 2-D surfaces (HepG2+ET). On 3-D surfaces, albumin production reduced significantly from 19.88±1.65 ng/mL to 13.6±2.12 ng/mL in response to 10µM ET treatment. Also, albumin synthesis decreased from 5.80± 1.32 to 1.39±0.30 when it was cultured in well plates after 48h incubation with etoposide but it's not statistically significant.
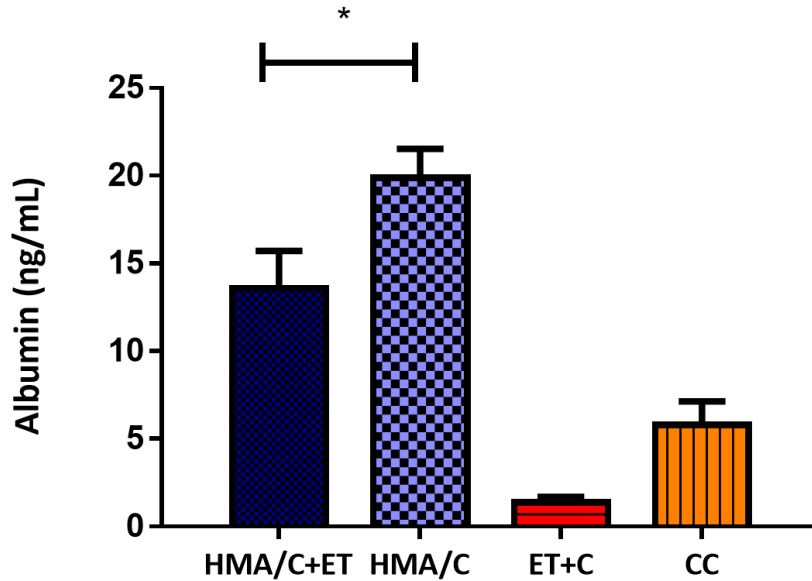
Figure 3.15. Secretion of albumin by HepG2 cells cultured on HEMA-MBA-Alginate (3-D surfaces) and 6-well plates (2-D surfaces) after incubation with 10 μM etoposide for 48h. The concentration of the albumin in the sample was determined by interpolating the blank control subtracted absorbance values against the standard curve. Data represent the mean±SD from three independent cultures. (*p<0.05) n=3 (**HMA/C +ET:** HEMA-MBA-Alginate with etoposide-treated HepG2 cells, **HMA/C**: HEMA-MBA-Alginate with HepG2, **ET+C:** Etoposide-treated HepG2 cells at 2-D surfaces**, CC:** Control cells**)**

3.4.2 Reduction of albumin gene expression in etoposide-treated HepG2 cells

The effect of etoposide on HepG2 cell synthetic activity was studied. HepG2 cells cultured on 2-D surfaces were exposed to etoposide at 10μM concentration for 48 hours. Albumin gene expression was measured by qRT-PCR in treated and non-treated cells. Figure 3.16 shows that the expression of the albumin gene in the etoposide-treated cells is down-regulated compared to albumin expression in non-treated cells (p<0.05).
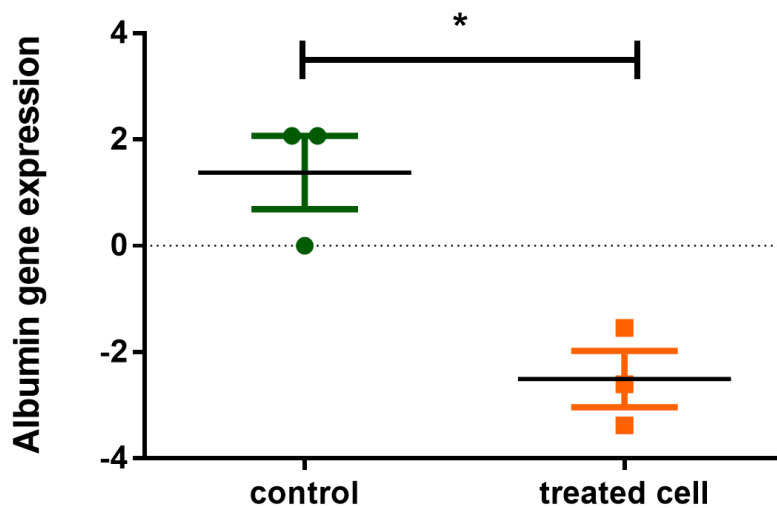
Figure 3.16. Effect of etoposide on albumin gene expression in HepG2 cells. The expression of actin was used as an internal control. Transcripts were normalised to actin and are shown as fold change over control levels. Data were analysed using an unpaired t-test. (p<0.05). n=3

3.4.3 Reduction of urea production in etoposide-treated cells

Urea production decreased significantly at 2-D and 3-D surfaces after treatment with 10µM etoposide for 48 h (p-value <0.001, figure 3.17). HepG2 at the 3-D surface (HM-alginate) in the non-treated group had an elevated level of urea production compared to a 2-D surface (increased from 3.3 to 4.2 mg/dL). However, this 3D culture system couldn't preserve the function of HepG2 after treatment with etoposide. Urea production reduced from 4.21±0.003 to 2.08±0.013 mg/dL and 3.38±0.007 to 0.722±0.050 mg/dL at 3-D and 2-D surfaces respectively.
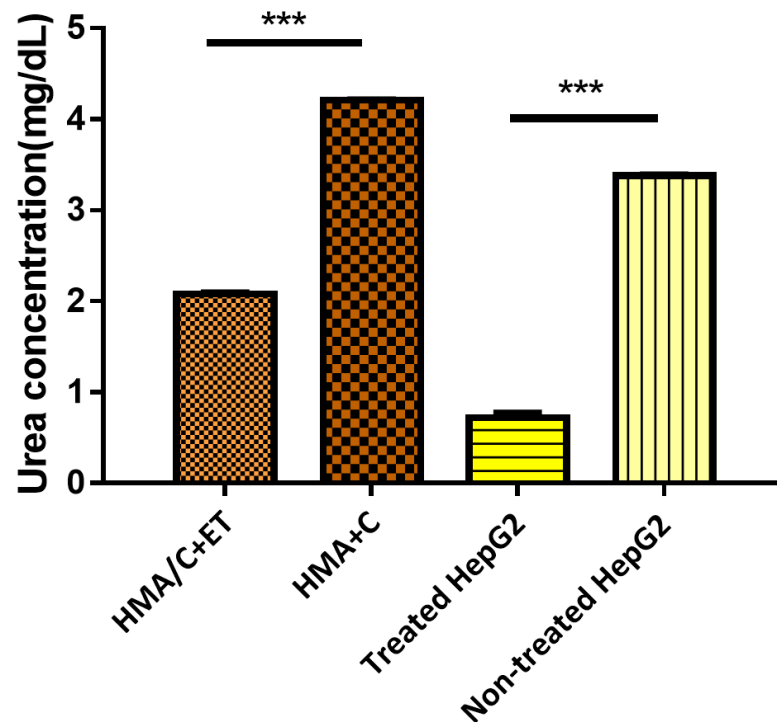
Figure 3.17. Urea production by HepG2 cells cultured on HEMA-MBA-Alginate (3-D surfaces) and 6-well plates (2-D surfaces) after incubation with 10 µM etoposide for 48h. Each sample was treated with 1mM ammonium chloride for 24 hours to stimulate urea production. Data represent the mean ± SD from three independent cultures and determinations using One-way ANOVA Tukey's multiple comparison test. (***p<0.001) **HMA/C +ET:** HEMA-MBA-Alginate with etoposide-treated HepG2 cells, **HMA+C**: HEMA-MBA-Alginate with HepG2.

3.5 Effects of liver toxins cocktail treatment on HepG2 cell proliferation and phenotype

3.5.1 HepG2 cell viability after treatment with liver toxins and cytokines on HEMA-MBA-alginate cryogels

The data in figure 3.18A shows that liver toxins and cytokines treatment did not have any significant effect on HepG2 viability. The number of viable cells reduced after both treatments (liver toxins, liver toxins+ cytokines) but it wasn't significant. This result is also confirmed by the live/dead staining performed 1 day after removing treatment.

Representative images of live cells taken with the confocal microscope at 10X magnification are reported in figure 18B.

A

B
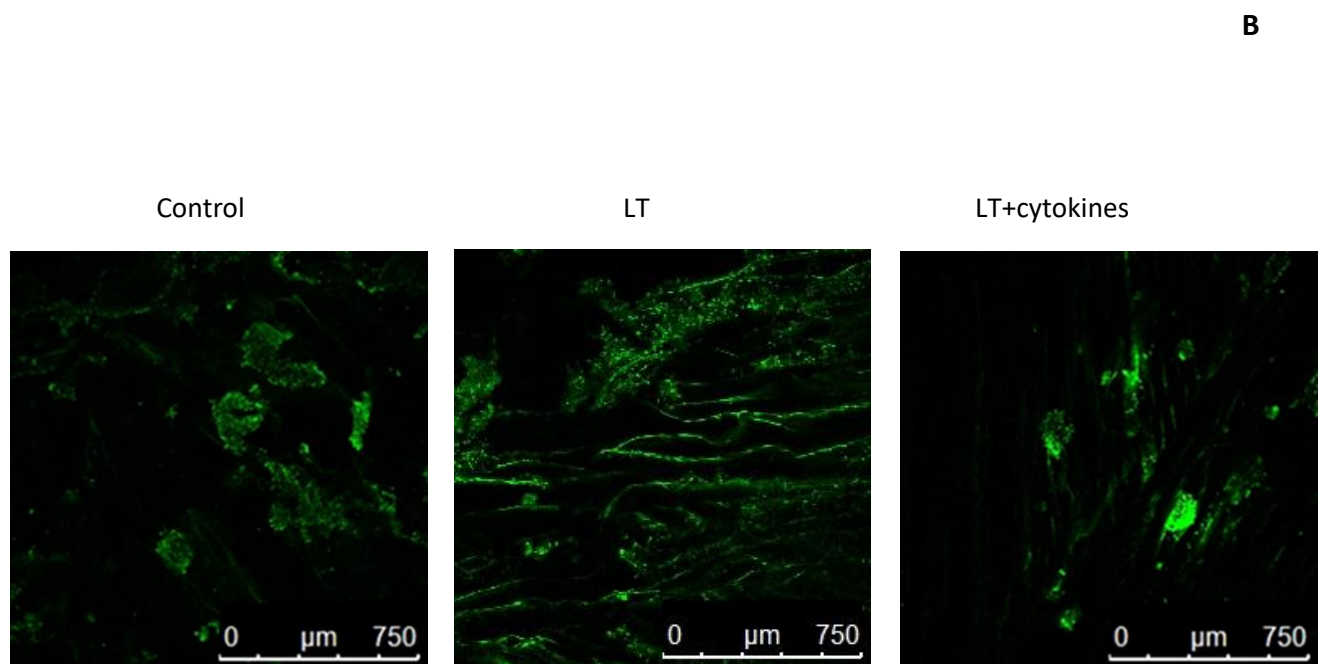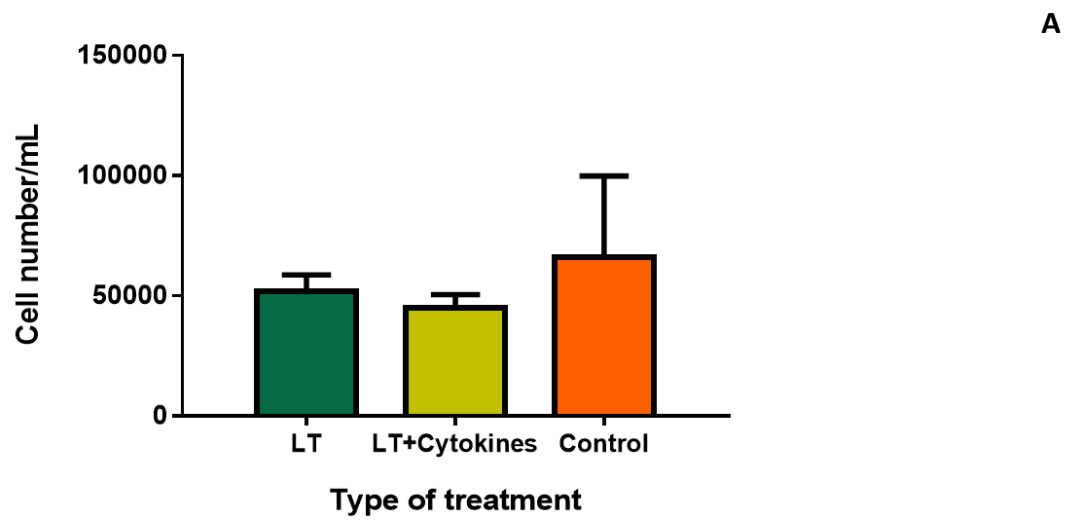
Figure 3.18. **A.** The number of viable cells on each HEMA-MBA-alginate cryogel was measured by MTT assay one day after removing treatment. Data were compared using One-Way ANOVA with Bonferroni's multiple comparison test. n=3 **B.** Live and dead staining of cryogels seeded with HepG2 cells after 6h treatment with liver toxins and cytokines treatment (LT: liver toxins). The scale bar is 750μm.

3.5.2 Induction of senescence markers after liver toxins treatment (EdU and Ki67)

- **The percentage of EdU positive cells reduced in liver toxins treated cell**

To develop an experimental system in which senescence is specifically induced after liver toxins treatment in HepG2 cells, etoposide drug an anticancer drug which causes DNA double-strand breaks was used as a positive control. Cells showing the senescence-like-growth arrest after exposure of HepG2 cells to 10µM etoposide for 48 hours (figure 3.19). The percentage of EdU positive cells reduced significantly after etoposide treatment compared to control cells (p<0.0001, figure 3.19). The cell growth inhibitory effect of liver toxins and cytokines on HepG2 cells was compared to etoposide. Similar to what had been observed about the reduction of EdU-positive cells in etoposide-treated cells, the percentage of EdU-positive cells was significantly reduced in HepG2 cells treated with liver toxins or liver toxins +cytokines (P value<0.0001). When HepG2 cells were treated with liver toxins for 6h, the percentage of EdU-positive cells decreased from 76.2% to 17.2%   and such decrease was even greater in the liver toxins+ cytokines treated group (14.78%) (figure 3.19).

| DAPI | EdU | Merged | B |

Negative control

Positive control

LT-treated

10µM

LT+ cytokines
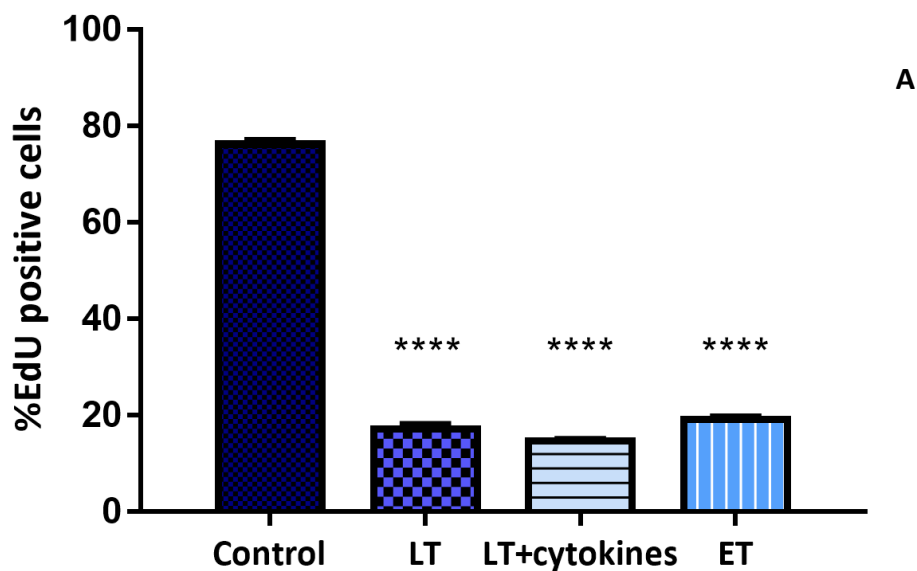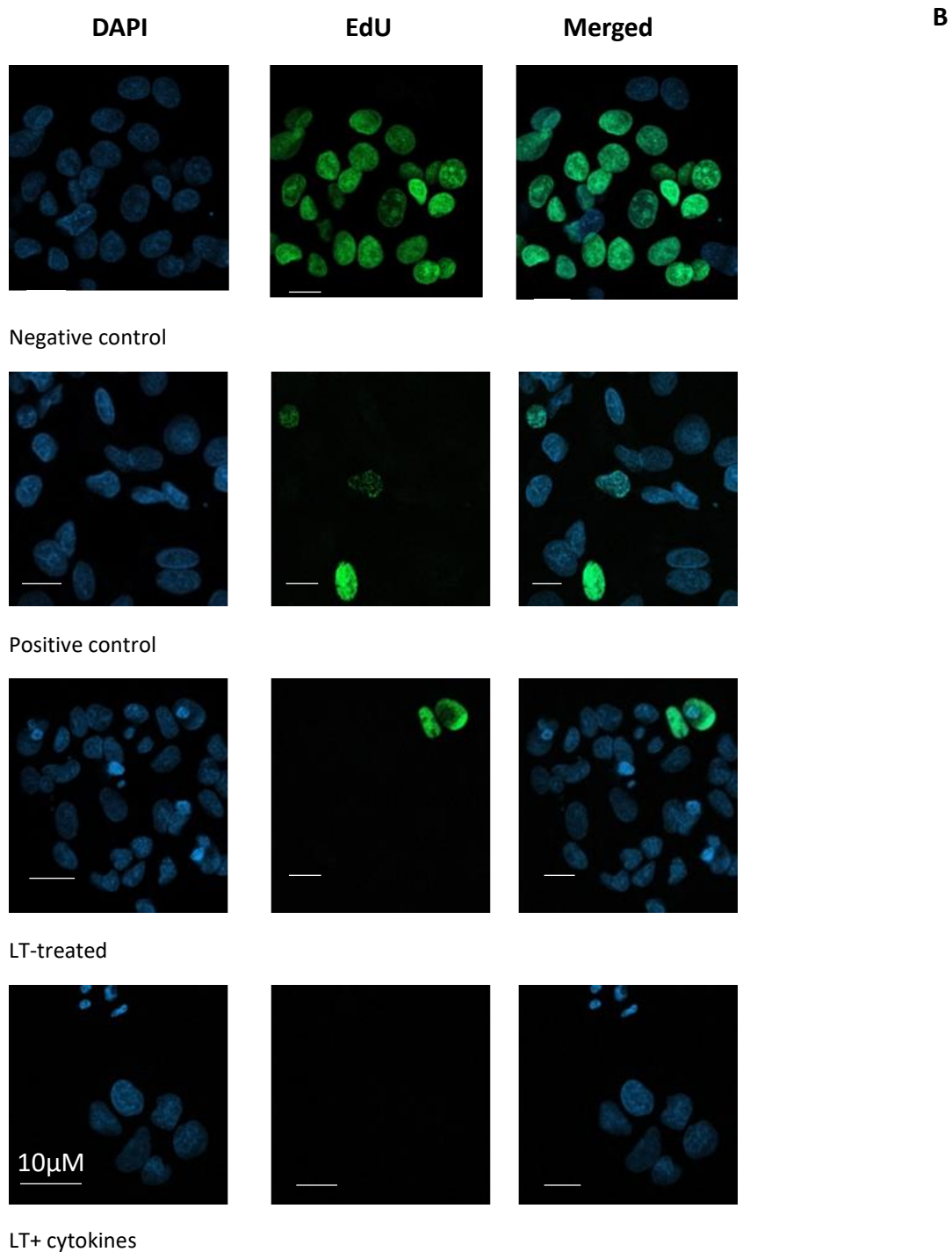
Figure 3.19. Effect of liver toxins treatment on the proliferation of HepG2 cells. **A**. The percentage of EdU-positive cells was quantified. The results are expressed as the Mean ± SD of three independent experiments using One-Way ANOVA with Bonferroni's Multiple Comparison Test (***$p < 0.0001$). **B.** Proliferating cells were labelled with EdU (green). Cell nuclei were stained with DAPI (blue). Negative control: un-treated cell, Positive control: Etoposide-treated, LT: liver toxins. Scale bar 10µm.

123

- **Reduced expression of Ki67 antigen in response to liver toxins treatment**

ICC assay with anti-Ki67 antibody staining was performed to measure the proliferative rate of HepG2 cells after liver toxins and cytokines treatment for 6h. Figure 3.20 demonstrates that Ki67 levels were reduced significantly in liver toxins and cytokines treatments compared to non-treated cells (***P value<0.001). The majority of non-treated HepG2 cells were positive for Ki67 labelling (%82). By contrast, less than %40 of liver toxins or liver toxins + cytokines treated cells were positive for Ki67 labelling, showing that HepG2 cells were not proliferating after both treatments.

A
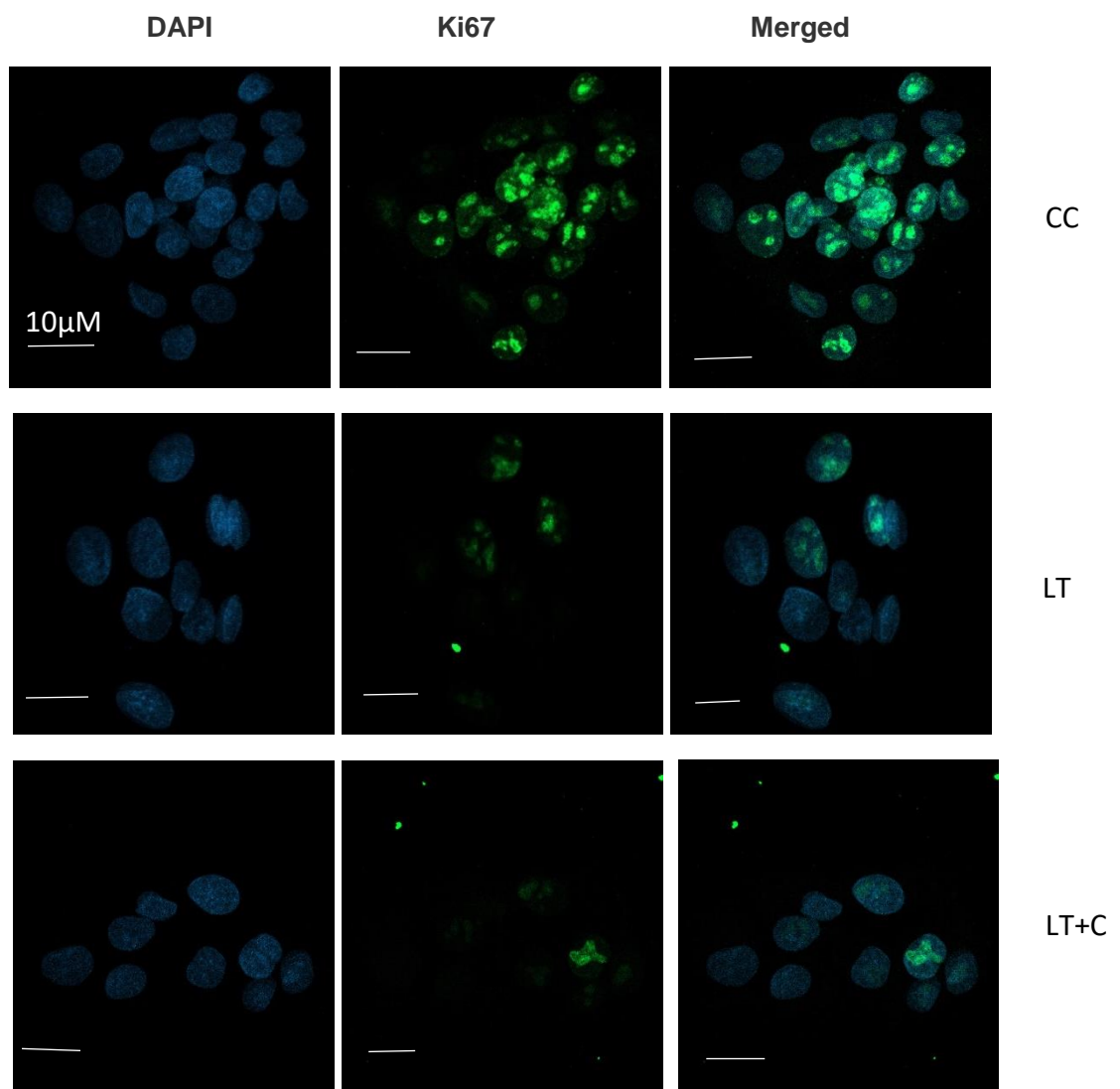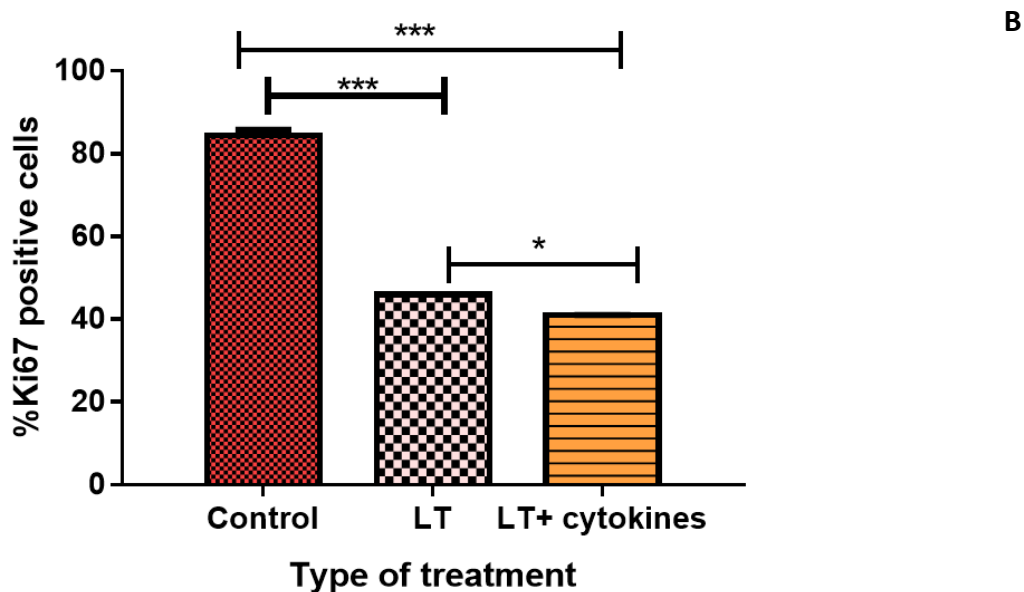
Figure 3.20. **A. Ki67 staining**. HepG2 cells were either untreated (control) or treated with liver toxins (LT) or liver toxins plus cytokines (LT+C) for 6h. HepG2 cells were stained with Ki67 antibody (green) and DAPI was used to counterstain nuclei (blue). (Scale bar 10μm) **B**. Ki67 staining was performed in duplicate and at least 500 cells were inspected to determine the percentage of Ki67 positive cells. The bar graph shows the percentage of Ki67 positive cells and data represent the average and standard deviation of three independent experiments using one-way ANOVA Bonferroni's multiple comparison test (***P value<0.0001. *P value<0.05).

3.5.3 Liver toxins, not cytokines are the primary mediators of senescence induction

Both liver toxins treatment and liver toxins plus cytokines induced senescence in HepG2 cells which resulted in a significant reduction of EdU positive cells from 56.9 ± 1.38 to 18 ± 0.94 and 14.7 ± 0.28 after both treatments, respectively (****p<0.0001, figure 3.21). The effect of individual cytokines on HepG2 proliferation was measured by EdU assay to assess whether proinflammatory cytokines in liver toxins cocktail affect HepG2 proliferation. As shown in figure 3. 21, IL-8 treatment caused a significant decrease in the percentage of EdU positive cells (p<0.05). While IL-6 and TNF-α treatments did not affect cell proliferation compared to other treatments.

125
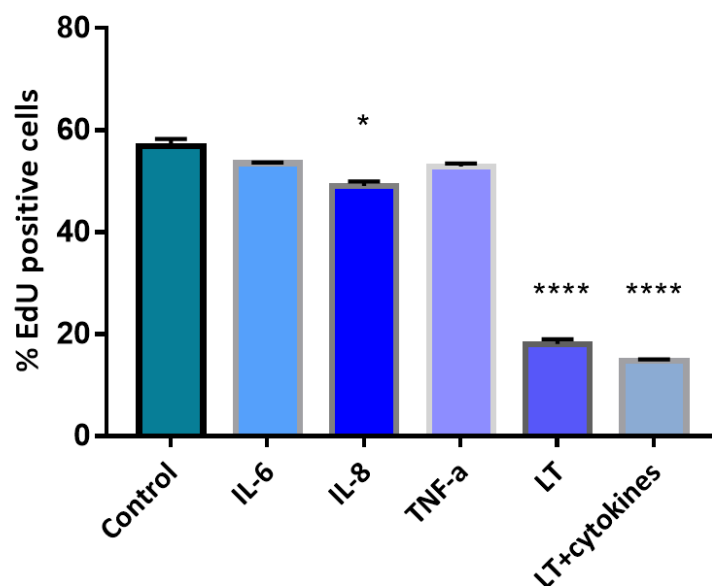
Figure 3.21. HepG2 cells were treated with individual cytokines (IL-6, IL-8 and TNF-α) at 1.0×10^{-6} cell/mL concentration and liver toxins plus cytokines combination for 6 h at 2-D surfaces. The percentage of EdU-positive cells was quantified. The results are expressed as the Mean ± SD of three independent experiments using One-Way ANOVA with Bonferroni's Multiple Comparison Test (*$p<0.05$, ****$p<0.0001$). **LT**: liver toxins-treated cell

3.5.4 Effect of liver toxins cocktail treatment on albumin and urea production

The results in figures 3.22 and 3.23 shows the loss of hepatocyte functions after liver toxins treatment. A significant decrease in albumin production by HepG2 cells was measured after liver toxins cocktail treatment at 2-D and 3-D surfaces, decreasing from 0.47 ± 0.05 to 0.019 ±0.04 µg/mL and 0.27 ±0.02 to 0.014 ± 0.01 µg/mL at 3-D and 2-D surfaces, respectively (figure 3.22). Similar to albumin production results, urea synthesis was reduced significantly after 6h exposure to liver toxins cocktail at 2-D and 3-D surfaces ($p<0.01$, $p<0.001$, figure 3.23). The level of urea synthesis at 3-D surfaces reduced from 12.08±0.40 to 1.33±0.80 mg/dL and at 2-D surfaces reduced from 7.03±1.12 to 0.90±0.09 mg/dL after liver toxins treatment.
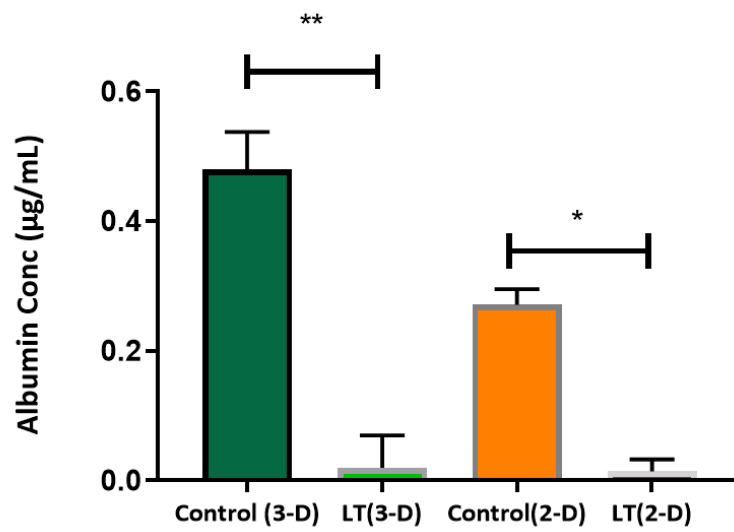
Figure *3.22.* Albumin production on 3-D (HEMA-MBA-alginate cryogel) and 2-D (12 well plates) surfaces (n=3) at 48 h after removing liver toxins treatment (LT). Values represent mean ± SD of three independent experiments. Statistical analysis was performed using one-way ANOVA with Bonferroni's post-hoc test (**p < 0.01, *p<0.05).
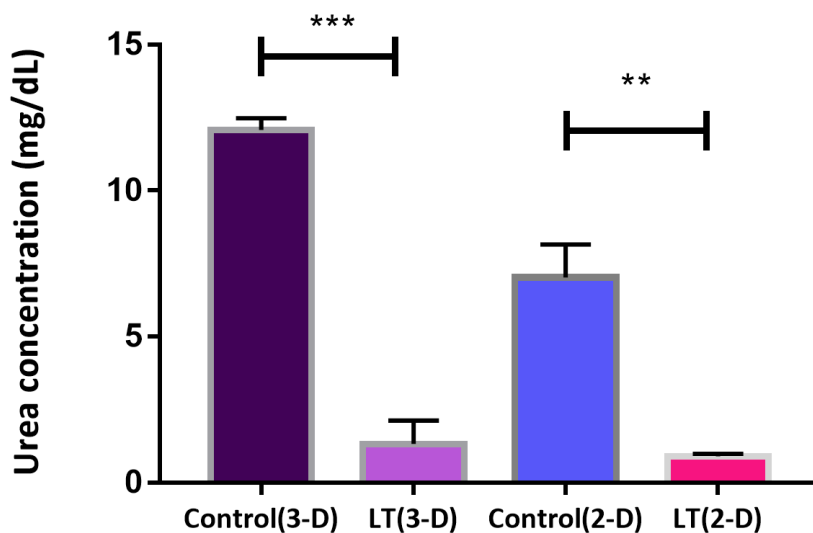
Figure 3. 23. Urea production after 24h post stimulation with ammonium chloride on 3-D (HEMA-MBA-alginate cryogel) and 2-D (12 well plates) surfaces (n=3) at 48 h after removing liver toxins treatment (LT). Values represent mean ± SD. Statistical analysis was performed using one-way ANOVA with Bonferroni's post-hoc test (***$p < 0.001$, **$p<0.01$).

3.6 Senescence induction can be blocked by pre-treatment with resveratrol

3.6.1 Dose-response curve of resveratrol

The effect of resveratrol on HepG2 cell proliferation was measured by an EdU assay to see whether resveratrol at 2, 5, 10 and 25 µM concentrations affects cell growth after 24 h incubation. Figure 3.24 shows the dose-response curve following exposure to resveratrol at the mentioned doses. The number of EdU positive cells increased significantly after 24h exposure to 2 and 5 µM doses of resveratrol ($p<0.05$, $p<0.01$) and more than 70% of the cell were stained positively for EdU. The percentage of EdU positive cells increased from 63.6%±0.74 to 75.03%±2.37 and 79.84±3.79 after treatment with 2 and 5µM concentrations of resveratrol respectively. While RSV at 10 µM concentration slightly inhibited the growth of HepG2 cells compared to the non-treated group (58.51±0.075 vs 63.6%±0.74). Also, resveratrol at 25 µM concentration caused about a 50% reduction in proliferation compared

128

to the non-treated cell (p<0.001, figure 3.24). The results suggest that resveratrol at a concentration ≥ 10 µM can inhibit cell proliferation. The subsequent experiments were carried out using 2 and 5 µM of resveratrol.
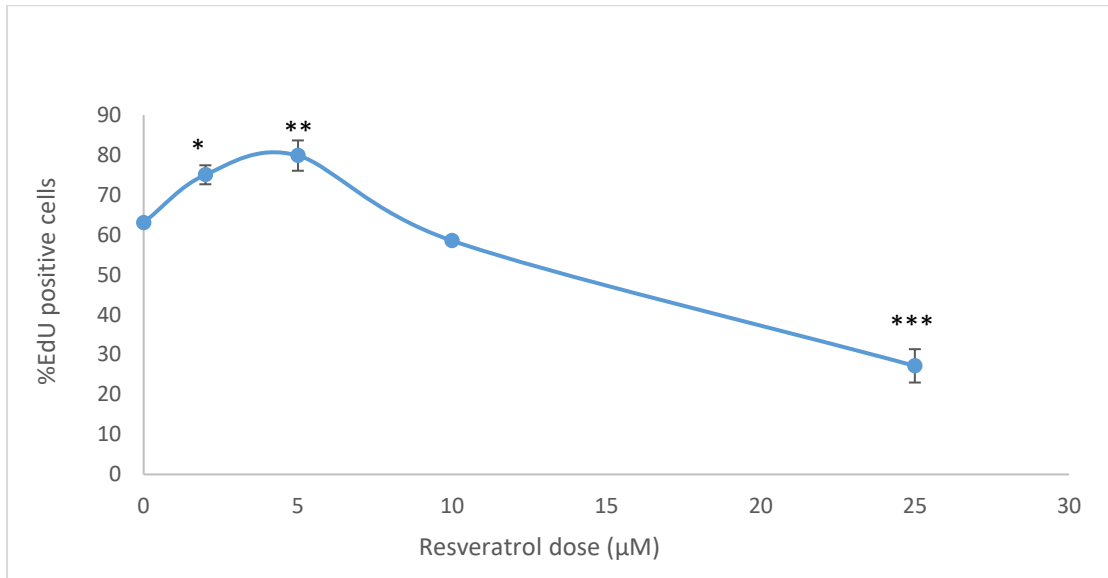
Figure 3.24. **Dose-response curve of RSV**. Results are expressed as mean±SD using One-way ANOVA Bonferroni's Multiple Comparison Test (***p< 0.001, **p<0.01, *p<0.05). n=3

3.6.2 The percentage of EdU positive cells increased after resveratrol treatment

The protective effect of resveratrol against senescence induced by liver toxins was measured by EdU labelling at 2-D and 3-D surfaces and it is shown in figures 3.25 and 3.26. The percentage of EdU-positive cells was reduced significantly at 2 and 3-D surfaces compared to the control cells after 6 h of treatment with liver toxins and cytokines (P<0.001) (figures 3.25 and 3.26). However, the percentage of EdU-positive cells increased significantly in the presence of 2 and 5 µM of resveratrol on both surfaces (p<0.01, p<0.001). The percentage of EdU positive cells at 3-D surfaces was 60.02%±0.35, 65.06%±1.82 and 42.28%±1.40 in 2 and 5µM resveratrol-treated cells and liver toxins-treaded cells respectively (figure 3.26). The EdU results show that RSV at 5 µM doses can better protect the cells against liver toxins effects compared to the 2 µM doses on both

129

surfaces. In 2-D surfaces, about 45% of cells were stained positively with EdU at 5µM concertation compared to the 2µM concertation (43%) ([figure 3.25](#)). Also, 65% of HepG2 cells were stained positively after 5µM resveratrol treatment on 3-D surfaces in comparison to 2µM (60%). The results in [figures 3.25](#) and [3.26](#) proved that resveratrol inhibits HepG2 cells senescence which is induced by liver toxins treatment and the level of protection is dose-dependent manner.

A
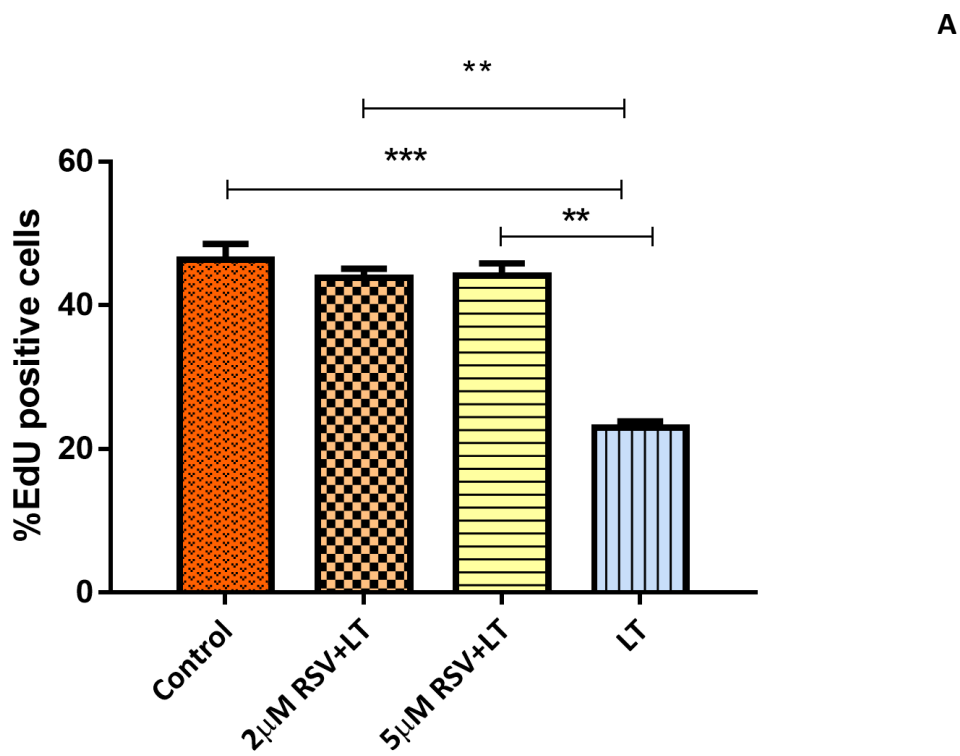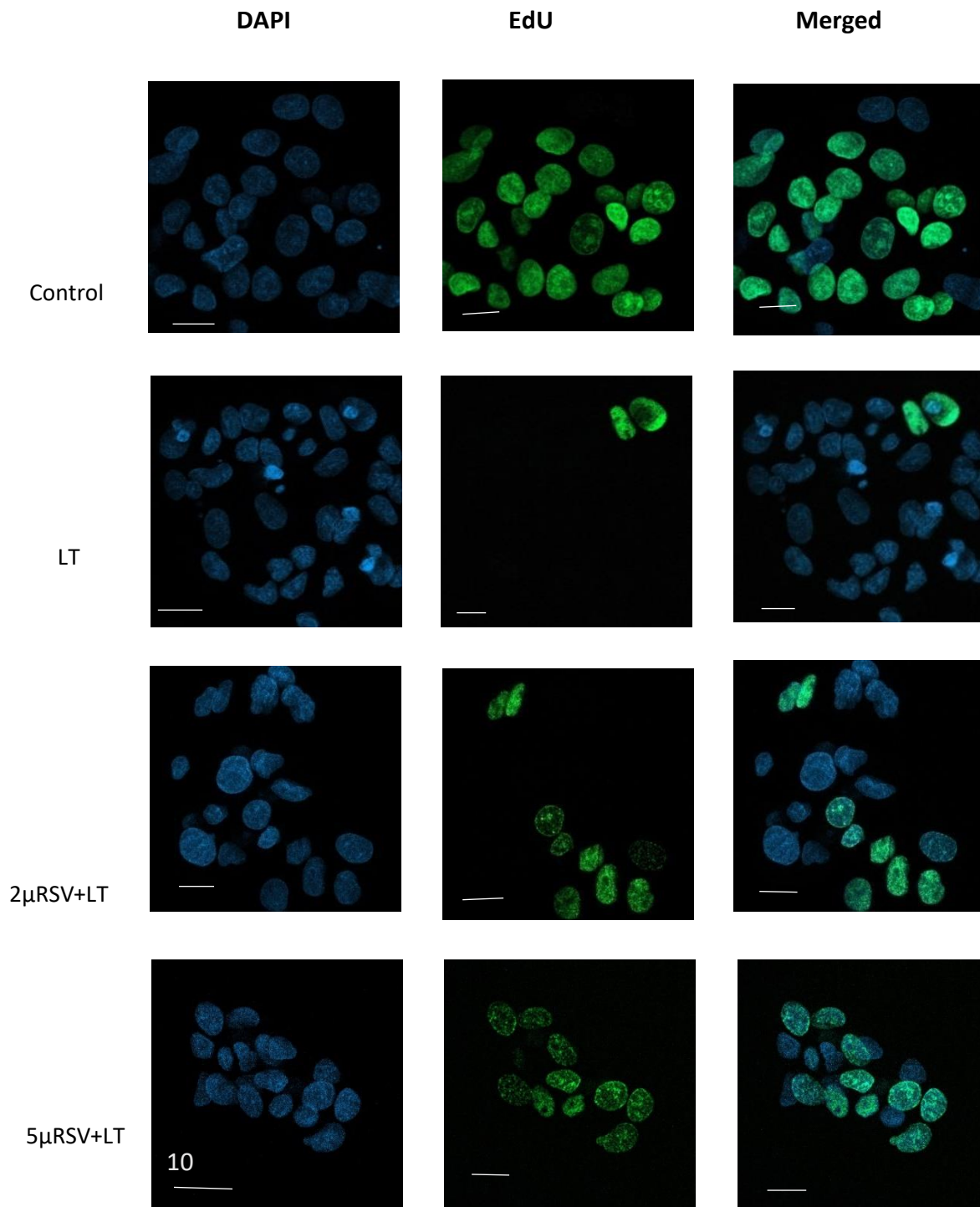
Figure 3.25. **The percentage of EdU-positive cells in 2-D surface (coverslips). A**. Data are presented as the Mean ± SD of EDU positive cells using One-Way ANOVA with Bonferroni's Multiple Comparison Test (***p< 0.001, **p<0.01) (n=3). At least 500 cells were counted on

each coverslip. **B**. Cells were counterstained with DAPI (blue) and EdU stain showed green light (scale bar 10μM). **RSV+ LT/RSV (2μM):** Pre-treated with RSV at 2μM concentration for 24 h and then treated with liver toxins and RSV at 2μM concentration and incubated for 6h. **RSV+ LT/RSV (5 μM):** Pre-treated with RSV at 5μM concentration for 24 h and then treated with liver toxins and RSV at 5μm concentration incubated for 6h. **LT**: liver toxins-treated cell.
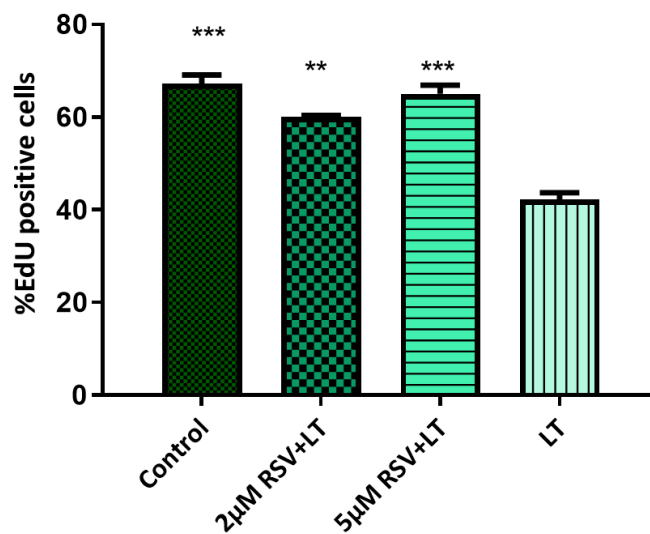
Figure 3.26. **The percentage of EdU-positive cells in 3-D surface (HEMA-MBA-alginate cryogel)**. Data are presented as the Mean ± SD of EDU positive cells using One-Way ANOVA with Bonferroni's Multiple Comparison Test (***p< 0.001, **p<0.01) (n=3). At least 300 cells were counted on each cryogels. **RSV+ LT/RSV (2μM)**: Pre-treated with RSV at 2μM concentration for 24 h and then treated with liver toxins and RSV at 2μM concentration and incubated for 6h. **RSV+ LT/RSV (5μM)**: Pre-treated with RSV at 5μM concentration for 24 h and then treated with liver toxins and RSV at 5μM concentration incubated for 6h. **LT**: liver toxins.

3.6.3 Increased Ki67 protein expression in response to resveratrol treatment at 2-D and 3-D surfaces

Immunostaining of Ki67 in HepG2 cells was carried out to assess if resveratrol can reverse the anti-proliferative effect of senescence induced by liver toxins. ICC analysis of Ki67 labelling showed that the total number of stained cells with Ki67 decreased significantly after exposure to liver toxins for 6h at both 2 and 3-dimensional surfaces ($p<0.001$ and $p<0.01$ respectively) (figure 3.26 and 3.27). Whereas the percentages of Ki67 positive cells in the liver toxins-treated group were increased from 22.78%±0.04 to about 56.09%±0.38 and 57.88±3.28 in the presence of 2 and 5 µM resveratrol at 2-D surfaces (figure 3.27). Consistent with these results, the percentage of Ki67 positive cells was increased remarkably in resveratrol treated groups compared to liver toxins treated cells at 3-D surfaces ($p<0.001$, figure 3.28). Ki67 positive cell counting revealed that treatment of HepG2 cells with resveratrol at 2 and 5 µM doses had a significantly higher proportion of proliferating cells (67% and 72% respectively) in comparison with the liver toxins treatment in 3-D surfaces (P value<0.01). On both surfaces, a fewer number of Ki67 positive cells were observed in 2 µM concentration of resveratrol versus 5 µM but there are not any significant differences.
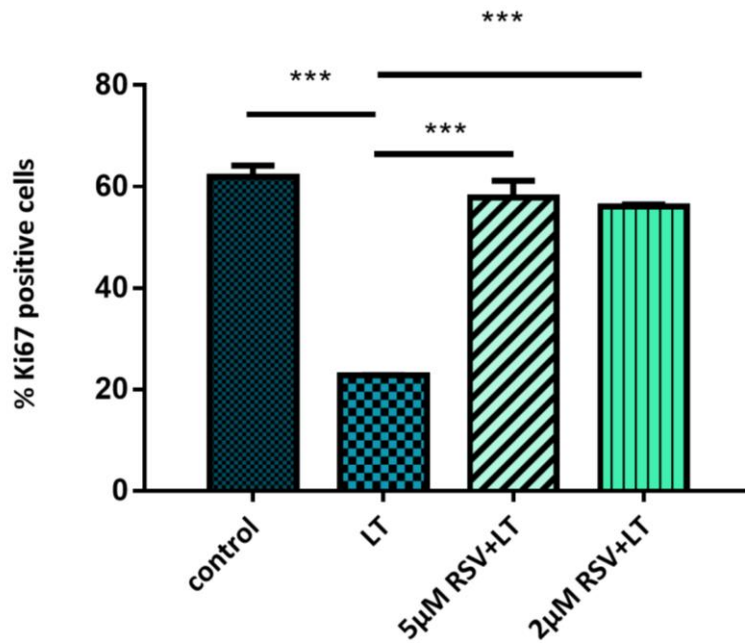
Figure 3.27. **The percentage of Ki67 positive cells in HepG2 cells cultured 2D matrices**. The bar graph shows the percentage of Ki67 positive cells and data represent the average and standard deviation of two independent counts of cells using one-way ANOVA Bonferroni's multiple comparison test ***P value<0.0001 (n=3). **RSV+LT/RSV**: pre-treated with resveratrol and then treated with liver toxins and resveratrol. **LT**: liver toxins
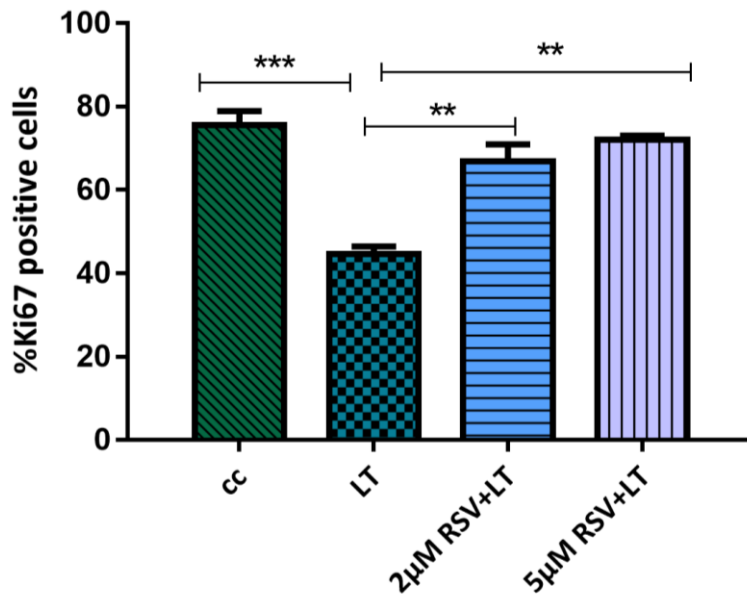
Figure 3.28. **The percentage of Ki67 positive cells in HepG2 cells cultured 3D matrices.** The bar graph shows the percentage of Ki67 positive cells and data represent the average and standard deviation of three independent experiments using one-way ANOVA Bonferroni's multiple comparison test. (**P value<0.01). (n=3)

3.7 Treatment with resveratrol protects key liver functions (albumin/urea)

3.7.1 Albumin production

Figure 3.29 shows that liver toxins treatment caused a significant reduction in albumin production at both 2 and 3-D culture systems (p<0.05, p<0.0001 respectively). Non-treated HepG2 secreted more albumin 0.479± 0.05 µg/mL than liver toxins-treated cells 0.0199±.04 µg/mL concentration of albumin at 3-D surfaces. The albumin production by non-treated HepG2 cultured on 2-D surfaces was 0.271±0.02 µg/mL which is significantly higher than albumin production by HepG2 -treated with liver toxins (0.014± 0.01 µg/mL). However, albumin production by HepG2 cells increased significantly in the presence of 2 and 5 µM doses of resveratrol in comparison to the liver toxins treated group. Conditioned media from HepG2 cultured on 3-D surfaces showed higher albumin when treated with 5 µM

135

resveratrol (0.471µg/mL) and 2 µM resveratrol (0.246µg/mL) in comparison to liver toxin-treated cells (0.0199 µg/mL) at 3-D surfaces (p<0.0001, p<0.05 respectively, figure 3.29).
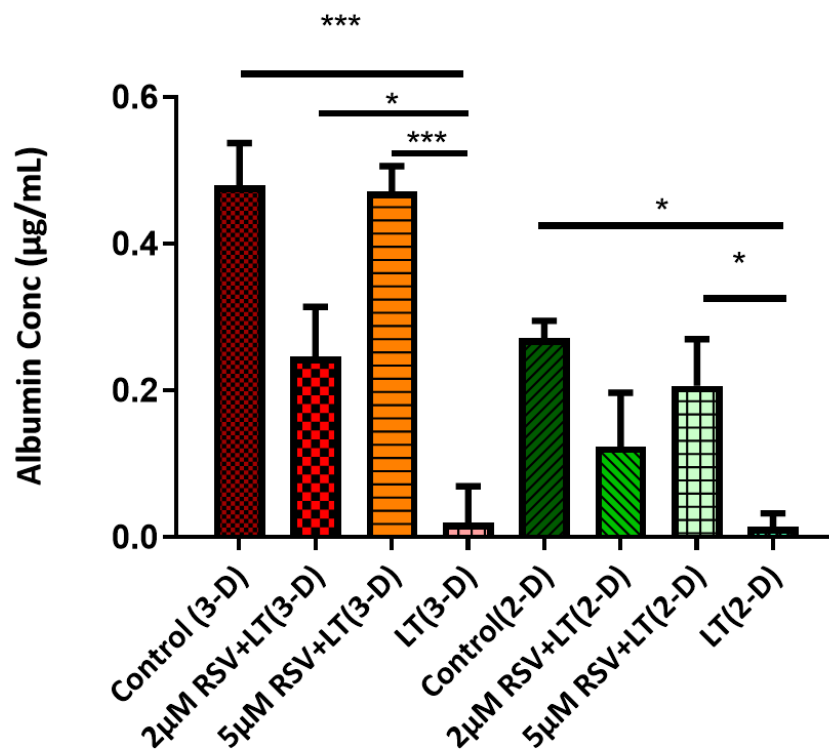
Figure 3.29. Secretion of albumin by HepG2 cells cultured on HEMA-MBA-Alginate (3-D surfaces) and 6-well plates (2-D surfaces) after treatment with liver toxins and resveratrol (RSV). The concentration of the albumin in the sample was determined by interpolating the blank control subtracted absorbance values against the standard curve. Data represent the mean± SD from three independent cultures and determinations using one-way ANOVA Bonferroni's multiple comparison test. ***P value<0.001, *p<0.05) (n=3). LT: liver-toxins treated cells.

3.7.2 Urea Synthesis

Figure 3.30 shows urea production measured at 24 h after stimulation with 1mM NH4Cl in the 24-well plate (2-D) and HEMA-MBA-alginate cryogels (3-D). The level of urea synthesis by HepG2 cells reduced significantly after liver toxins treatment at both 2 and 3-D surfaces (p <0.05, p<0.0001 respectively). At 3-D and 2-D surfaces, non-treated HepG2 (control) cells produced more urea 12.083 and 7.034 mg/dL respectively compared to liver toxins treated cells (1.33 mg/dL at 3-D and 0.901mg/dL at 2-D). HepG2 cells cultured on 3-D surfaces after 2 and 5 µM resveratrol with liver toxins treatment showed significantly higher (p<0.0001) conversion of ammonia to urea (11.652, 12.166 mg/dL respectively) compared to liver toxins treated cells (1.33 mg/dL). So, resveratrol at 2 and 5µM concentrations can protect the urea synthesis from liver toxins effects (figure 3.30).
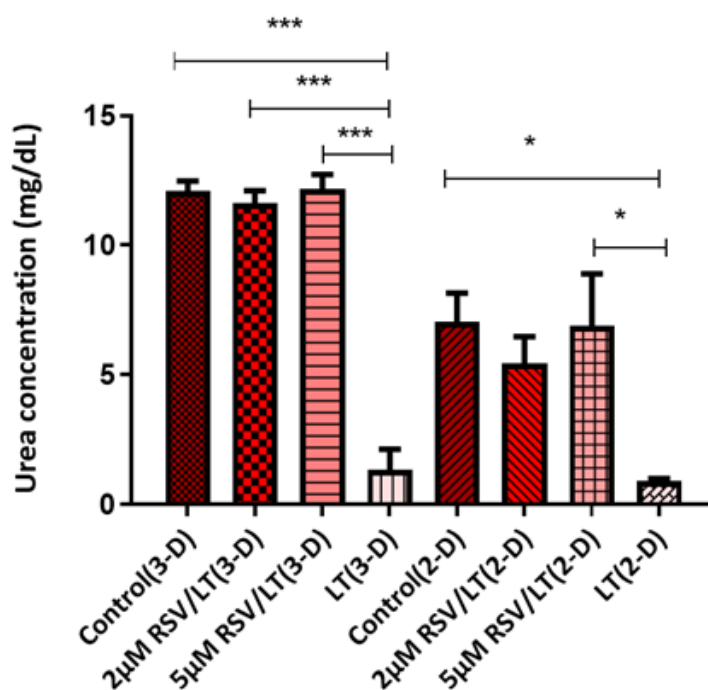
Figure 3.30. Urea production by HepG2 cells cultured on HEMA-MBA-Alginate (3-D surfaces) and 6-well plates (2-D surfaces) after incubation with liver toxins for 6h. Data represent the mean± SD from three independent cultures and determinations using One-Way ANOVA with Bonferroni's Multiple Comparison Test (***p<0.0001, *p<0.05). (n=3)

3.8 Resveratrol and resveralogues protected HepG2 cells growth against liver toxins treatment at 2-D surfaces

The result in figure 3.31 shows that HepG2 cell growth was protected against liver toxins effect. Vitamin-C, resveratrol, dihydroresveratrol and resveralogues (V34, V31 and V29) showed a significant increase in HepG2 proliferation compared to liver toxins treated cells ($p < 0.0001$, figure 3.31). The percentage of EdU positive cells in non-treated (control) cells reduced from 50% to 18% in liver toxins-treated cells. However, the number of EdU positive cells increased significantly in the presence of different SIRT-1 dependent and independent compounds and more than 40% of the cells were stained positively with EdU. Although, the number of EdU positive cells increased significantly after treatment with V29 ($p < 0.001$) compared to liver toxins treated cells, at the same concentration V29 was found to be less effect on cell protection against liver toxins than other compounds.
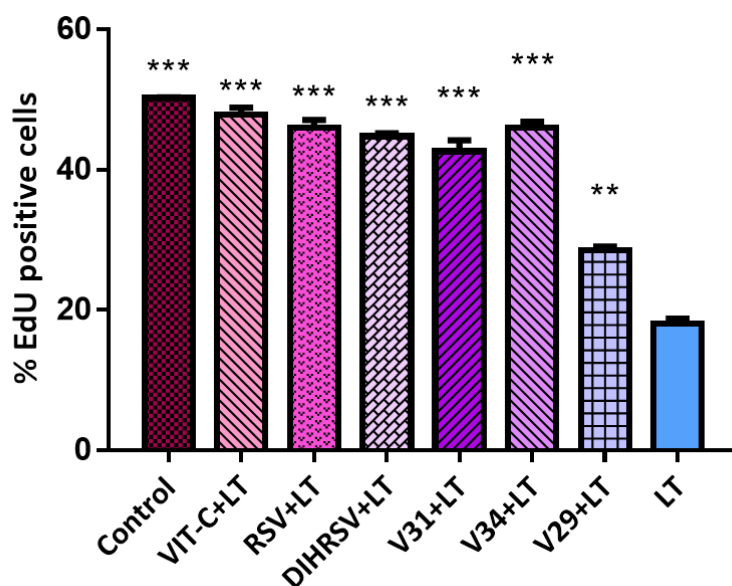
Figure 3.31. The bar graph shows the percentage of EdU positive cells and data represent the average and standard deviation of two independent counts of cells using one-way ANOVA Bonferroni's multiple comparison test ***P value<0.001 **P value<0.01 (n=3). At least 500 cells were counted on each coverslip. (**VIT+C +LT**: pre-treated with 5µM Vitamin-C for 24 h and then treated with liver toxins and vitamin-C at mentioned dose for 6h. **RSV+LT**: Pre-treated with resveratrol at 5µM concentration for 24 h and then treated with liver toxins

and resveratrol for 6h. **DIHRSV+LT**: Pre-treated with dihydro-resveratrol at 5µM concentration for 24 h and then treated with liver toxins and Dihydro-RSV for 6h. **LT**: Liver toxins).

3.9 Resveratrol derivatives protected HepG2 metabolic function against liver toxins effect in 3-D culture system

The data obtained from the albumin ELISA assay showed that the level of albumin production was increased significantly after treatment with resveratrol, dihydro resveratrol and V29 compared to liver toxins treated cells (p<0001, figure 3.32A). Similarly, a notable increase was observed in urea synthesis after treatment with resveratrol and dihyro-resveratrol (p<0.01), v29 (p<0.01) and vitamin-C (p<0.01) in comparison to liver toxins treated cells (figure 3.32 B).

Column1	Control	RSV+LT	LT	DIHRSV+LT	V29+LT
Albumin Conc(ng/ml)	21.90060852	21.74509804	12.4820825	21.03515889	21.03515889
STDEV	0.0593043	0.029194748	0.17267407	0.074312404	0.068602721
Albumin Conc ng/ml (*20 dilution factor)	438.0121704	434.9019608	249.64165	420.7031778	420.7031778
Albumin Conc µg/ml	0.43801217	0.434901961	0.24964165	0.420703178	0.420703178

A   **B**
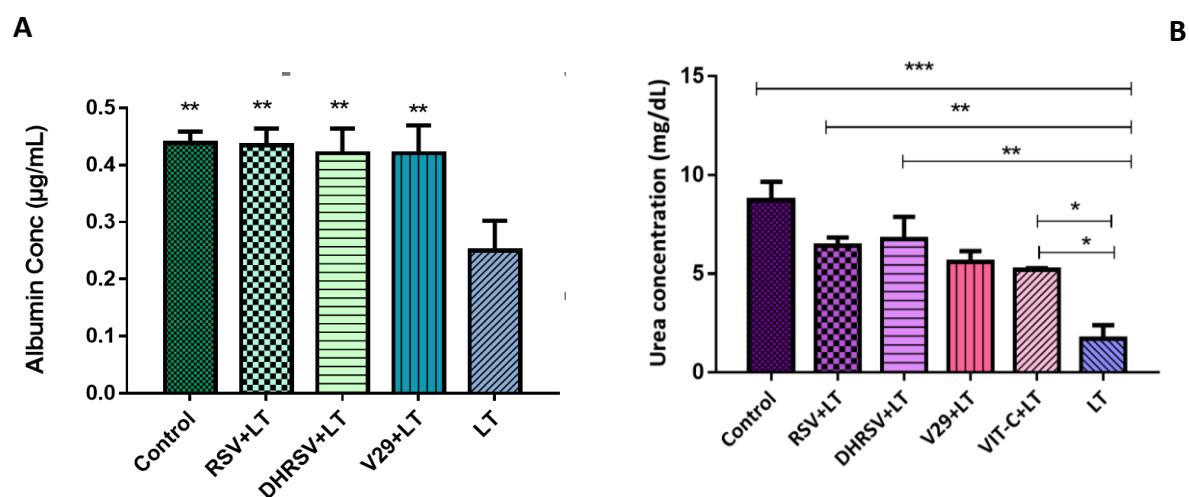
Figure 3.32. Secretion of albumin and urea by HepG2 cells cultured on 3-D surfaces (HEMA-MBA-Alginate) after treatment with liver toxins and resveratrol derivatives. Data represent the mean SD from two independent cultures and determinations using one-way ANOVA Bonferroni's multiple comparison test. ***p<0.001, **p<0.01, *p<0.05) (n=3)

3.10 Design the bioreactor prototype to measure hepatocyte key metabolic functions after exposure to a medium containing liver toxins and cytokines

3.10.1 Live/dead imaging

The cell viability in the multi-layered bioreactor was assessed using Live and dead assay 3 days after resveratrol and liver toxins treatment. The confocal images demonstrate that most cells were viable even after liver toxins treatment. Most of the DAPI-stained cells were stained positively with Calcin-AM which represents the number of live cells (figure 3.33).
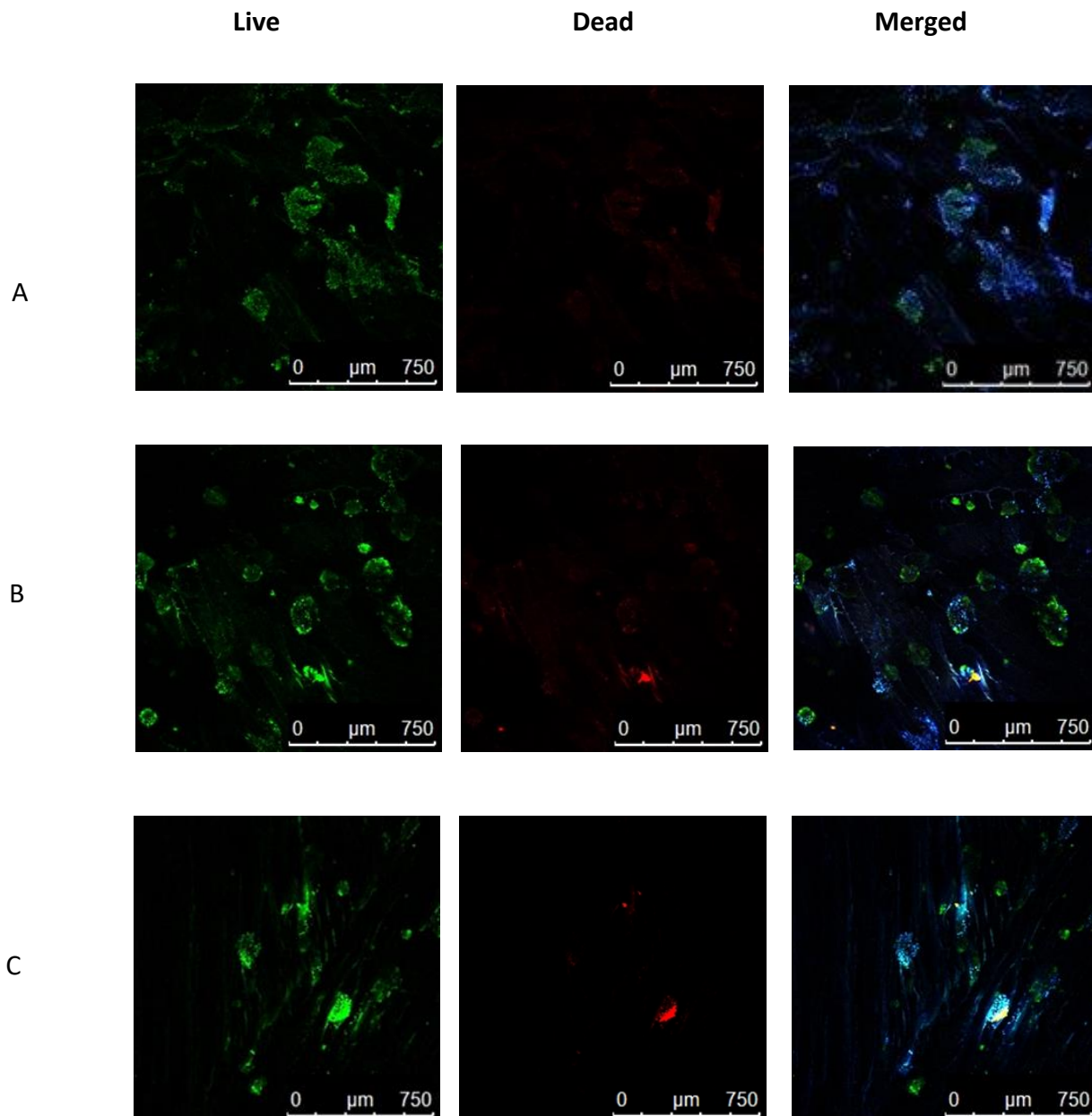
Figure 3.33. Representative live/dead confocal images of cryogel discs after 5µM resveratrol and liver toxins treatment in multi-layered bioreactor prototype. (A: control, B: 5µM RSV+LT, C: LT)

3.10.2 Liver toxins treatment-induced senescence in HepG2 cell in a multi-layered bioreactor

Figure 3.34B shows the percentage of EdU-positive cells in a multi-layered bioreactor porotype. The percentage of EdU positive cells reduced from 75% in control cells to 40% in liver-toxins treated cells. While there are not any significant differences in the percentage of EdU positive cells between control and 5µM resveratrol plus liver toxins-treated cells. The number of cells which stained positively with EdU in the resveratrol-treated group increased significantly in comparison to the liver toxins treated group (p<0.001, figure 3.34).

DAPI

EdU

5μM
RSV+LT

100μM
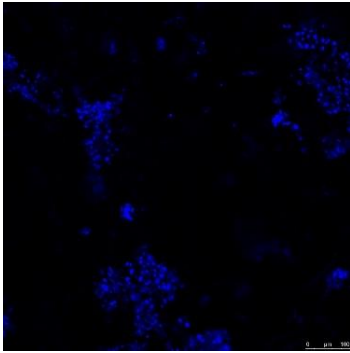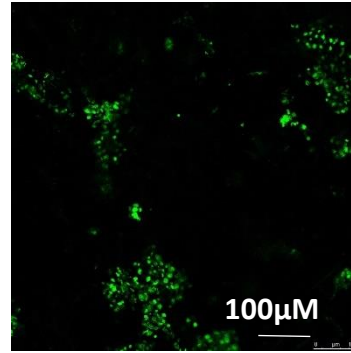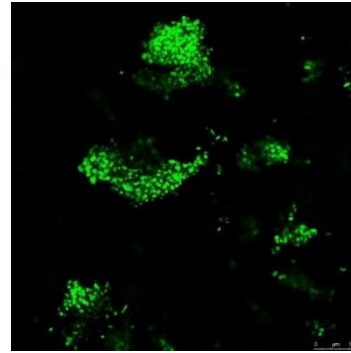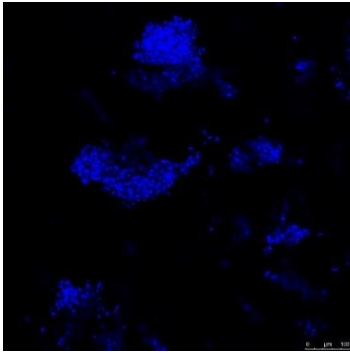
Control
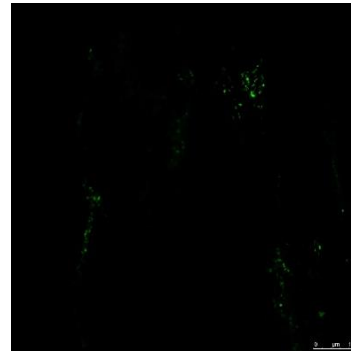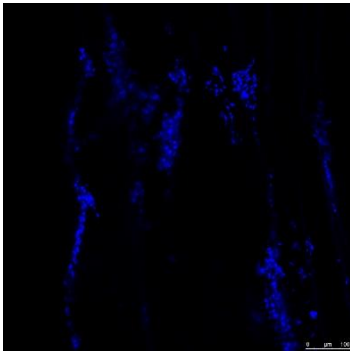
LT
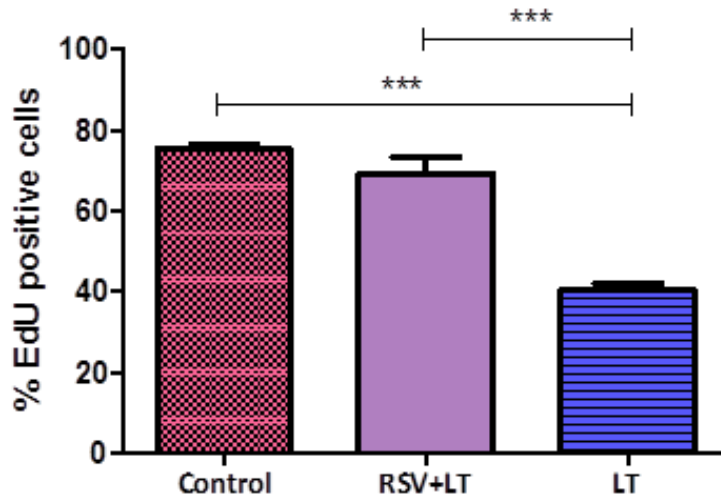
Figure 3.34. **A.** Proliferating cells were labelled with EdU (green). Cell nuclei were stained with DAPI (blue). Scale bar = 100 µm**. B.** The percentage of EdU-positive cells was quantified in cryogels. Data are presented as the Mean ± SD of EDU positive cells using One-Way ANOVA with Bonferroni's Multiple Comparison Test (***p< 0.001) (n=2). At least 500 cells were counted on each cryogel. **Control**: un-treated cell, **RSV+LT**: Pre-treated with RSV at 5µM concentration for 24 h and then treated with liver toxins and RSV at 5µM concentration for 6h. **LT**: liver toxins).

3.10.3 Loss of phenotypic function in cultured hepatocytes within a BAL cryogel prototype

Figures 3.35A and B show markedly reduced albumin production and urea synthesis in HepG2 cells after exposure to the liver toxin cocktail in the bioreactor. Albumin production measured 48 h after removing liver toxins treatment in the multi-layered bioreactor, was 0.964584 µg/ml for the control cells and was significantly higher than albumin produced by liver toxins-treated cells (0.320162 µg/mL) (p<0.01, figure 3.35A). Also, HepG2 produced a higher level of albumin after resveratrol treatment (0.869655 µg/mL) compared to the liver toxins treated cells (p<0.01). There weren't any significant differences between resveratrol treated and non-treated cells (figure 3.35A). Urea synthesis measured 24 h after stimulation with NH4Cl in the multi-layered bioreactor was 5.223684 mg /dl in the control group and was significantly higher than the urea produced by liver-toxins treated cells which were

3.526316 mg/dl (p<0.001, figure 3.35B). 5µM resveratrol caused a significant increase in urea production by HepG2 cells in comparison to liver-toxin-treated cells (p<0.05, figure 3.35B).
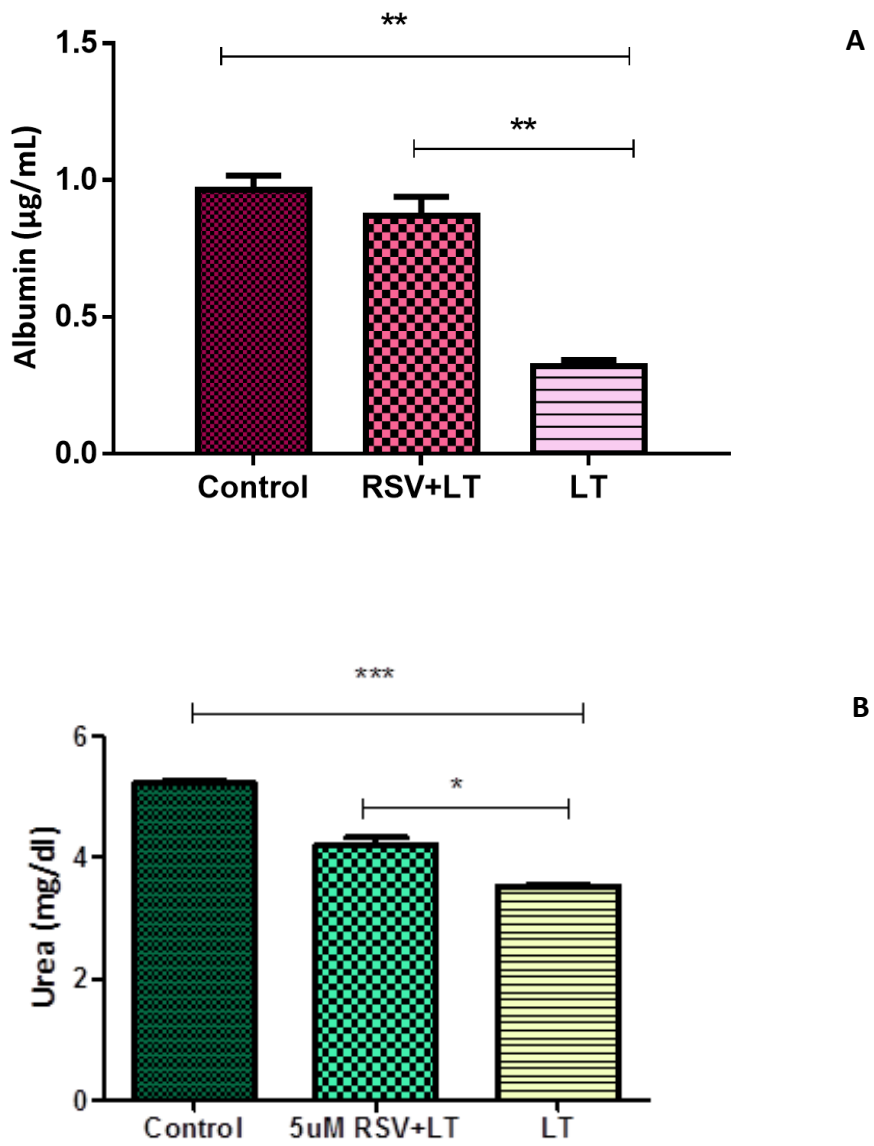
Figure 3.35. Albumin production in multi-layered bioreactors (n=3) 48 h post liver toxins treatment and urea synthesis 24h post-stimulation with ammonium chloride in multilayers bioreactors (n=3). Values represent mean ± SD. Statistical analysis was performed using ANOVA with Bonferroni's post-hoc test (*p<0.05, ***p < 0.001).

3.10.4 Liver toxins treatment led SASP induction in hepatocytes and reversal using resveratrol within a BAL cryogel prototype

The results of the cytokine production by HepG2 cells are shown in figures 3.36 and 3.37. As it's shown in figure 3.36, IL-6 concentration increased significantly in liver toxins-treated cells compared to the non-treated group (p<0.01). The IL-6 concentration decreased significantly from 116.36±14.09 pg/mL in liver toxins- treated group to 55.68±2.67pg/mL in resveratrol-treated cells (p<0.05, figure 3.36).

Regarding IL-8 production, HepG2 cells produced a significant level of IL-8 after treatment with liver toxins compared to non-treated cells (p<0.001, figure 3.37). The control cells and liver toxins-treated cells produced IL-8 at 136.44±4.45 pg/mL and 546.72±6.68pg/mL concentrations respectively. However, the IL-8 concentration decreased significantly after 5µM resveratrol treatment compared to the liver toxins-treated group (p<0.001) (figure 3.37).
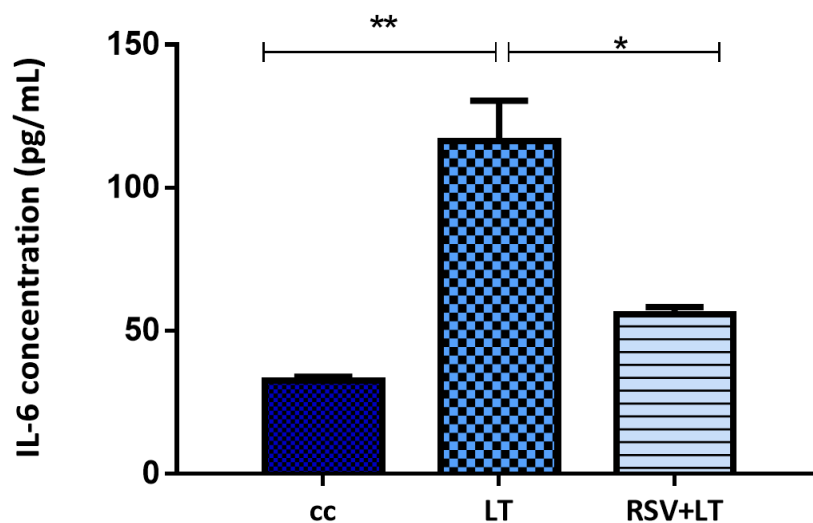
Figure 3.36. The protein level of IL-6 was measured by ELISA assay. HepG2 cells were seeded on discs in the bioreactor and pre-treated with 5µM resveratrol (RSV) for 24 h and then treated with liver toxins and 5µM RSV (**RSV+LT**) for a further 6h. The medium was collected from each bioreactor 3 days after removing treatment and kept at -20°C until further experiments. Control cells (**CC**) were grown in medium only. The values are shown as the means ± SD using one-way ANOVA with Bonferroni's multiple comparison test (*p< 0.05, **p< 0.01) n=3. **LT:** liver toxins-treated cells.

145
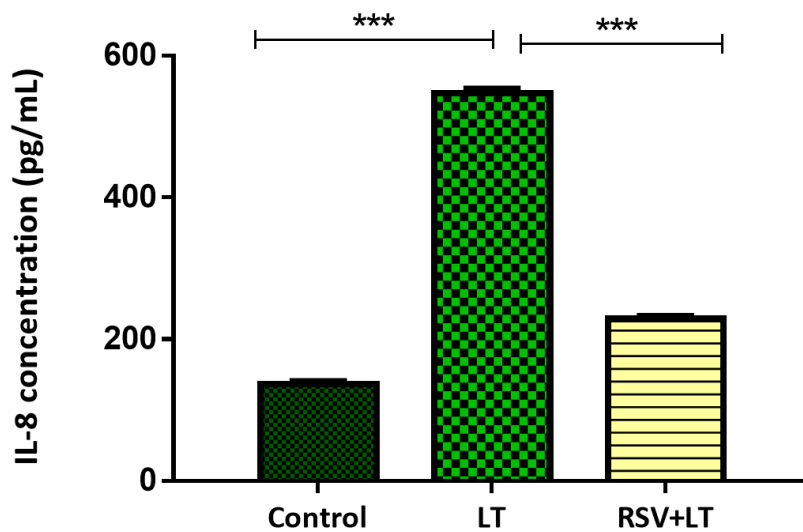
Figure 3.37. The values are shown as the means ± SD using one-way ANOVA with Bonferroni's multiple comparison test (***p < 0.001) n=3. **LT**: liver toxins-treated cell. **RSV+LT**: cells pre-treated with 5μM resveratrol (RSV) for 24 h and then treated with liver toxins and 5μM RSV for a further 6h.

Chapter 4 Discussion

4.1 Introduction

Hepatocyte senescence is known to promote the development of liver disease and is linked to liver dysfunction in chronic liver disease through changes in hepatocellular regenerative capacity and function. Progressive accumulation of senescent hepatocytes can adversely affect hepatic function leading to liver cirrhosis. In patients with acute or acute on chronic liver failure, the loss of detoxification, synthesis, and metabolic processing normally carried out by hepatocytes leads to complications associated with toxin accumulation. Biological liver replacement devices incorporating a hepatoma cell line or primary hepatocytes into a bioreactor to process blood or plasma have been developed to partially replace the liver's metabolic and regulatory functions besides detoxifying the patient's plasma as a bridge to transplant or organ recovery after liver decompensation. However, such devices fail to significantly enhance clinical survival in patients with ALF or ACLF. A severe decline in hepatocyte function has been observed in monolayer and BAL cultures of hepatocytes after exposure to ALF plasma. Toxins and inflammatory cytokines present at high concentrations in the patient's blood as a result of their liver disease and evidence from other studies exposing hepatocytes to ALF plasma suggests that there is a cytotoxic effect on liver cells in addition to a reduction in cell function. These alterations in hepatocyte function within BAL systems may be associated with cytotoxic compounds accumulating in blood during ALF. This can lead to cell death and/or induction of senescence in hepatocytes as a direct result of exposure to patient plasma loaded with liver toxins and cytokines and these changes induced by senescence should be considered a critical factor in mediating device failure after exposure to perfused liver toxins. However, no studies have directly investigated the role and significance of senescence in bio artificial liver performance over time or whether senescence suppression strategies may be incorporated to improve bio artificial liver function by using senescence inhibitor compounds. In this study, these knowledge gaps were addressed by investigating the impact of senescence on hepatocyte function within a BAL bioreactor after exposure to the perfused liver toxin and considering routes to mitigate any effects in bio artificial organ design to represent a novel enhancement of artificial organ function.

To fulfil the aims of this project, firstly, human hepatocyte phenotypes were characterised for use in a cryogel BAL and to establish a suitable cell model to study hepatocyte senescence in a BAL prototype. Then, a cryogel matrix including alginate cryogel was synthesised to establish a 3-dimensional BAL model and to study the effect of senescence on hepatocyte proliferation and function in a 3-D model. Next, the effect of liver toxins treatment on induction of senescence in tumour-derived hepatocytes was studied on 2 and 3-D surfaces, and their key synthetic functions such as albumin and urea synthesis were measured on both surfaces after liver toxins treatment. Also, the effect of senescence inhibitor compounds including resveratrol and resveralogues were investigated to test if they can block senescence after liver toxins exposure and reverse bio-artificial liver prototype failure. Finally, as a conclusion of this study, a cryogel-based multi-layered bioreactor was used as an in *vitro* model of liver failure to assess the induction of senescence and its role in declining device function. Resveratrol was used in this model to investigate if it can improve this bio-artificial liver prototype function by increasing cell growth and developing hepatocyte's key functions.

4.2 Characterisation of human hepatocyte phenotypes for use in a cryogel BAL to investigate liver toxin-induced hepatocyte senescence

Human hepatocyte lines (HHLs), derived from healthy human liver, have been developed as an alternative to tumour-derived and primary hepatocytes for research on hepatitis virus and hepatocyte function. In previous work by Bonalumi et al in 2021 [150] the HHLs were characterised and compared with HepG2 cells for potential use in a cryogel BAL prototype. In this work, the HHLs were characterised and compared with HepG2 cells for potential use to investigate the impact of liver toxin-induced senescence on hepatocyte functional performance in a cryogel BAL prototype. These cells were analysed by the ICC assay for cytokeratin expression and their features were compared with established human hepatoma cell lines (HepG2) and non-liver cells (NIH-3T3) to confirm that these cells retain the primary hepatocyte phenotype. The results of the ICC assay in this study showed that HHLs expressed both parenchymal CK8 and non-parenchymal CK7 phenotype markers which is inconsistent with published data (figure 3.1) [141]. HepG2 cell expressed CK8, but it did not stain positively with non-parenchymal marker CK7 which is in line with published data

149

showing the lack of CK7 expression in hepatic metastatic adenocarcinomas[152]. CK7 is usually expressed in bile duct epithelium in the healthy liver [153] and is also found in fibrolamellar carcinoma of the liver [154]and primary biliary cirrhosis[155] depending on the affected tissue. Both CK7 and CK8 were absent in NIH-3T3 cells because of their fibroblastic origin. The result of this assay confirmed that HHLs retained some aspects of the phenotype of primary hepatocytes, and they are the same cells supplied.

4.3 Hepatocyte proliferation and phenotype studies on HEMA-based cryogels

Cryogels are supermacroporous hydrogels with interconnecting pores. These interconnected porous networks of cryogels are beneficial in supporting cell proliferation and migration. Such structures make them suitable for many tissue engineering applications including within bioreactor systems, cell separation, and scaffolding [156]. Cryogels have been widely used as cell scaffolds inside a bioreactor unit for BAL purposes. The interconnected porous network of cryogels forms a capillary network and these are beneficial to support hepatocyte growth in the bioreactor. In addition, cryogels provide a large surface area to volume ratio for cell immobilisation [150]. The initial aim of this study was to use previously characterised cryogel matrices [150] in comparing 2-D and 3-D cultures and establishing a model of BAL hepatocyte senescence. In this study, cryogel matrices composed of the HEMA-MBA and HEMA-PEGDA cryogels were synthesised by the cryogelation technique and were modified with alginate to enhance the non-fouling properties of the cryogel surface and increase cell adherence. These cryogels were previously characterised with a range of physical assays including FTIR characterisation, Zeta potential measurements, and scanning electron microscope (SEM) which indicated that the HEMA-based cryogels possessed open porosity, the interconnectivity of pores, and pore size up to 100 μm to allow hepatocyte colonisation and proliferation [150]. The mentioned cryogels were tested in this study to verify the biocompatibility and compare 2D and 3D growth parameters, and also to establish a model for the first testing of liver toxin-induced senescence in hepatocytes. The result of the MTT assay showed that all the mentioned cryogels maintained cell proliferation over 1 week period (figure 3.2). In the first 24 h, there were no significant differences in cell number among the different cryogel versions. After

150

one week of incubation, alginate-containing cryogels showed a significant increase in cell viability compared to the non-alginate-containing versions (figure 3.2, p<0.0010). At each time point, HEMA-MBA-alginate cryogels possessed a higher number of viable cells compared to non-alginate-containing cryogels indicating that this cryogel supported hepatocyte proliferation better than the plain versions.

Albumin synthesis and the detoxification of toxic ammonia into soluble urea through the urea cycle are the most important functions carried out by hepatocytes. Since HEMA-MBA-alginate cryogels supported the long-term growth of cultured cells, their main functions were measured at the 3-D culture conditions, and it was compared to 2-D surfaces. Time courses of albumin production and urea synthesis over 7 days showed higher albumin and urea concentrations in a culture grown on the cryogel discs (3-D) in comparison with the cell growth on the 2-D surface indicating that a 3-D environment is more beneficial to cell function (figure 3.5 and 3.6). The data obtained show that the material used in this study is able to support the long-term growth and function of cultured hepatocytes and it was used to establish a model for the first testing of liver toxin-induced senescence in hepatocytes.

4.4 HHL-7 hepatocytes cannot be induced to senesce in culture

To study the effect of senescence on human hepatocyte cell lines, HHL-7 cells were treated with hydrogen peroxide and Mitomycin C which are both known as producers of reactive oxygen species and can cause premature senescence through the production of a persistent DNA damage response. Several studies show premature senescence (SIPS) caused by oxidative stress such as H_2O_2 in fibroblasts [51, 157, 158] and human hepatoma-derived cell line HepG2 [159].

Mitomycin C alkylates DNA, and produces inter-strand as well as intra-strand DNA cross-links, thereby inhibiting DNA synthesis [160]. In this study, Mitomycin C and hydrogen peroxide were used to address the question if these two treatments can induce senescence in HHL-7 cell lines. The concentration values and incubation time of each treatment were cited in the literature review and subsequently used in this study [161]. The HHL-7 cell line was firstly treated with 100μM, 200μM, and 300μM of H_2O_2 for 24 hours to select a dose that did not affect HHL-7 cell viability. The result of the viability assay (MTT) showed that

H$_2$O$_2$ at all mentioned concentrations was toxic to the HHL-7 cells and the percentage of viable cells was less than 40% compared to non-treated cells ([figure 3.7](#)). These cells were also treated with 1µg/mL and 10µg/mL Mito-C for 24 and 1 h respectively and the number of viable cells was measured at 0,1 and 3 days after removing treatment. The result of the MTT assay showed that Mito-C at all doses was cytotoxic to the HHL-7 cell line and caused a significant reduction in the number of viable cells at each time point compared to non-treated cells ([figure 3.9](#)). In contrast, in the study by Kabiri et al in 2019 [162], transitional cell carcinoma (TCC) and normal mouse L929 fibroblast cells were treated with higher doses of Mito-C including 25 and 50 µg/mL for 24 h and remained viable after the mentioned doses. But, in our study Mito-C at lower concentrations was toxic to the HHL-7 cell line. The result of this study showed that both H$_2$O$_2$ and Mito-C treatments have a cytotoxic effect on the HHL-7 cell line.

This study also showed that exposure to subtoxic concentrations of H$_2$O$_2$ including 10, 50, and 100 µM for 24 h didn't induce senescence in HHL-7 cells. Lack of proliferation markers such as Ki67 protein is a hallmark of cellular senescence. The result of the ICC assay showed that H$_2$O$_2$-treated cells all stained positively with Ki67 and there were no differences between treated and control cells ([figure 3.8](#)). The incorporation of thymidine analogue EdU (5-ethynyl-2'-deoxyuridine) into newly synthesised DNA is usually used as a marker to detect and quantify cell proliferation by directly measuring DNA synthesis. Therefore, an EdU assay was performed to measure if Mito C treatment at the mentioned doses can induce cell cycle arrest in the HHL-7 cell line. The result of EdU staining in [figure 3.10](#) indicates that there were no significant differences in the percentage of EdU positive cells between control and Mito-C treated cells and more than 80% of treated cells were stained positively with this marker. According to the results obtained, H$_2$O$_2$ and Mito-C could not induce senescence growth arrest in HHL-7 cell lines because these cell lines lack important markers for transformation. The HHLs were examined by indirect immunofluorescence assay for the expression of P53 protein in a study by Clayton in 2005 [141] and all of them were negative for P53 protein expression due to the immortalisation technique which was applied to them [141]. HHL-7 cells were immortalised by retrovirus-mediated transduction of HPV E6 and E7 oncoproteins. These proteins' effects are well known to induce cell-cycle disruption because of interference with cellular p53 and retinoblastoma protein (Rb). During HPV16 infection,

E6 links and inactivates p53 by forming a stable bond with p53 leading to p53 degradation [163]. As it was shown by a previous study [141] that HHL-7 cells do not have a functional p53 protein, therefore, induction of cell cycle arrest after using senescence-inducing compounds was not achieved.

Since the absence of p53 meant that the HHL-7 cell line could not be induced to senescence and therefore was not suitable for the study, HepG2 cells were selected for further experiments in this project. The induction of senescence in HepG2 cells is well established in the literature [6, 159, 164]. In addition, the result of this project suggested that HHL- 7 does not completely retain the primary hepatocyte phenotype and also did not show suitable functionality for use in a BAL system in comparison to HepG2 cells. Albumin production and urea synthesis by HHL-7 and HepG2 cells were measured at 2-D and 3-D surfaces over 3- and 7-day incubation and the results in figure 3.5 and figure 3.6 indicate that HepG2 cells at both surfaces produced a higher amount of albumin and urea than the HHL-7. However, there was no significant difference in the number of viable cells between HepG2 and HHL-7 over 3- and 7-day incubation on the 3-D cryogel disc surfaces (figures 3. 3 and 3.4) indicating that whilst metabolic function was significantly increased in the HepG2s support of viable hepatocyte growth and proliferation was the same.

4.5 HepG2 hepatocytes are a better cell type to study hepatocyte senescence in a BAL prototype

4.5.1 Genotoxic damage induces a senescent phenotype in HepG2 cells that combines growth arrest and loss of key functional phenotypes

In this study, the effect of senescence on hepatocyte key functional phenotypes was analysed using HepG2 cells. As mentioned in the previous section, these cells were chosen as an alternative to hepatocytes, since the number of available primary hepatocytes is limited and other commonly used hepatocyte cell lines including HHLs, Huh7, and Hep3B have fundamental mutations in p53 [165], which may interfere with the induction of cellular senescence. Induction of senescence was achieved through a well-characterised inducer of senescence with a low concentration of etoposide that causes DNA double-strand breaks

153

and has been used in various cell types [164, 166]. Treatment of HepG2 cells with a lower dose of etoposide (10 and 20μM) for 48h induced growth arrest which was confirmed by the reduced percentage of EdU positive cells after both concentrations (figure 3.12). The number of viable cells reduced significantly after 24 and 48h treatment with 20μM etoposide. While HepG2 cells remained viable after 48 h treatment with 10μM Etoposide (figure 3.11). Consequently, a threshold concentration of 10μM was chosen to treat HepG2 cells for 48h and avoid cytotoxic damage. In addition to reduced DNA synthesis, senescence was also confirmed by reduced expression of the proliferation-associated protein Ki67 (figure 3.13), together with increases in p53 positive nuclei and p53 gene expression (figure 3.14) in HepG2 cells after 48 h treatment with 10μM etoposide. These results are in agreement with published data that demonstrated that senescence is induced by the low dose of etoposide in HepG2 cells[164].In conclusion, senescence in HepG2 cells was confirmed by reduced expression of proliferative-associated protein Ki67, reduced DNA synthesis, and expression of cell cycle inhibitor p53. Etoposide at 10μM concentration caused replicative arrest and senescence in HepG2 cells.

4.5.2 HepG2 senescence induced a significant reduction in albumin and urea production, and this is more pronounced in HepG2 cells grown on HEMA-MBA-alginate cryogels

Significant changes in metabolism have been shown in human fibroblasts undergoing oncogene-induced senescence [167]. Also, the induction of senescence in HepG2 cells through oxidative stress resulted in reduced hepatocyte synthetic function, with reduced levels of α-fetoprotein, fibrinogen, and retinal binding protein in senescent HepG2 cells [6]. However, this is the first time that this study investigated the effect of senescence on key metabolic functions of hepatocytes including albumin and urea production. In this study, for evaluation of the functional capacity of senescent hepatocytes, albumin production and urea synthesis were measured in treated and non-treated HepG2 cells grown at HEMA-MBA-alginate cryogels (3-D surface) and 12 well plates (2-D surface). The result of this study shows that the level of albumin and urea production reduced significantly after induction of senescence at both surfaces suggesting impaired key synthetic functions in these cells (Figures 3.15 and 3.17). The level of albumin production by HepG2 cells was more reduced

154

(p<0.05) on 3-D surfaces than on 2-D surfaces in response to 10μM etoposide treatment which indicates even a 3D culture system could not preserve the function of HepG2 after induction of senescence.

To further demonstrate the effect of senescence on synthetic function, the expression of the albumin gene in the Etoposide-treated cells was measured on 2-D surfaces and compared with non-treated cells. The result shows that albumin gene expression was downregulated in HepG2 senescence compared to the control cells which confirms the result obtained by the ELISA assay measuring protein expression (figure 3.16). In summary, these results demonstrated that levels of albumin synthesis and urea production were significantly reduced in the conditioned media of senescent HepG2 cells compared to the non-treated cells suggesting that senescence compromises important hepatocyte functions even when cultured in the 3D systems used in liver devices which maximise differentiation. In addition, these data may explain the relation of hepatocyte senescence with hepatic dysfunction and adverse liver-related outcome seen in chronic liver disease [5].

4.6 HepG2 cells enter a senescent state in response to the liver toxin and inflammatory cytokine exposure

As senescence plays a role in the development of liver disease due to alterations in hepatocyte metabolic and synthetic functions, it is possible that liver toxins in the plasma of patients with acute or chronic liver disease can negatively affect hepatocyte functions by induction of senescence. Since it was demonstrated that the onset of senescence perturbs other features of the HepG2 phenotype central to liver detoxification and albumin synthesis functions, it was hypothesised that some component of the hepatotoxic mixture that builds up during liver failure induces senescence directly compromising the performance of bioartificial liver devices. In order to assess the effect of liver toxins treatment on induction of senescence in tumour-derived hepatocytes, HepG2 cells were treated with a liver toxins cocktail at physiological doses and over physiologically relevant times (6 h). A combination or mixture of liver toxins is termed a "liver toxin cocktail" herein. The liver toxin cocktail consists of creatinine, bilirubin, sodium chenodesoxycholate (C-Doca), ammonia, urea, and

cytokines (IL-6, IL-8, and TNF-α); this combination of toxins is well-known to be representative of the toxin composition of blood in subjects suffering from liver failure. The concentrations of mentioned liver toxins and cytokines are physiologically relevant, and they are representative of the concentrations found in the blood of a subject with hepatic functional impairment, suffering from liver disease, or liver failure requiring liver dialysis [100, 101, 168, 169]. HepG2 cells were treated with liver toxins only and liver toxins plus cytokines for 6h on HEMA-MBA-alginate cryogel3-D surfaces and their viability was measured 24 h after removing treatment. The data in figure 3.18 A shows that liver toxins and cytokines treatment had no significant effect on HepG2 viability, and many of the cells remained viable after both treatments. In contrast, the number of proliferating cells reduced significantly after both treatments which was confirmed by a significant reduction in EdU and Ki67 (p<0.0001) labelling (figures 3.19 and 3.20). As it has already been shown in figure 3.18, the majority of HepG2 cells remained viable after liver toxins and cytokines treatment. The reduction of radiolabelling thymidine incorporation into DNA synthesis after liver toxins cocktail treatment suggested that liver toxins and cytokines could induce cell cycle arrest in the S phase of the cell cycle and promote senescence of HepG2 cells which was not dependent on a decrease in cell viability.

These findings parallel previous studies which reported that bile acids and bilirubin, the main components of liver toxins, can inhibit DNA synthesis and cell proliferation in different cell sources [170-172]. For example, smooth muscle cell cycle progression at the G1 phase was inhibited after treatment with 200 µmol/L bilirubin through inhibition of the mitogen-activated protein kinase signal transduction pathways and inhibition of hyperphosphorylation of the retinoblastoma tumour suppressor protein Rb. Bilirubin at supranormal concentrations of 200 µmol/L was not cytotoxic, nor did it induce necrosis or apoptosis but arrested cell cycle progression in the late G1 phase in VSMCs [170]. Here this study demonstrated that liver toxins induced premature senescence in HepG2 cells which was confirmed by a significant reduction in cell proliferation markers, and it is most likely mediated by a regulatory mechanism activated by DNA damage response. The fact that senescence was induced after only a 6-hour exposure to the liver toxin was consistent with a telomere-*independent* induction of the senescent state.

Both Liver toxins cocktail and liver toxins plus cytokines induced senescence in HepG2 cells after 6 h treatment. HepG2 cells were treated with individual cytokines for 6h to understand which factors affect cell growth and mediate induction of senescence. The results in figure 3.21 demonstrate a significant reduction of cell proliferation after 6 h treatment with IL-8 (p<0.05). In contrast, other cytokines such as IL-6 and TNF-α had no significant effect on HepG2 proliferation. This result suggests that HepG2 cells are less sensitive to cytokines-induced senescence and liver toxins, not cytokines are the primary mediators of senescence induction.

4.7 Does senescence induced by liver toxins (SILT) compromise the performance of the bio artificial liver?

Knowledge of cell culture conditions for hepatocytes including important components of culture media has been developed which allowed successful culturing of freshly isolated hepatocytes in the BAL systems. Facilities such as oxygenation and perfusion systems have become available that support the maintenance of large amounts of viable and functionally active hepatocytes in bioreactors[173]. Nevertheless, when these systems are used in clinical application, hepatocytes directly or indirectly become in contact with ALF patient's plasma which is less optimal for cell culture in comparison to culture media and may affect hepatocytes viability and functionality. It has been suggested by some studies in *vitro* that plasma of patients from ALF had negative effects on freshly isolated and cultured porcine hepatocytes viability and functions [173, 174]. For example, it has been shown by Catapano et al in 1996 [174] that high concentration's of ammonia and lactate negatively affected the viability and detoxification function of rat hepatocytes including urea synthesis and ammonia elimination. In the mentioned studies, reduced hepatocyte viability after exposure to ALF plasma was considered the main reason for the reduction of hepatocyte function in BAL. However, the effects of ALF serum or plasma on synthetic and detoxification functions of cultured hepatocytes have not been clearly explained. This study showed that 6h exposure to a liver toxin cocktail did not affect hepatocytes viability but, reduced cell proliferation and DNA synthesis plus synthetic and detoxification functions. Albumin and urea synthesis both reduced significantly after liver toxins treatment at 2 and 3-D surfaces

157

when compared to pre-treatment values ([figures 3.22](#) and [3.23](#)). In contrast, the cell viability of HepG2 cells did not significantly change when compared to their functions after liver toxins exposure. These results are in line with observations of Abrahmse et al in 2002 [149], who demonstrated a reduction of cell function of porcine hepatocytes in bioreactors after 24-hour treatment of anhepatic pigs. Their results showed that urea synthesis, ammonia clearance, and ethoxycoumarin O-deethylase (ECOD) activity decreased significantly in bioreactors after treatment of anhepatic pigs when compared to pre-treatment values (p<0.05)[149]. The combination of loss of protein synthesis and detoxification functions of primary porcine hepatocyte populations with undiminished cell viability reported by these researchers after exposure to the hepatotoxins in the plasma of these animals is strongly reminiscent of SILT. This loss of hepatocyte function, and thence the ability to keep the donor animals alive, clearly does not result from deficits in the bioengineering of the device itself because identical AMC-BAL bioreactors not exposed to toxin-laden plasma were able to support autologous hepatocytes with high levels of function over the same period. In conclusion, our results indicate that liver toxins induce both senescence and loss of phenotypic function in cultured hepatocytes, and senescence induced by liver toxins can compromise the performance of bioartificial liver devices.

4.8 Resveratrol can reverse liver toxin-induced hepatocyte senescence

This study has already shown that the senescent state caused by exposure to the liver toxin cocktail induced a loss of hepatocyte-specific activity in the cells; after exposure to the liver toxin cocktail, the cells showed markedly reduced albumin production and urea synthesis. In this study, resveratrol was used to see if it can prevent or recover liver toxin-induced loss of hepatocytes proliferation and phenotype. Resveratrol (RSV), or trans-3,5,4'-trihydroxystibene, is a polyphenol naturally occurring compound found in wine that has been shown to have antioxidant and anticancer properties. This molecule improved the lifespan of lower organisms such as yeast, worms, and flies through activation of the NAD-dependent protein deacetylase which is considered a potent SIRT1 activator compared to other polyphenols. Resveratrol showed a 13-fold increase in deacetylase activity of SIRT1 protein and demonstrated beneficial effects on senescence phenotypes through other

pathways such as SIRT1 activity [24] and also through effects on the senescence-associated secretory phenotype (SASP).

Firstly, HepG2s were treated with resveratrol at 2, 5, 10, and 25 µM concentrations for 24h and the EdU assay was performed to measure the cell proliferation at the mentioned doses. The result of the dose-response curve (figure 3.24) showed that cell proliferation increased significantly after 2 and 5µM concentrations of resveratrol. However, resveratrol at 25µM concentration inhibited cell proliferation and it caused about a 35% reduction in cell growth. Therefore, HepG2 cells were pre-treated with resveratrol at 2 and 5µM concentrations for 24 h and then treated with a liver toxins cocktail plus resveratrol at the mentioned doses for 6h. This study demonstrated that cell proliferation markers (as measured by EdU and Ki67 staining) at 2-D (figures 3.25 and 3.26) and 3-D (figures 3.26 and 3.27) surfaces were markedly increased upon resveratrol treatment at both doses, indicating cell cycle entry. This result is consistent with other reports on resveratrol indicating that under low treatment dose (less than 25µM) and short time (24 h), cells viability and proliferation including human breast cancer cell line MCF-7 and human epidermoid carcinoma cells (A431) were not affected. But resveratrol can significantly decrease cell viability and inhibit cell proliferation at higher concentrations (more than 25µM) even at a low incubation period [175, 176]. So, resveratrol at 2 and 5 µM doses were more effective to protect HepG2 cell growth against the growth inhibitory effect of liver toxins.

4.9 The loss of growth capacity in senescence-induced by liver toxins occurs in a SIRT1 dependent and independent manner

In order to understand the mechanism of protection by resveratrol, HepG2 cells were also treated with resveratrol-related compounds (resveralogues) which all exhibited differential activity against SIRT1 and SASP. These compounds were chosen based on structural novelty and low cytotoxicity and previously observed increases in the Ki67 positive fraction of MRC5 cultures at 5 µM concentration [177, 178]. The HepG2 cells also treated with 5µM vitamin-C which is a well-known antioxidant that can scavenge highly reactive free radicals generated constantly by the cellular machinery [179, 180]. The result of figure 3.31 shows the significant increases in growth fraction (as measured by EdU labelling) after treatment with

159

vitamin-C, SIRT1 interacting compounds including resveratrol, dihydroresveratrol, V34, and V31 (p<0.0001), and SIRT-1 non –interacting compounds including V29 (p<0.001) compared to liver-toxins treated cells only. However, V29 (which does not activate SIRT1) had less effect on HepG2 cell protection against senescence induced by liver toxins compared to resveratrol and other resveralogues with variable SIRT-activation activity (v31 and v34, DHRSV) and vitamin-C (figure 3.31). Since resveratrol and other SIRT-1 activating compounds prevent the growth inhibitory effect of liver toxins, this study suggested that a decline in SIRT-1 expression upon liver toxins treatment may be a reason for induction of senescence which is most likely mediated by a regulatory mechanism activated by DNA damage response. However, SIRT-1 non –interacting compounds including V29 and vitamin-C caused a significant increase in cell growth and protected cells against liver toxins effect indicating that liver toxins also induced senescence in HepG2 cells in SIRT-1 independent manner. So, it can be concluded that the increase in cell proliferation markers expression on resveralogues treatment can occur either dependently or independently of SIRT1 activation. In addition, the loss of growth capacity in senescence induced by liver toxins occurs in a SIRT1-dependent and independent manner.

4.10 The loss of phenotype in SILT occurs in a SIRT1 independent manner

This study already showed that liver toxins impair hepatocyte key functions including albumin and urea synthesis. Since these key functions were compromised by liver toxins, HepG2 cells were treated with resveratrol at 2 and 5µM concentrations to see if they can protect cell synthetic functions against liver toxins' effects. These concentrations were based on previous data (figures 3.25 and 3.26) which confirmed that resveratrol at 2 and 5µM concentrations can improve HepG2 cell proliferation and block the growth inhibitory effect of liver toxins. The results in figures 3.29 and 3.30 show that resveratrol at both concentrations can protect key hepatocyte functions including albumin and urea synthesis at 2-D and 3-D surfaces. The level of albumin production after 2 and 5µM concentrations of resveratrol was %91 and %95 higher than liver toxins treated cells at 3-D surfaces. In addition, when cells treated with resveratrol at 5µM concentration produced 48% higher albumin than at 2µM concentration (figure 3.29). Urea synthesis after 2 and 5µM

160

concentrations of resveratrol was also 88% and 89% higher than liver toxins treated cells at the 3-D surface. Resveratrol at the mentioned doses increased urea synthesis even at 2-D surfaces but the level of protection was higher at the 5μM dose of resveratrol at the 2-D surface (figure 3.30). So, these results suggest that resveratrol has the potential to block or reverse cellular senescence with a consequent positive impact on hepatocyte's key metabolic functions.

Resveratrol increases both the expression and the activity of SIRT1 [181, 182]. This study found that treatment with resveratrol protected HepG2 proliferation against the liver toxins-induced reduction in SIRT1 levels and led to significantly higher EdU-positive cells. The inhibitory effect of resveratrol on liver toxins-induced senescence also happened independent of SIRT1 activation which can be related to the other protective effects of resveratrol including both free radical scavenging and antioxidant or anti-inflammatory effects.

Since resveratrol protected HepG2 functions against liver toxins effects, HepG2 cells treated with SIRT1 interacting compounds and SIRT-1 non –interacting compounds to investigate whether the beneficial activities of resveratrol on hepatocyte functions that may be mediated through SIRT1 or independent of SIRT1 activation. HepG2 cells were pre-treated with a 5μM concentration of resveratrol, dihydroresveratrol, and V29 for 24 h and then co-treated with the mentioned compounds and liver toxins for a further 6h. The result in figure 32 shows that a 75% reduction in albumin synthesis was observed after 6h treatment with liver toxins. While resveratrol and resveralogues caused a more than 60% increase in albumin production compared to liver toxins–treated cells. The level of albumin production by resveratrol, dihydrorevratrol, and V29-treated cells was about 74%, 69%, and 69% higher than in liver toxins-treated cells. The mentioned compounds also recovered urea synthesis function after liver toxins treatment which caused a significant increase in urea production after treatment with a 5μM concentration of resveratrol, dihydroresveratrol, V29, and vitamin-C (figure 3.32). Treatment with liver toxins caused about an 80% reduction in urea synthesis by HepG2. However, about 70% and 65% of this function were recovered in the presence of SIRT-1 and non-SIRT1 interacting compounds, respectively. V29, a non-SIRT1 interacting compound displayed the same effect of protection to that of resveratrol against

liver toxins indicating that loss of albumin and urea synthesis after liver toxins treatment occurs in a SIRT1 independent manner.

4.11 Modelling the impact of hepatocyte senescence on BAL using a multi-layered HEMA-MBA-alginate cryogel bioreactor

A multi-layered bioreactor designed and characterised by Bonalumi et al in 2021 [150] was used for this study. In the bioreactor, the cryogel column was sectioned into discs and they were spaced by using a 3D PLA printed spacer which was designed to re-arrange the flow by disrupting the laminar flow from a disc and maximise blood or medium/cell interaction. The aim of this study was to use the BAL bioreactor as a *vitro* model of liver failure to assess the induction of senescence and its role in declining device function and also evaluate the effect of and mechanisms by which senescence inhibitor compounds may reverse bio-artificial liver prototype failure. The results showed that the number of proliferating cells reduced significantly ($p<0.001$) after liver toxins treatment and more than 35% of HepG2 cells lost their proliferation after liver toxins treatment (figure 3.34). However, cell proliferation was improved in the presence of resveratrol, and about 69% of cells re-entered the cell cycle. The reduction of cell proliferation was independent of the reduced number of viable cells as they remained viable after liver toxins treatment (figure 3.33). Similar to results observed in 2 and 3-D culture conditions about HepG2 functions, albumin, and urea production was significantly decreased in the bioreactor after exposure to liver toxins treatment ($p<0.001$, $p<0.01$ respectively) (figure 3.35). However, both functions increased significantly in the presence of 5µM resveratrol treatment. It was also observed that a spiked medium with liver toxins induced the HepG2 to produce cytokines and led to SASP induction in HepG2. The level of IL-6 and IL-8 were measured 3 days after removing treatment and the results showed that exposure to a liver toxins cocktail for 6 h induced the hepatocytes to produce IL-8 and IL-6 about 75% and 71% higher than non-treated group (figures 3.36 and 3.37). The level of IL-8 and IL-6 reduced significantly after using 5µM resveratrol ($p<0.001$, $p<0.05$) suggesting that the SASP induction in HepG2 was reversed using senescence inhibitors within a BAL cryogel prototype. In summary, these results indicate that senescence was induced in HepG2 cells in the bioreactor when they were exposed to liver toxins for 6h, and

162

senescence induced by liver toxins had a significant effect on declining cell function and subsequently device performance. However, senescence inhibitor compounds such as resveratrol reverse this bio-artificial liver prototype functions by improving cell growth and hepatocyte's key functions including protein synthesis and detoxification functions, and also develop device performance.

5. Conclusion

In summary, the main goal of this study was to investigate the role and significance of hepatocyte senescence in bio artificial liver failure using a hepatocyte-loaded macroporous cryogel prototype device. The initial results of this study showed that genotoxic damage induced a senescent phenotype in HepG2 cells that includes growth arrest and loss of key functional phenotypes. Etoposide caused replicative arrest and senescence in HepG2 which was confirmed by reduced expression of proliferative-associated protein Ki67, reduced DNA synthesis, and expression of cell cycle inhibitor p53. Further, induction of senescence impaired important synthetic functions in the HepG2 cells which caused a significant reduction in albumin and urea production and this was more pronounced in HepG2 cells grown on 3-D surfaces than 2-D surfaces. Therefore, this study suggested that senescence compromises important hepatocyte functions even when cultured in the 3D systems used in liver devices which maximise differentiation.

This study also investigated the effect of liver toxins treatment on the induction of senescence in tumour-derived hepatocytes. The results produced in this work showed that treatment with a cocktail of liver toxins and inflammatory cytokines *in vitro* for six hours induces a senescent state in HepG2 cells (confirmed by loss of pKi67 reactivity and EdU label exclusion) alongside a near complete loss of albumin synthesis and urea production. So, these results contributed to addressing a new knowledge regarding the alterations in hepatocyte function within the BAL system after exposure to a patient's plasma occurs as a consequence of senescence induced by exposure to perfused liver toxins. It was also demonstrated in this study that the induction of senescence by liver toxins can be prevented by treatment with resveratrol and resveralogues. Cell proliferation markers (as measured by EdU and Ki67 staining) at 2-D and 3-D surfaces were markedly increased upon

163

resveratrol treatment indicating cell cycle entry. Also, significant increases in growth fraction and hepatocyte's key synthetic functions were shown in this study after treatment with SIRT1 interacting compounds including resveratrol, dihydroresveratrol, V34, and V31 (p<0.0001) and SIRT-1 non –interacting compounds including V29. Therefore, this study concluded that both resveratrol and resveralouges have the potential to delay or reverse cellular senescence after liver toxins treatment with a consequent positive impact on hepatocyte's key metabolic functions.

Finally, BAL bioreactor was used in this study as a *vitro* model of liver failure to assess induction of senescence and its role in declining device function and also evaluate the effect of and mechanisms by which senescence inhibitor compounds may reverse bio-artificial liver prototype failure. Similar to results observed in 2 and 3-D culture conditions, loss of growth capacity and key functional phenotypes, and SASP induction were observed in the bioreactor after exposure to a spiked medium with liver toxins which demonstrates the primary reason for the failure of all bioartificial liver devices. However, senescence inhibitor compounds such as resveratrol reverse this bio-artificial liver prototype failure by improving cell growth and hepatocyte synthetic functions and also developing device performance. This protection from senescence represents a novel enhancement of artificial organ function.

In conclusion, this study showed that a physiologically reflective mixture of the hepatotoxins found in the plasma of patients with liver failure induces a senescent state in which albumin and urea production drop dramatically. However, this can be prevented by the use of polyphenolic compounds to protect the cells in the device from senescence in a SIRT1 dependent or independent manner.

6. Future work

The next step would be to test this multi-layered cryogel-based BAL with cells for safety and tolerability in a rat model of liver failure and use resveralouges to measure if these compounds can improve the performance of BAL devices. Furthermore, this study needs to be expanded to measure the effect of each single toxin effect on the induction of senescence in hepatocytes to see which toxin has a major effect to induce senescence in hepatocytes. Strategy to identify the key pathways mediating protection by resveratrol and resveralouges will be considered in the next step. HepG2 represents the only realistic current source of hepatocyte material for BALS that does not carry the risk of interspecies viral transmission and they are easy to expand in culture to generate sufficient biomass to populate the hollow-fibre system. However, this cells have approximately 20% of the urea production capacity of primary hepatocytes. Therefore, Co-transfected HepG2 cells with complete urea cycle activity and ammonia detoxification function developed by Mavri-Damelin et al in 2007 [183] would be better suited in the future work. The phenotypes of control cultures of HepG2 cells, primary human hepatocytes, and primary porcine hepatocytes will be compared after maintaining under physiologically reflective conditions with those treated with liver toxins to induce senescence by liver toxins.

7. Bibliography

1. Bram, Y., et al., *Cell and Tissue Therapy for the Treatment of Chronic Liver Disease.* Annual review of biomedical engineering, 2021. **23**: p. 517-546.

2. *Findings in Liver Transpls Reported from King's College Hospital NHS Foundation Trust (Adult liver transplantation: UK clinical guideline - part 2: surgery and post-operation).* 2020, NewsRX LLC. p. 488.

3. Dhandayuthapani, B., et al., *Polymeric Scaffolds in Tissue Engineering Application: A Review.* International Journal of Polymer Science, 2011. **2011**: p. 1-19.

4. Pless, G., *Bioartificial liver support systems.* Methods in molecular biology (Clifton, N.J.) Journal Article, 2010. **640**: p. 511-523.

5. Aravinthan, A., et al., *Hepatocyte senescence predicts progression in non-alcohol-related fatty liver disease.* Journal of hepatology, 2012. **58**(3): p. 549-556.

6. Aravinthan, A., et al., *The senescent hepatocyte gene signature in chronic liver disease.* Experimental gerontology, 2014. **60**: p. 37-45.

7. Fridlyanskaya, I., L. Alekseenko, and N. Nikolsky, *Senescence as a general cellular response to stress: A mini-review.* Experimental gerontology, 2015. **72**: p. 124-128.

8. , B.G., et al., *Senescence and apoptosis: dueling or complementary cell fates?* EMBO reports, 2014. **15**(11): p. 1139-1153.

9. Terzi, M.Y., M. Izmirli, and B. Gogebakan, *The cell fate: senescence or quiescence.* Molecular biology reports, 2016. **43**(11): p. 1213-1220.

10. Deursen, J.M.A.v., *The role of senescent cells in ageing.* Nature (London), 2014. **509**(7501): p. 439-446.

11. Faragher, R., et al., *Senescence in the aging process.* 2017.

12. Hayflick, L., *The Cell Biology of Aging.* Journal of investigative dermatology, 1979. **73**(1): p. 8-14.

13. Shay, J.W. and W.E. Wright, *Hayflick, his limit, and cellular ageing.* Nature reviews. Molecular cell biology, 2000. **1**(1): p. 72-76.

14. Fridman, A.L. and M.A. Tainsky, *Critical pathways in cellular senescence and immortalization revealed by gene expression profiling.* Oncogene, 2008. **27**(46): p. 5975-5987.

15. Avelar, R.A., et al., *A multidimensional systems biology analysis of cellular senescence in aging and disease.* Genome biology, 2020. **21**(1): p. 91-91.

16. Mohamad Kamal, N.S., et al., *Aging of the cells: Insight into cellular senescence and detection Methods.* European journal of cell biology, 2020. **99**(6): p. 151108-151108.

17. Bodnar, A.G., et al., *Extension of Life-Span by Introduction of Telomerase into Normal Human Cells.* Science (American Association for the Advancement of Science), 1998. **279**(5349): p. 349-352.

18. Caliri, A.W., et al., *Spontaneous and photosensitization-induced mutations in primary mouse cells transitioning through senescence and immortalization.* The Journal of biological chemistry, 2020. **295**(29): p. 9974-9985.

19. Odell, A., et al., *How to become immortal: Let MEFs count the ways.* Aging (Albany, NY.), 2010. **2**(3): p. 160-165.

20. Zhao, X., et al., *Spontaneous immortalization of mouse liver sinusoidal endothelial cells.* International journal of molecular medicine, 2015. **35**(3): p. 617-624.

21. Reddel, R.R., *The role of senescence and immortalization in carcinogenesis.* Carcinogenesis (New York), 2000. **21**(3): p. 477-484.

22. Herranz, N. and J. Gil, *Mechanisms and functions of cellular senescence.* The Journal of clinical investigation, 2018. **128**(4): p. 1238-1246.

23. Faragher, R.G.A., et al., *Senescence in the aging process.* F1000 research, 2017. **6**: p. 1219.

24. Evans, R.J., et al., *A P53-dependent, telomere-independent proliferative life span barrier in human astrocytes consistent with the molecular genetics of glioma development.* Cancer research (Chicago, Ill.), 2003. **63**(16): p. 4854-4861.

25. Kumari, R. and P. Jat, *Mechanisms of Cellular Senescence: Cell Cycle Arrest and Senescence Associated Secretory Phenotype.* Frontiers in cell and developmental biology, 2021. **9**: p. 645593-645593.

26. Campisi, J., *Aging, cellular senescence, and cancer.* Annual review of physiology, 2013. **75**: p. 685-705.

27. Suzuki, M. and D.A. Boothman, *Stress-induced Premature Senescence (SIPS).* Journal of radiation research, 2008. **49**(2): p. 105-112.

28. Burova, E., et al., *Sublethal Oxidative Stress Induces the Premature Senescence of Human Mesenchymal Stem Cells Derived from Endometrium.* Oxidative medicine and cellular longevity, 2013. **2013**: p. 474931-12.

29. Zhan, H., et al., *Ataxia Telangiectasia Mutated (ATM)-mediated DNA Damage Response in Oxidative Stress-induced Vascular Endothelial Cell Senescence[S].* The Journal of biological chemistry, 2010. **285**(38): p. 29662-29670.

30. Seoane, M., J.A. Costoya, and V.M. Arce, *Uncoupling Oncogene-Induced Senescence (OIS) and DNA Damage Response (DDR) triggered by DNA hyper-replication: Lessons from primary mouse embryo astrocytes (MEA).* Scientific reports, 2017. **7**(1): p. 12991-7.

31. d'Adda di Fagagna, F., et al., *Oncogene-induced senescence is a DNA damage response triggered by DNA hyper-replication.* Nature (London), 2006. **444**(7119): p. 638-642.

32. Shelton, D.N., et al., *Microarray analysis of replicative senescence.* Current biology, 1999. **9**(17): p. 939-945.

33. McHugh, D. and J. Gil, *Senescence and aging: Causes, consequences, and therapeutic avenues.* The Journal of cell biology, 2018. **217**(1): p. 65-77.

34. Kang, T.-W., et al., *Senescence surveillance of pre-malignant hepatocytes limits liver cancer development.* Nature (London), 2011. **479**(7374): p. 547-551.

35. Borodkina, A.V., et al., *"Social life" of senescent cells: What is SASP and why study it?* Actanaturae, 2018. **10**(1): p. 4-14.

36. Krizhanovsky, V., et al., *Senescence of Activated Stellate Cells Limits Liver Fibrosis.* Cell, 2008. **134**(4): p. 657-667.

37. Coppé, J.-P., et al., *The senescence-associated secretory phenotype: The dark side of tumor suppression.* Annual review of pathology, 2010. **5**: p. 99-118.

38. Coppé, J.-P., et al., *Senescence-associated secretory phenotypes reveal cell-nonautonomous functions of oncogenic RAS and the p53 tumor suppressor.* PLoS biology, 2008. **6**(12): p. 2853-2868.

39. Kim, K.M., et al., *Identification of senescent cell surface targetable protein DPP4.* Genes & development, 2017. **31**(15): p. 1529-1534.

40. Kim, K.M., et al., *SCAMP4 enhances the senescent cell secretome.* Genes & development, 2018. **32**(13-14): p. 909-914.

41. Rossi, M. and K. Abdelmohsen, *The Emergence of Senescent Surface Biomarkers as Senotherapeutic Targets.* Cells, 2021. **10**(7): p. 1740.

42. Baker, D.J., et al., *Clearance of p16Ink4a-positive senescent cells delays ageing-associated disorders.* Nature (London), 2011. **479**(7372): p. 232-236.

43. Zhu, Y., et al., *The Achilles' heel of senescent cells: from transcriptome to senolytic drugs.* Aging cell, 2015. **14**(4): p. 644-658.

44. Vasileiou, P.V.S., et al., *Mitochondrial Homeostasis and Cellular Senescence.* Cells (Basel, Switzerland), 2019. **8**(7): p. 686.

45. Kwon, S.M., et al., *Metabolic features and regulation in cell senescence.* BMB reports, 2019. **52**(1): p. 5-12.

46. Passos, J.F., et al., *Mitochondrial dysfunction accounts for the stochastic heterogeneity in telomere-dependent senescence.* PLoS biology, 2007. **5**(5): p. 1138-1151.

47. González-Gualda, E., et al., *A guide to assessing cellular senescence in vitro and in vivo.* The FEBS journal, 2021. **288**(1): p. 56-80.

48. Alcorta, D.A., et al., *Involvement of the Cyclin-Dependent Kinase Inhibitor p16 (INK4a) in Replicative Senescence of Normal Human Fibroblasts.* Proceedings of the National Academy of Sciences - PNAS, 1996. **93**(24): p. 13742-13747.

49. Yaswen, P., et al., *Reversal of human cellular senescence: roles of the p53 and p16 pathways.* The EMBO journal, 2003. **22**(16): p. 4212-4222.

50. Dulic, V., et al., *Uncoupling between Phenotypic Senescence and Cell Cycle Arrest in Aging p21-Deficient Fibroblasts.* Molecular and Cellular Biology, 2000. **20**(18): p. 6741-6754.

51. Chen, Q. and B.N. Ames, *Senescence-Like Growth Arrest Induced by Hydrogen Peroxide in Human Diploid Fibroblast F65 Cells.* Proceedings of the National Academy of Sciences - PNAS, 1994. **91**(10): p. 4130-4134.

52. Faragher, R.G.A., *Simple Detection Methods for Senescent Cells: Opportunities and Challenges.* Frontiers in Aging, 2021. **2**(17).

53. Schneider, E.L. and Y. Mitsui, *The Relationship between in Vitro Cellular Aging and in Vivo Human Age.* Proceedings of the National Academy of Sciences - PNAS, 1976. **73**(10): p. 3584-3588.

54. Sherwood, S.W., et al., *Defining Cellular senescence in IMR-90 Cells: A Flow Cytometric Analysis.* Proceedings of the National Academy of Sciences - PNAS, 1988. **85**(23): p. 9086-9090.

55. Perillo, N.L., et al., *Human T lymphocytes possess a limited in vitro life span.* Experimental gerontology, 1989. **24**(3): p. 177-187.

56. Hernandez-Segura, A., J. Nehme, and M. Demaria, *Hallmarks of Cellular Senescence.* Trends in cell biology, 2018. **28**(6): p. 436-453.

57.   Freund, A., et al., *Lamin B1 loss is a senescence-associated biomarker.* Molecular biology of the cell, 2012. **23**(11): p. 2066-2075.

58.   Dimri, G.P., et al., *A Biomarker that Identifies Senescent Human Cells in Culture and in Aging Skin in vivo.* Proceedings of the National Academy of Sciences - PNAS, 1995. **92**(20): p. 9363-9367.

59.   Cho, S.H.U.o.S.S.R.o.K., J.H.Y.s.P.C.S.R.o.K. Park, and E.S.U.o.S.S.R.o.K. Hwang, *Kinetics of the Cell Biological Changes Occurring in the Progression of DNA Damage-Induced Senescence.* Molecules and cells, 2011. **31**(6): p. 539-546.

60.   Martin, C., et al., *Changed genome heterochromatinization upon prolonged activation of the Raf/ERK signaling pathway.* PloS one, 2010. **5**(10): p. e13322-e13322.

61.   Michaloglou, C., et al., *BRAFE600-associated senescence-like cell cycle arrest of human naevi.* Nature (London), 2005. **436**(7051): p. 720-724.

62.   Narita, M., et al., *Rb-Mediated Heterochromatin Formation and Silencing of E2F Target Genes during Cellular Senescence.* Cell, 2003. **113**(6): p. 703-716.

63.   Kosar, M., et al., *Senescence-associated heterochromatin foci are dispensable for cellular senescence, occur in a cell type- and insult-dependent manner, and follow expression of p16(ink4a).* Cell cycle (Georgetown, Tex.), 2011. **10**(3): p. 457-468.

64.   Matjusaitis, M., et al., *Biomarkers to identify and isolate senescent cells.* Ageing research reviews, 2016. **29**: p. 1-12.

65.   Carnero, A. *Markers of cellular senescence*. United States.

66.   Barry, A.E., et al., *Hepatic Stellate Cells and Hepatocarcinogenesis.* Frontiers in cell and developmental biology, 2020. **8**: p. 709-709.

67.   Damm, G., et al., *Human parenchymal and non-parenchymal liver cell isolation, culture and characterization.* Hepatology International, 2013. **7**(4): p. 951-958.

68.   !!! INVALID CITATION !!! [56].

69.   Kholodenko, I.V. and K.N. Yarygin, *Cellular Mechanisms of Liver Regeneration and Cell-Based Therapies of Liver Diseases.* BioMed research international, 2017. **2017**: p. 1-17.

70.   Tao, Y., et al., *Liver Regeneration: Analysis of the Main Relevant Signaling Molecules.* Mediators of inflammation, 2017. **2017**: p. 4256352-9.

71.   Huard, J., et al., *An integrative model links multiple inputs and signaling pathways to the onset of DNA synthesis in hepatocytes.* The FEBS journal, 2012. **279**(18): p. 3290-3313.

72.   Koniaris, L.G., et al., *Liver regeneration*. 2003, Elsevier Inc: NEW YORK. p. 634-659.

73.   Manco, R., et al., *Liver regeneration: Different sub-populations of parenchymal cells at play choreographed by an injury-specific microenvironment.* International journal of molecular sciences, 2018. **19**(12): p. 4115.

74.   Dewhurst, M.R., et al., *Loss of hepatocyte cell division leads to liver inflammation and fibrosis.* PLoS genetics, 2020. **16**(11): p. e1009084-e1009084.

75.   Wang, M.J., et al., *Reversal of hepatocyte senescence after continuous in vivo cell proliferation.* Hepatology (Baltimore, Md.), 2014. **60**(1): p. 349-361.

76.   Tabibian, J.H., et al., *Cholangiocyte senescence by way of N-ras activation is a characteristic of primary sclerosing cholangitis.* Hepatology (Baltimore, Md.), 2014. **59**(6): p. 2263-2275.

77. Sasaki, M., et al., *Bile ductular cells undergoing cellular senescence increase in chronic liver diseases along with fibrous progression.* American journal of clinical pathology, 2010. **133**(2): p. 212-223.

78. Meng, L., et al., *Functional Role of Cellular Senescence in Biliary Injury.* The American journal of pathology, 2015. **185**(3): p. 602-609.

79. Cheng, Y., et al., *Aging-associated oxidative stress inhibits liver progenitor cell activation in mice.* Aging (Albany, NY.), 2017. **9**(5): p. 1359-1374.

80. Carpentier, B., A. Gautier, and C. Legallais, *Artificial and bioartificial liver devices: present and future.* Gut, 2009. **58**(12): p. 1690-1702.

81. Sykes, M. and D.H. Sachs, *Transplanting organs from pigs to humans.* Science immunology, 2019. **4**(41).

82. Pinzani, M., *Pathophysiology of Liver Fibrosis.* Digestive diseases (Basel), 2015. **33**(4): p. 492-497.

83. Schuppan, D.D. and N.H.M.D. Afdhal, *Liver cirrhosis.* The Lancet (British edition), 2008. **371**(9615): p. 838-851.

84. Osna, N.A., T.M. Donohue, and K.K. Kharbanda, *Alcoholic Liver Disease: Pathogenesis and Current Management.* Alcohol research, 2017. **38**(2): p. 147-161.

85. Neuschwander-Tetri, B.A., *Non-alcoholic fatty liver disease.* BMC medicine, 2017. **15**(1): p. 45-45.

86. Sayiner, M., et al., *Epidemiology of Nonalcoholic Fatty Liver Disease and Nonalcoholic Steatohepatitis in the United States and the Rest of the World.* Clinics in liver disease, 2016. **20**(2): p. 205-214.

87. De Silva, H.J. and A.S. Dassanayake, *Non-alcoholic fatty liver disease: Confronting the global epidemic requires better awareness.* Journal of gastroenterology and hepatology, 2009. **24**(11): p. 1705-1707.

88. Blackmore, L. and W. Bernal, *Acute liver failure.* Clinical medicine (London, England), 2015. **15**(5): p. 468-472.

89. Shalimar and S.K. Acharya, *Management in Acute Liver Failure.* Journal of clinical and experimental hepatology, 2014. **5**(1): p. S104-S115.

90. Zaccherini, G., E. Weiss, and R. Moreau, *Acute-on-chronic liver failure: Definitions, pathophysiology and principles of treatment.* JHEP Reports, 2021. **3**(1): p. 100176-100176.

91. Zamora Nava, L.E., et al., *Acute-on-chronic liver failure: A review.* Therapeutics and clinical risk management, 2014. **10**(1): p. 295-303.

92. Aravinthan, A., et al., *Hepatocyte Expression of the Senescence Marker p21 Is Linked to Fibrosis and an Adverse Liver-Related Outcome in Alcohol-Related Liver Disease.* PloS one, 2013. **8**(9): p. e72904.

93. Katharine, M.I.R.S.N.J.B.M.M.G.P.T.D.L.B.G.M.M.H.M.J.S.A.D.C.E.E., *Senescent human hepatocytes express a unique secretory phenotype and promote macrophage migration.* World journal of gastroenterology : WJG, 2014. **20**(47): p. 17851-17862.

94. Sekoguchi, S., et al., *Role of cell-cycle turnover and oxidative stress in telomere shortening and cellular senescence in patients with chronic hepatitis C.* Journal of gastroenterology and hepatology, 2007. **22**(2): p. 182-190.

95. Moustakas, I.I., et al., *Hepatic Senescence Accompanies the Development of NAFLD in Non-Aged Mice Independently of Obesity.* International journal of molecular sciences, 2021. **22**(7): p. 3446.

96.   Ferreira-Gonzalez, S., et al., *Paracrine cellular senescence exacerbates biliary injury and impairs regeneration.* Nature communications, 2018. **9**(1): p. 1020-1020.

97.   Ramakrishna, G., et al., *From Cirrhosis to Hepatocellular Carcinoma: New Molecular Insights on Inflammation and Cellular Senescence.* Liver cancer (Basel), 2013. **2**(3-4): p. 367-383.

98.   Ande, S., et al., *Hepatocyte telomere shortening and senescence are general markers of human liver cirrhosis.* Journal of Hepatology, 2002. **36**: p. 44-44.

99.   Aini, W., et al., *Accelerated telomere reduction and hepatocyte senescence in tolerated human liver allografts.* Transplant immunology, 2014. **31**(2): p. 55.

100.   Acar, U., et al., *Impact of Cytokine Adsorption Treatment in Liver Failure.* Transplantation proceedings, 2019. **51**(7): p. 2420-2424.

101.   Selden, C., et al., *A clinical-scale BioArtificial Liver, developed for GMP, improved clinical parameters of liver function in porcine liver failure.* Scientific reports, 2017. **7**(1): p. 14518-19.

102.   He, Y.-T., et al., *Bioartificial liver support systems for acute liver failure: A systematic review and meta-analysis of the clinical and preclinical literature.* World journal of gastroenterology : WJG, 2019. **25**(27): p. 3634-3648.

103.   Rust, C., et al., *Bile Acid-induced Apoptosis in Hepatocytes Is Caspase-6-dependent.* The Journal of biological chemistry, 2009. **284**(5): p. 2908-2916.

104.   Martinez-Diez, M.C., et al., *Comparison of the effects of bile acids on cell viability and DNA synthesis by rat hepatocytes in primary culture.* Biochimica et biophysica acta. Molecular basis of disease, 2000. **1500**(2): p. 153-160.

105.   Sugita, T., et al., *Analysis of the Serum Bile Acid Composition for Differential Diagnosis in Patients with Liver Disease.* Gastroenterology research and practice, 2015. **2015**: p. 717431-10.

106.   Choi, S.H., K.E. Yun, and H.J. Choi, *Relationships between serum total bilirubin levels and metabolic syndrome in Korean adults.* Nutrition, Metabolism and Cardiovascular Diseases, 2011. **23**(1): p. 31-37.

107.   Rawat, V., et al., *Bilirubin-Induced Oxidative Stress Leads to DNA Damage in the Cerebellum of Hyperbilirubinemic Neonatal Mice and Activates DNA Double-Strand Break Repair Pathways in Human Cells.* Oxidative medicine and cellular longevity, 2018. **2018**: p. 1-11.

108.   Qaisiya, M., et al., *Bilirubin mediated oxidative stress involves antioxidant response activation via Nrf2 pathway.* Cellular signalling, 2014. **26**(3): p. 512-520.

109.   Slack, A.J., et al., *Ammonia clearance with haemofiltration in adults with liver disease.* Liver international, 2014. **34**(1): p. 42-48.

110.   Cauli, O., et al., *Inflammation and hepatic encephalopathy: Ibuprofen restores learning ability in rats with portacaval shunts.* Hepatology, 2007. **46**(2): p. 514-519.

111.   Rozga, J., *Liver support technology – an update.* Xenotransplantation, 2006. **13**(5): p. 380-389.

112.   Lesaffer, G., et al., *Intradialytic removal of protein-bound uraemic toxins: Role of solute characteristics and of dialyser membrane.* Nephrology, dialysis, transplantation, 2000. **15**(1): p. 50-57.

113.   Pless, G., *Artificial and Bioartificial Liver Support.* Organogenesis, 2007. **3**(1): p. 20-24.

114.   Freeman, J.G., K. Matthewson, and C.O. Record, *Plasmapheresis in acute liver failure.* The International journal of artificial organs, 1986. **9**(6): p. 433.

171

115.   Van De Kerkhove, M.P., et al., *Clinical application of bioartificial liver support systems.* Annals of Surgery, 2004. **240**(2): p. 216-230.

116.   Schaefer, B., et al., *Comparison of Molecular Adsorbents Recirculating System (MARS) dialysis with combined plasma exchange and haemodialysis in children with acute liver failure.* Nephrology, dialysis, transplantation : official publication of the European Dialysis and Transplant Association - European Renal Association Journal Article, 2011. **26**(11): p. 3633.

117.   Klammt, S., et al., *Extracorporeal liver support by recirculating albumin dialysis: analysing the effect of the first clinically used generation of the MARSystem: Extracorporeal liver support.* Liver (Copenhagen), 2002. **22**: p. 30-34.

118.   Guo, L.-M., et al., *Application of Molecular Adsorbents Recirculating System to remove NO and cytokines in severe liver failure patients with multiple organ dysfunction syndrome.* Liver international, 2003. **23**(s3): p. 16-20.

119.   Donati, G., et al., *Extracorporeal Detoxification for Hepatic Failure Using Molecular Adsorbent Recirculating System: Depurative Efficiency and Clinical Results in a Long-Term Follow-Up.* Artificial organs, 2014. **38**(2): p. 125-134.

120.   Santoro, A., et al., *Prometheus System: A Technological Support in Liver Failure.* Transplantation proceedings, 2006. **38**(4): p. 1078-1082.

121.   Sponholz, C., et al., *Molecular adsorbent recirculating system and single-pass albumin dialysis in liver failure - a prospective, randomised crossover study.* Critical Care, 2016. **20**(1): p. 2-2.

122.   Struecker, B., N. Raschzok, and I.M. Sauer, *Liver support strategies: Cutting-edge technologies.* Nature Reviews Gastroenterology and Hepatology, 2014. **11**(3): p. 166-176.

123.   Joseph, N. and L. Kumar, *Liver support devices: Bridge to transplant or recovery.* Indian journal of respiratory care, 2017. **6**(2): p. 807.

124.   Ellis, A.J., et al., *Pilot-controlled trial of the extracorporeal liver assist device in acute liver failure.* Hepatology (Baltimore, Md.), 1996. **24**(6): p. 1446-1451.

125.   Millis, J.M., et al., *Initial experience with the modified extracorporeal liver-assist device for patients with fulminant hepatic failure: System modifications and clinical impact.* Transplantation, 2002. **74**(12): p. 1735-1746.

126.   Thompson, J., et al., *Extracorporeal cellular therapy (ELAD) in severe alcoholic hepatitis: A multinational, prospective, controlled, randomized trial.* Liver transplantation, 2018. **24**(3): p. 380-393.

127.   Jalan, R., S. Sen, and R. Williams, *PROSPECTS FOR EXTRACORPOREAL LIVER SUPPORT.* Gut, 2004. **53**(6): p. 890-898.

128.   Mullon, C. and Z. Pitkin, *The HepatAssist® Bioartificial Liver Support System: Clinical study and pig hepatocyte process.* Expert opinion on investigational drugs, 1999. **8**(3): p. 229-235.

129.   Sauer, I.M., et al., *Clinical extracorporeal hybrid liver support - phase I study with primary porcine liver cells.* Xenotransplantation (København), 2003. **10**(5): p. 460-469.

130.   van de Kerkhove, M.P., et al., *Phase I clinical trial with the AMC-bioartificial liver.* International journal of artificial organs, 2002. **25**(10): p. 950-959.

131.   Chew, S.C., et al., *Clinical experience with a porcine hepatocyte-based liver support system.* International journal of artificial organs, 1996. **19**(11): p. 664-669.

132. Sauer, I.M., et al., *Clinical extracorporeal hybrid liver support – phase I study with primary porcine liver cells.* Xenotransplantation (København), 2003. **10**(5): p. 460-469.

133. Struecker, B., N. Raschzok, and I.M. Sauer, *Liver support strategies: Cutting-edge technologies.* Nature reviews. Gastroenterology & hepatology, 2014. **11**(3): p. 166-176.

134. Schrem, H., et al., *Physiological incompatibilities of porcine hepatocytes for clinical liver support.* Liver Transplantation, 2006. **12**(12): p. 1832-1840.

135. Sauer, I.M., et al., *Clinical extracorporeal hybrid liver support – phase I study with primary porcine liver cells.* Xenotransplantation, 2003. **10**(5): p. 460-469.

136. Arzumanian, V.A., O.I. Kiseleva, and E.V. Poverennaya, *The curious case of the HepG2 cell line: 40 years of expertise.* International journal of molecular sciences, 2021. **22**(23): p. 13135.

137. Yan, Q., et al., *Establishment and characterization of an immortalized human hepatocyte line for the development of bioartificial liver system.* Cytotechnology, 2018. **70**(2): p. 665-674.

138. Pan, X., et al., *Establishment and characterization of immortalized human hepatocyte cell line for applications in bioartificial livers.* Biotechnology letters, 2012. **34**(12): p. 2183-2190.

139. Ramboer, E., et al., *Strategies for immortalization of primary hepatocytes.* Journal of hepatology, 2014. **61**(4): p. 925-943.

140. Kobayashi, N., *Artificial Cells for the Development of Cell Therapy.* 2008, SAGE Publications: Los Angeles, CA. p. 3-9.

141. Clayton, R.F., et al., *Liver cell lines for the study of hepatocyte functions and immunological response.* Liver International, 2005. **25**(2): p. 389-402.

142. Pien, G.C., et al., *Capsid antigen presentation flags human hepatocytes for destruction after transduction by adeno-associated viral vectors.* Journal of Clinical Investigation, 2009. **119**(6): p. 1688-1695.

143. Deurholt, T., et al., *Novel immortalized human fetal liver cell line, cBAL111, has the potential to differentiate into functional hepatocytes.* BMC biotechnology, 2009. **9**(1): p. 89-89.

144. Zhao, L., et al., *Evaluation of a reversibly immortalized human hepatocyte line in bioartificial liver in pigs.* African Journal of Biotechnology, 2012. **11**(17): p. 4116-4126.

145. David, B., et al., *In vitro assessment of encapsulated C3A hepatocytes functions in a fluidized bed bioreactor.* Biotechnology Progress, 2004. **20**(4): p. 1204-1212.

146. van Wenum, M., et al., *HepaRG-Progenitor Cell Derived Hepatocytes Cultured in Bioartificial Livers Are Protected from Healthy- and Acute Liver Failure-Plasma Induced Toxicity.* Cellular physiology and biochemistry, 2018. **48**(5): p. 2189-2204.

147. Matthew, H.W.T., et al., *Effects of plasma exposure on cultured hepatocytes: Implications for bioartificial liver support.* Biotechnology and bioengineering, 1996. **51**(1): p. 100-111.

148. Hoekstra, R., et al., *The effect of rat acute-liver-failure plasma on hepaRG cells.* International journal of artificial organs, 2012. **35**(11): p. 1006-1014.

149. Abrahamse, S.L., et al., *Treatment of acute liver failure in pigs reduces hepatocyte function in a bioartificial liver support system.* International journal of artificial organs, 2002. **25**(10): p. 966-974.

173

150. Bonalumi, F., et al., *Bioengineering a cryogel-derived bioartificial liver using particle image velocimetry defined fluid dynamics.* MATERIALS SCIENCE & ENGINEERING C-MATERIALS FOR BIOLOGICAL APPLICATIONS, 2021. **123**: p. 111983-111983.

151. Ingavle, G.C., et al., *Affinity binding of antibodies to supermacroporous cryogel adsorbents with immobilized protein A for removal of anthrax toxin protective antigen.* Biomaterials, 2015. **50**(1): p. 140-153.

152. Shimonishi, T., K. Miyazaki, and Y. Nakanuma, *Cytokeratin profile relates to histological subtypes and intrahepatic location of intrahepatic cholangiocarcinoma and primary sites of metastatic adenocarcinoma of liver: CK expression in cholangiocarcinoma.* Histopathology, 2000. **37**(1): p. 55-63.

153. Rubio, C.A., *The detection of bile ducts in liver biopsies by Cytokeratin 7.* In vivo (Athens), 1998. **12**(2): p. 183-186.

154. Eyken, P.V., et al., *Abundant expression of cytokeratin 7 in fibrolamellar carcinoma of the liver.* Histopathology, 1990. **17**(2): p. 101-107.

155. Yabushita, K., et al., *Aberrant expression of cytokeratin 7 as a histological marker of progression in primary biliary cirrhosis.* Liver (Copenhagen), 2001. **21**(1): p. 50-55.

156. Savina, I.N., et al., *Cryogels from poly(2-hydroxyethyl methacrylate): Macroporous, interconnected materials with potential as cell scaffolds.* Soft matter, 2007. **3**(9): p. 1176-1184.

157. Toussaint, O., E.E. Medrano, and T. von Zglinicki, *Cellular and molecular mechanisms of stress-induced premature senescence (SIPS) of human diploid fibroblasts and melanocytes.* Experimental gerontology, 2000. **35**(8): p. 927-945.

158. Frippiat, C., et al., *Subcytotoxic H2O2 stress triggers a release of transforming growth factor-beta 1, which induces biomarkers of cellular senescence of human diploid fibroblasts.* The Journal of biological chemistry, 2001. **276**(4): p. 2531-2537.

159. Irvine, K.M., et al., *Senescent human hepatocytes express a unique secretory phenotype and promote macrophage migration.* World journal of gastroenterology : WJG, 2014. **20**(47): p. 17851-17862.

160. Wang, A.S. and O. Dreesen, *Biomarkers of cellular senescence and skin aging.* Frontiers in Genetics, 2018. **9**: p. 247-247.

161. Alili, L., et al., *A drug-induced accelerated senescence (DIAS) is a possibility to study aging in time lapse.* AGE, 2014. **36**(3): p. 1329-1343.

162. Kabiri, L., et al., *Inhibitory and Apoptotic Effects of Mannan-Mitomycin C Conjugate Against Transitional Cell Carcinoma and Normal Mouse Fibroblasts.* Reports of biochemistry and molecular biology, 2019. **8**(1): p. 63-71.

163. Squarzanti, D.F., et al., *Human papillomavirus type 16 E6 and E7 oncoproteins interact with the nuclear p53-binding protein 1 in an in vitro reconstructed 3D epithelium: New insights for the virus-induced DNA damage response.* Virology journal, 2018. **15**(1): p. 176-176.

164. Nagano, T., et al., *Identification of cellular senescence-specific genes by comparative transcriptomics.* Scientific reports, 2016. **6**(1): p. 31758-31758.

165. Bressac, B., et al., *Abnormal Structure and Expression of p53 Gene in Human Hepatocellular Carcinoma.* Proceedings of the National Academy of Sciences - PNAS, 1990. **87**(5): p. 1973-1977.

166. Gu, L. and M. Kitamura, *Sensitive Detection and Monitoring of Senescence-Associated Secretory Phenotype by SASP-RAP Assay.* PloS one, 2012. **7**(12): p. e52305-e52305.

167.	Quijano, C., et al., *Oncogene-induced senescence results in marked metabolic and bioenergetic alterations.* Cell cycle (Georgetown, Tex.), 2012. **11**(7): p. 1383-1392.

168.	Ding, Y., *LIVER Other 88: The Development of a New Bioartificial Liver and its Application in 12 Acute Liver Failure Patients.* Journal of gastrointestinal surgery, 2003. **7**(2): p. 285-285.

169.	Stiffel, M., et al., *24-Hour Performance of Albumin Dialysis Assessed by a New Two-Compartment In Vitro Model.* Therapeutic apheresis and dialysis, 2014. **18**(1): p. 79-86.

170.	Ollinger, R., et al., *Bilirubin - A natural inhibitor of vascular smooth muscle cell proliferation.* Circulation (New York, N.Y.), 2005. **112**(7): p. 1030-1038.

171.	Öllinger, R., et al., *Bilirubin inhibits tumor cell growth via activation of ERK.* Cell cycle (Georgetown, Tex.), 2007. **6**(24): p. 3078-3085.

172.	Martinez-Diez, M.C., et al., *Comparison of the effects of bile acids on cell viability and DNA synthesis by rat hepatocytes in primary culture.* BIOCHIMICA ET BIOPHYSICA ACTA-MOLECULAR BASIS OF DISEASE, 2000. **1500**(2): p. 153-160.

173.	Gove, C.D., R.D. Hughes, and R. Williams, *Rapid inhibition of DNA synthesis in hepatocytes from regenerating rat livers by serum from patients with fulminant hepatic failure.* British journal of experimental pathology, 1982. **63**(5): p. 547-553.

174.	Catapano, G., et al., *The effect of catabolite concentration on the viability and functions of isolated rat hepatocytes.* International journal of artificial organs, 1996. **19**(4): p. 245-250.

175.	Kim, A.L., et al., *Resveratrol inhibits proliferation of human epidermoid carcinoma A431 cells by modulating MEK1 and AP-1 signalling pathways.* Experimental dermatology, 2006. **15**(7): p. 538-546.

176.	Kim, Y.-A., et al., *Resveratrol inhibits cell proliferation and induces apoptosis of human breast carcinoma MCF-7 cells.* Oncology reports, 2004. **11**(2): p. 441-446.

177.	Latorre, E., et al., *Small molecule modulation of splicing factor expression is associated with rescue from cellular senescence.* BMC cell biology, 2017. **18**(1): p. 31-15.

178.	Birar, V.C., et al., *A facile, stereoselective, one-pot synthesis of resveratrol derivatives.* Chemistry Central journal, 2015. **9**(1): p. 26-26.

179.	Nimse, S.B. and D. Pal, *Free radicals, natural antioxidants, and their reaction mechanisms.* RSC advances, 2015. **5**(35): p. 27986-28006.

180.	Traber, M.G. and J.F. Stevens, *Vitamins C and E: Beneficial effects from a mechanistic perspective.* Free radical biology & medicine, 2011. **51**(5): p. 1000-1013.

181.	Jian, B., et al., *Resveratrol restores sirtuin 1 (SIRT1) activity and pyruvate dehydrogenase kinase 1 (PDK1) expression after hemorrhagic injury in a rat model.* Molecular medicine (Cambridge, Mass.), 2014. **20**(1): p. 10-16.

182.	Zhang, P., et al., *Resveratrol Ameliorated Vascular Calcification by Regulating Sirt-1 and Nrf2.* Transplantation proceedings, 2016. **48**(10): p. 3378-3386.

183.	Mavri-Damelin, D., et al., *Ornithine transcarbamylase and arginase I deficiency are responsible for diminished urea cycle function in the human hepatoblastoma cell line HepG2.* The international journal of biochemistry & cell biology, 2007. **39**(3): p. 555-564.
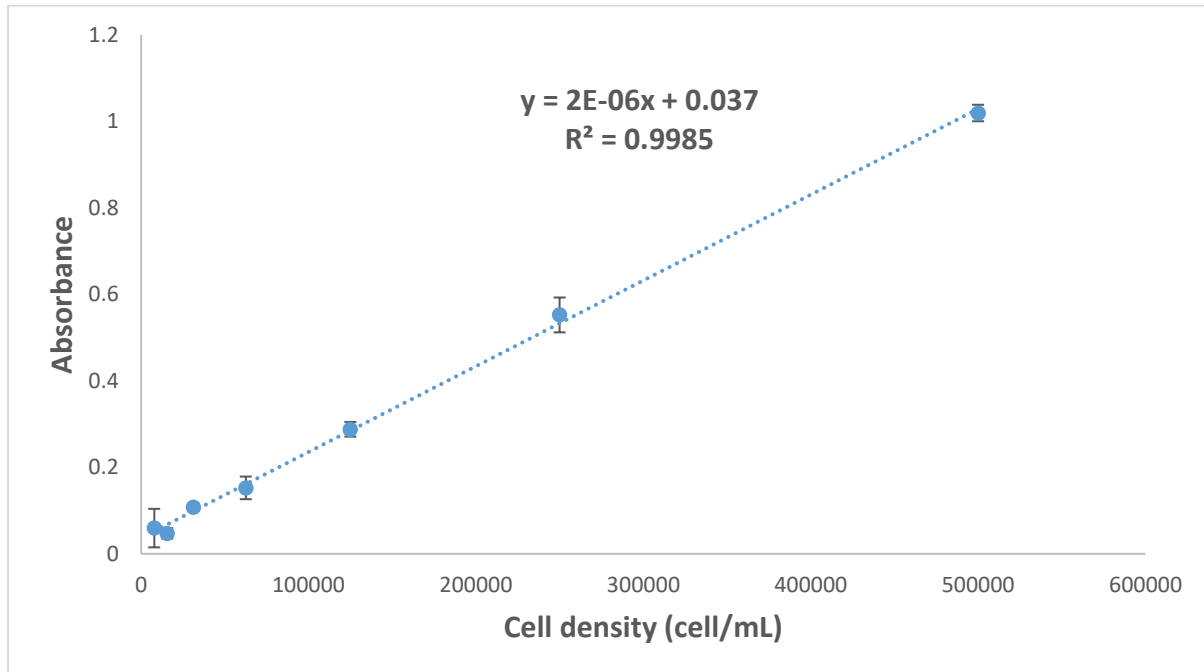
Appendix

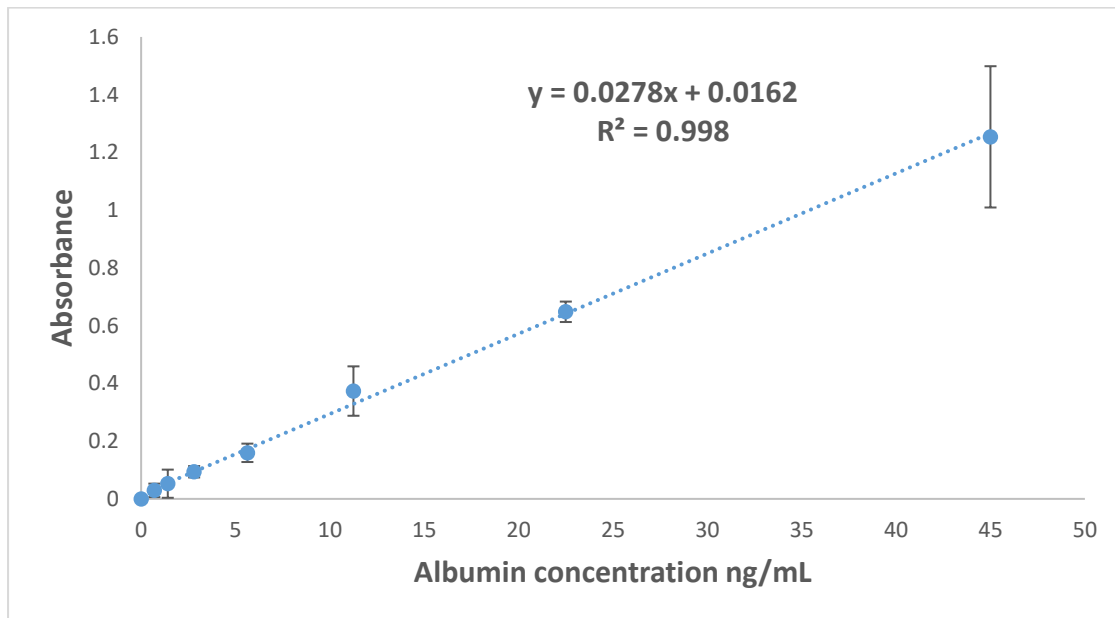**MTT assay 1**

$y = 2E\text{-}06x + 0.0322$

$R^2 = 0.9916$
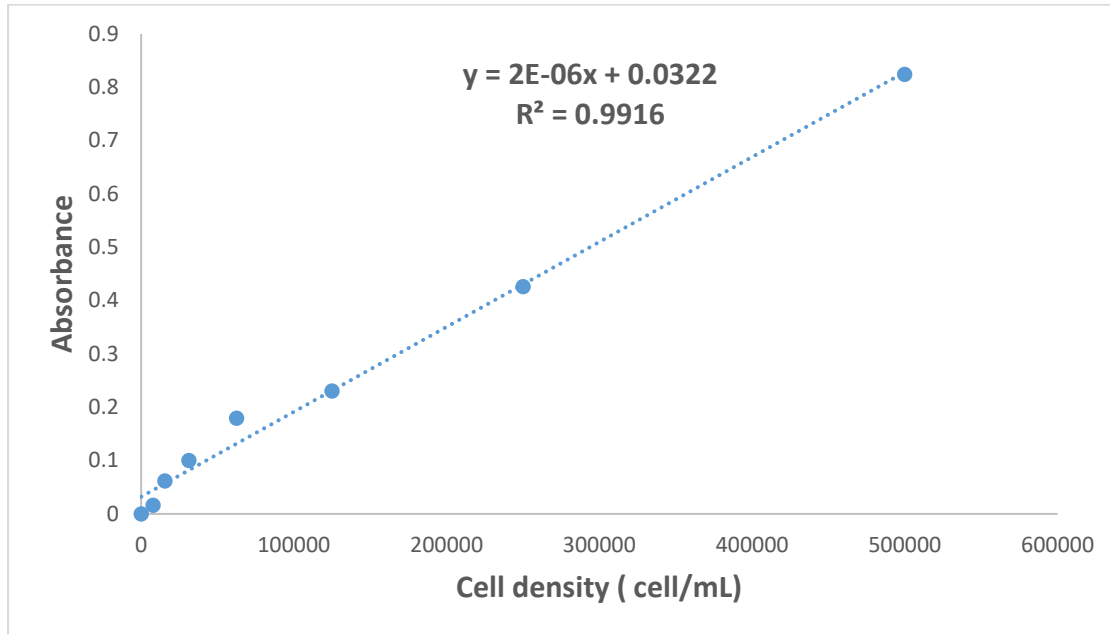
Increase in absorbance with increasing in HHL7 density is shown in the standard curve. Absorbance was measured after 24-h incubation.
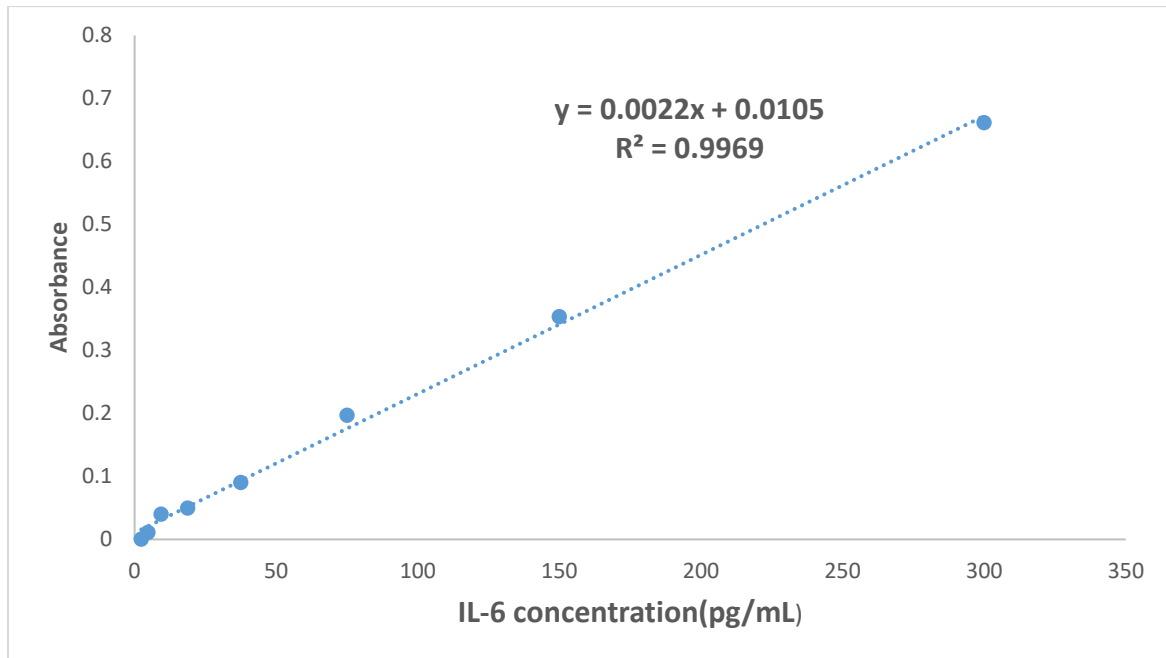
MTT assay 2

The standard curve shows a linear increase of absorbance with increasing in HepG2 cell density. Absorbance was measured after 24-h incubation.
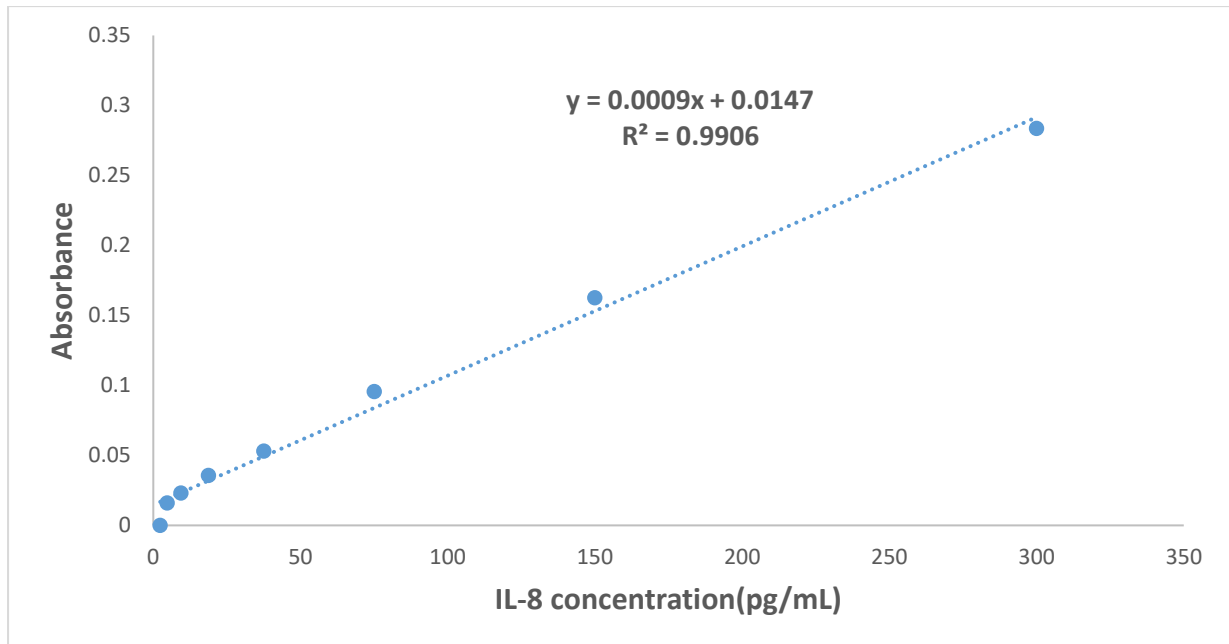
ELISA assay

Human albumin ELISA assay standard curve validation shows the linear increase of absorbance with increasing albumin concentration.

ELISA assay for cytokines measurement

Human IL-6 ELISA assay validation shows linear increase of absorbance with increasing of IL-6 concentration.

ELISA assay for cytokines measurement

Human IL-8 ELISA assay validation shows the linear increase of absorbance with increasing IL-8 concentration.

Immunostaining of Ki67 in HepG2 cells cultured on HEMA-MBA-alginate cryogels after liver toxins and resveratrol treatment
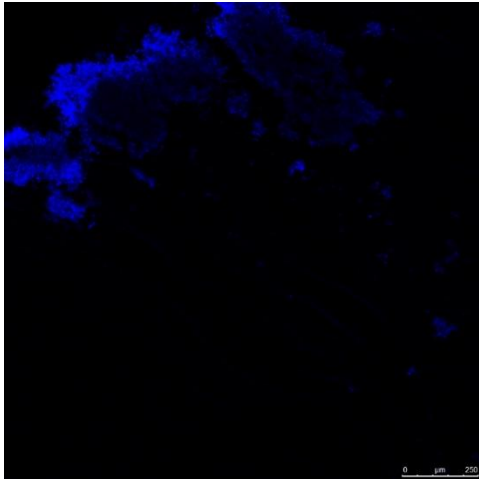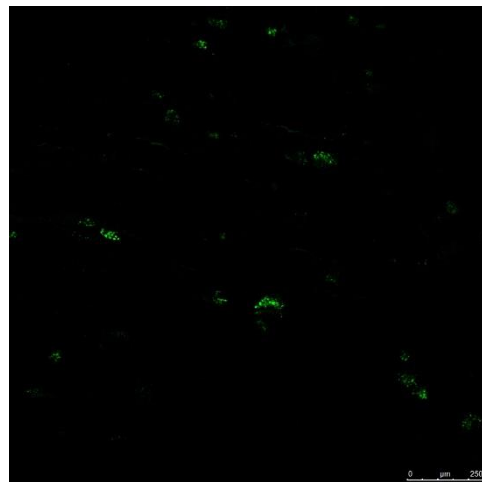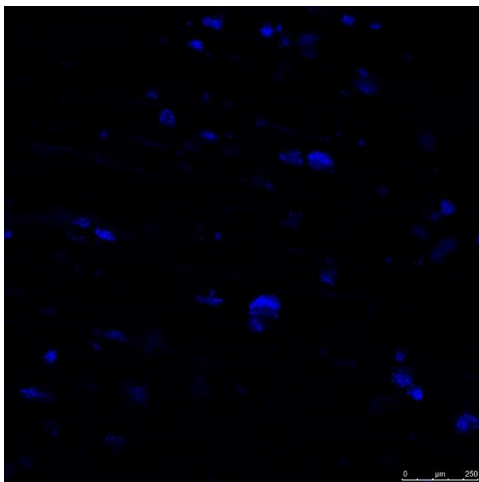
DAPI　　　　　　　　　　　　　　**Ki67**

Control

2µM RSV+LT

5μM RSV+LT

LT